

DESIGN FOR DYNAMIC PERFORMANCE OF AN AIR SEPARATION
UNIT

**DESIGN FOR DYNAMIC PERFORMANCE:
APPLICATION TO AN AIR SEPARATION UNIT**

by

Yanan Cao, B. Eng. Mgt. (Chemical Engineering & Management)

A Thesis

Submitted to the School of Graduate Studies

in Partial Fulfillment of the Requirements

for the Degree

Master of Applied Science

McMaster University

© Copyright by Yanan Cao, April 2011

MASTER OF APPLIED SCIENCE (2011)
(Chemical Engineering)

McMaster University
Hamilton, Ontario, Canada

TITLE: Design for Dynamic Performance: Application to an Air
Separation Unit

AUTHOR: Yanan Cao, B.Eng.Mgt. (Chemical Engineering & Management)
(McMaster University, Hamilton, Ontario, Canada)

SUPERVISOR: Dr. C.L.E. Swartz

NUMBER OF PAGES: xv, 124

ABSTRACT

The significant effect that the design of a plant can have on its dynamic performance has led to methodologies for systematic analysis of the interaction between design and control, and for inclusion of dynamic performance considerations in plant design. In this thesis, an optimization-based framework is presented for improving the agility of a N_2 plant in response to the highly dynamic market, particularly demand and electricity price fluctuations. In this research, a decomposition optimization strategy is followed to identify limiting plant constraints and investigate selected design modifications using a rigorous dynamic air separation plant model.

The plant model comprises of dynamic models for the distillation column with an integrated reboiler/condenser and a primary heat exchanger, and algebraic models for a compressor and turbine. The models presented follow first principles and/or empirical approaches. An index reduction procedure is utilized to reduce a high-index dynamic distillation model to an index-1 system. The proposed plant model is validated and reconciled using plant data through parameter estimation. Excellent prediction accuracy is obtained.

Steady state optimization is the first tier of the optimization problem. In this stage, different scenarios in terms of demand changes and electricity price fluctuations are explored. In all optimized cases, the liquid nitrogen (LN_2) production rate and rate of evaporation remain at their lower bounds due to the zero revenue for LN_2 product and the high cost of evaporation. It is demonstrated that operating close to the maximum allowable impurity level is optimal as it gives a high recovery rate. Two major findings in this stage are: (1) the operating window of the plant is defined by the flooding constraint of the distillation column and the surge constraint of the compressor when the feed flow rate is considered; and (2) there is a break-even point between revenue generated from and compression cost required by one mole of air feed into the system when electricity price fluctuates.

Dynamic optimization is performed to switch the system from the base case operating point to the new operating point determined from the steady state optimization without violating plant constraints. A trajectory tracking objective function with endpoint constraints to “pin-down” the final states to the pre-determined optimal values is solved in each case. With optimized control action, a fast transition without constraint violations can be achieved. Plants can complete the transition in less than 30 minutes with step-like responses of gas nitrogen (GN_2) production. Two plant modifications for aiding transitions are evaluated: (1) introducing external LN_2 during transitions for cases of increasing demand, and (2) allowing a vent stream after the compressor for cases of decreasing demand. Even though for this particular plant setup (impurity requirements, tray design, etc.), introducing external LN_2 may not be cost-effective, this design modification is very attractive as it allows a smaller operating safety margin in the impurity requirement, which could result in more profitable steady state operation.

ACKNOWLEDGEMENTS

I wish to express my gratitude to my supervisor, Dr. Christopher Swartz, for his continued support, advice and guidance throughout the course of this research. This thesis would certainly not be possible without his vision and direction.

I wish to acknowledge the McMaster Advanced Control Consortium and the Department of Chemical Engineering at McMaster University for financial support. I would like to thank all the professors, who have taught me since my first day at McMaster University. They have provided me with an excellent background. Special thanks go to Dr. Thomas E. Marlin, who taught me my first course in this field, and led me into the interesting area of process control.

Thanks also go to the industrial partner, Praxair, Inc., for graciously providing the key motivation for and continued participation in this project. Special thanks go to Michael Baldea and Stephane Blouin for their insights and suggestions.

In addition, I would like to thank all my friends and my colleagues in the control group, especially Zhiwen Chong. Their friendship and moral support are indeed appreciated.

This thesis is dedicated to my parents, Wendu Cao and Ying Zhang, for their financial and emotional support all these years, particularly during the difficult periods of my life. Their sacrifices in order to provide me with an education can never be repaid.

Table of Contents

1	Introduction	1
1.1	Motivation and Goals	2
1.2	Main Contributions	4
1.3	Thesis overview	5
2	Literature Review	7
2.1	Air Separation Process	7
2.1.1	Process Description	7
2.1.2	Modeling of Cryogenic Distillation Column	11
2.1.3	Control of Cryogenic Air Separation Process	12
2.1.4	Optimization for Design and Operation of Air Separation Processes	15
2.2	Dynamic Optimization	16
2.2.1	General Form	16
2.2.2	Solution Strategies	17

2.3	Differential Algebraic Equations	21
2.3.1	Ordinary Differential Equations	21
2.3.2	Mathematical Structure and Index of Differential Algebraic Equations	24
2.3.3	Numerical Solution	26
3	Mathematical Model	27
3.1	Physical Property Estimation	28
3.1.1	Vapor-Liquid Phase Equilibrium (VLE)	28
3.1.2	Vapor Phase Compressibility Factor and Molar Density	29
3.1.3	Liquid Phase Molar Density	30
3.1.4	Liquid Phase Surface Tension	31
3.2	Distillation Column Tray	31
3.2.1	General Approach	32
3.2.2	Index Reduction	38
3.3	Integrated Reboiler/Condenser (IRC)	41
3.3.1	Condenser Side Model	42
3.3.2	Reboiler Side Model	44
3.4	Sump at the Column Bottom	45
3.5	Primary Heat Exchanger (PHX)	46
3.5.1	Volume Calculation	47

3.5.2	Dynamic Heat Exchanger Model	50
3.6	Compressor	54
3.6.1	Modeling Equations	54
3.6.2	Obtaining Surface Fits for Compressor Maps	57
3.7	Turbine	61
3.8	Integrated Plant Model	63
3.9	Data Reconciliation and Parameter Estimation	64
3.10	Simulation Results	68
4	Optimization Formulation	72
4.1	Optimization Approach - Decomposition Strategy	72
4.2	Tier 1: Economic Steady-state Optimization	73
4.2.1	General Form	73
4.2.2	Constraints	75
4.3	Tier 2: Dynamic Optimization	78
4.3.1	General Form	78
4.3.2	Constraints	79
4.4	Handling Optimization Decision Variables	81
4.4.1	Filter on the Inputs	81
4.4.2	Control Vector Parametrization	81

5	Case Studies	84
5.1	Optimization Platform	84
5.2	Steady-state Optimization	85
5.2.1	Demand Fluctuation	86
5.2.2	Electricity Price Change	88
5.3	Dynamic Optimization for Existing Design	90
5.3.1	Positive 20 % Demand Change	91
5.3.2	Positive 10 % Demand Change	94
5.3.3	Negative 20 % Demand Change	94
5.3.4	Negative 10 % Demand Change	97
5.4	Effect of Introducing External Liquid Nitrogen during Transitions	98
5.4.1	Multiple Trays	100
5.4.2	Single Tray	107
5.4.3	Remarks	108
5.5	Effect of Vent after the Compressor	108
6	Conclusions and Recommendations	111
6.1	Conclusions	111
6.1.1	Process Modeling	111
6.1.2	Steady State Optimization	113

6.1.3	Dynamic Optimization	113
6.2	Recommendations for Further Work	115
6.2.1	Distillation Column Modeling	115
6.2.2	Varying Efficiency	115
6.2.3	Disturbance and Uncertainty	116
6.2.4	Multiple Column Air Separation Plants	116
	References	118
	A Numerical Issues	125
A.1	Step-wise Discontinuity	125
A.2	Variable Scaling	127
A.3	Constraint Formulation	129
	B Manual Index Reduction	131
	C Results of Introducing External Liquid Nitrogen to Top Tray	136

List of Figures

2.1	A cryogenic air separation plant that produces argon in addition to oxygen and nitrogen diagram, as depicted in Miller <i>et al.</i> [2008b]. LAr = Liquid Argon; LO ₂ = Liquid Oxygen; GO ₂ = Gas Oxygen; LN ₂ = Liquid Nitrogen; GN ₂ = Gas Nitrogen; PHX = Primary Heat Exchanger; LC = Lower Column; UC = Upper Column.	9
2.2	Nitrogen plant process diagram, as depicted in Zhu <i>et al.</i> [2001]. LN ₂ = Liquid Nitrogen; GN ₂ = Gas Nitrogen; PHX = Primary Heat Exchanger.	10
2.3	Example control variable profiles for control vector parameterization, adapted from Chachuat [2009] and Biegler [2007].	18
2.4	Example collocation, as depicted in Biegler [2007]. Black dots denote the collocation points.	20
3.1	Schematic representation of a column tray.	32
3.2	Schematic representation of the integrated reboiler/condenser.	42
3.3	Simplified illustration of a brazed aluminium plate-fin heat exchanger used in air separation processes, modified from ALPEMA [2000]. A detailed illustration of a brazed aluminium plate-fin heat exchanger is available in ALPEMA [2000].	48

3.4	Sectional view of the primary heat exchanger, as modelled.	48
3.5	Schematic of each layer of the primary heat exchanger. Modified from ALPEMA [2000].	49
3.6	Segment division and numbering in each zone.	50
3.7	Example compressor maps of inlet guide vane angle and rotation speed effects with surge lines shown (Brown [2005], Neerken [1984]).	58
3.8	The surface fit for the discharge pressure map. Circles are data points collected from the compressor map.	60
3.9	Scaled compressor map for the pilot plant. Scaled values were obtained according to the fan law and the predicted curves were generated using the surface fit expressions. Percentages correspond to the percentage closure of the IGVA.	62
3.10	Dynamic response of selected scaled variables to a negative step change in the air feed.	70
3.11	Dynamic response of selected scaled variables to a positive step change in the gas draw fraction to the primary heat exchanger.	71
4.1	A nitrogen plant configuration with indicated decision variables for the optimization problems.	74
4.2	Filter on the inputs.	81
4.3	Piecewise linear control profile.	82
5.1	Fraction of vapor velocity to flooding velocity at critical tray for 20 % demand increase case	92

5.2	Responses of the scaled variables for the 20 % demand increase case with optimized control actions.	93
5.3	Responses of the scaled variables for the 10 % demand increase case with optimized control actions.	95
5.4	Responses of the scaled variables for the 20 % demand decrease case with optimized control actions.	96
5.5	Responses of the scaled variables for the 10 % demand decrease case with optimized control actions.	97
5.6	A schematic representation of the design modification for introducing pre-stored liquid nitrogen.	99
5.7	Magnified views of gas nitrogen production and fractional flooding at the critical tray in responses to: optimized control actions of only the four manipulated variables (MVs); four MVs together with external LN ₂ with and without cost considerations.	102
5.8	Optimized trajectories of scaled variables for 20 % demand increase cases with and without external liquid nitrogen. No cost penalty applied to external liquid.	103
5.9	Optimized trajectories of scaled variables for 20 % demand increase case with cost penalty for external LN ₂ usage.	105
5.10	Optimized trajectories of scaled variables for 20 % demand increase case without cost penalty for external LN ₂ usage and with tightened impurity constraint.	106
5.11	Optimized trajectories of scaled variables for 20 % demand decrease case, with and without a vent stream.	110
A.1	Step-wise discontinuity in vapor phase molar enthalpy coefficients.	126

C.1	Magnified views of gas nitrogen production and fractional flooding at the critical tray in responses to: optimized control actions of only the four manipulated variables (MVs); four MVs together with external LN ₂ with and without cost considerations.	137
C.2	Optimized trajectories of scaled variables for 20 % demand increasing case with fixed duration time and no cost penalty applied to using external LN ₂	138
C.3	Optimized trajectories of scaled variables for 20 % demand increasing case with fixed duration time and cost penalty applied to using external LN ₂	139
C.4	Optimized trajectories of scaled variables for 20 % demand increase case without cost penalty for external LN ₂ usage and with tightened impurity constraint.	140

List of Tables

2.1	Advantages and disadvantages of direct solution methods (Biegler and Grossmann [2004], Cervantes and Biegler [2009], Chachuat [2009]).	22
3.1	Set of variable specifications in the integrated plant model.	65
3.2	Parameters in the integrated plant model.	66
3.3	Table of the measured variables.	68
5.1	Steady-state optimization results for changing demand and electricity price.	87
5.2	Dynamic Optimization Setup	91
5.3	Active constraints for case studies with tightened impurity constraints during transitions with and without external LN_2 to multiple trays.	107
C.1	Active constraints for case studies with tightened impurity constraints during transitions with and without external LN_2 to single tray.	141

Chapter 1

Introduction

The importance that the design of a plant has on its dynamic performance has received an increased amount of attention in recent years. Poor dynamic performance can lead to many practical problems such as failure to meet product specifications, safety and environmental constraints, as well as expected economic performance. Hence, extensive studies have been carried out over the past three decades to explore systematic analyses of design limitations to control performance, and incorporation of dynamic performance considerations within a plant design framework (van Schijndel and Pistikopoulos [2000], Morari [1983]).

Dynamic optimization provides a useful framework for the assessment of control performance limitations. Economic evaluation (e.g. Narraway and Perkins [1993]), trajectory tracking (e.g. Swartz [1996], Cao *et al.* [1996]), speed of response (e.g. White *et al.* [1996]) and plant startup/shutdown (e.g. Miller *et al.* [2008a]) are typical performance criteria. In optimization-based approaches to simultaneous plant and control system design, dynamic performance is accounted for implicitly through an economic objective function and path constraints on the input and response trajectories (Sakizlis *et al.* [2004], Mohideen *et al.* [1996], Baker and Swartz [2004]).

In this project, we will apply an optimization-based approach to investigate limiting factors for dynamic performance of an air separation plant. Historically, dynamic performance of air separation plants was judged based on the ability to reject disturbances. The agility and switchability (i.e. ability to switch between operating points quickly and optimally) were of little importance (White *et al.* [1996], Miller *et al.* [2008a]). This is mainly because such plants used to experience infrequent changes in operation conditions. This is no longer the case since electricity price deregulation has resulted in fluctuations in electricity price. Since electricity consumption is the major operational cost for an air separation plant, with a total electricity consumption by gas producers of over \$700 million/year in the USA (Zhu *et al.* [2001]), responding optimally to electricity price changes could yield significant economic benefit. On the one hand, electricity price variations create a great economic incentive for the air separation plants to introduce more frequent changes in operating conditions, such as producing at full capacity at the minimum price while reducing production when the electricity is at the peak. On the other hand, customers may also adjust their demand requirements in accordance to the electricity price. Those economic factors ultimately translate into frequent plant load changes that must be performed within a given time window. Hence, the use of steady-state simulation tools to design plants that will be subject to highly dynamic demand and utility price patterns has limitations. Also, such transition-time constraints make a stronger case for an integrated and dynamic design and control strategy. Systematic approaches to the design of dynamically operable plants have been the subject of many research studies over the past three decades (e.g. Sakizlis *et al.* [2004], Mohideen *et al.* [1996], Baker and Swartz [2004]). However, most studies on air separation processes have been limited to single process units, often represented by highly simplified models.

1.1 Motivation and Goals

This project is motivated by the need for a systematic approach for the identification of design factors that limit the capability of an air separation plant to respond to the highly

dynamic market, and investigation of promising design alternatives. The overall research goal is to develop an optimization-based framework to identify design characteristics that limit plant agility in the face of production demand and electricity price changes. To achieve this, two sub-objective are defined:

1. develop a rigorous and robust plant model that captures an air separation plant's dynamics and constraint structure, and adequately represents the nonlinear nature of the plant; and
2. through dynamic optimization, determine the best achievable dynamic performance, identify limiting plant constraints, and investigate selected design modifications to improve plant agility.

The first sub-objective — model development, validation and simulation is the foundation for the optimization-based approach. Mathematical representations of the essential process equipment will be derived following first principles and empirical approaches that capture the nonlinear nature of the process. Then, models of individual units will be assembled in accordance with the plant configuration. The proposed model will address critical safety and operational issues in the system. Model validation will be accomplished through parameter estimation. Prediction capability of the finalized model will then be tested through dynamic simulation case studies.

The second sub-objective involves large-scale nonlinear dynamic optimization. The rigorous dynamic plant model derived in the previous sub-objective will be utilized. Optimization would be performed first with only the pre-defined control inputs in the actual plant with fixed plant design. Thereafter, selected scenarios with plant modifications will be investigated. Consideration of uncertainties and disturbances are not within the scope of this research project.

1.2 Main Contributions

The first contribution of this project is the development of a mathematical representation for a nitrogen plant. Individual unit models considered in this study include:

- stage-by-stage distillation column model with integrated reboiler/condenser, resulting in a system of differential algebraic equations (DAEs);
- primary heat exchanger model, comprising a system of DAEs; and
- compressor and turbine models, comprising systems of algebraic equations only.

Other studies on air separation processes are either based on simplified distillation models or focus only on the distillation column rather than the whole plant. In addition, the stage-by-stage distillation model developed in this research considers dynamics of the energy holdup. The common assumption of negligible vapor holdup usually leads to a high-index dynamic distillation column model. An index reduction procedure is proposed to reduce the original high-index model to an index-1 system. This approach is effective, illustrated by a noticeable improvement in model robustness and a significant reduction in simulation time. The proposed model for the primary heat exchanger involves three countercurrent streams and allows a phase change in the air feed stream. The proposed plant model is validated and reconciled using plant data through parameter estimation.

The second contribution of this thesis is developing a decomposition optimization strategy for determining the best achievable dynamic performance, identifying limiting plant constraints, and investigating selected design modifications to improve plant agility. A full stage-by-stage dynamic distillation column model is employed in the optimization studies. The decomposition strategy involves economic based steady-state optimization followed by trajectory tracking dynamic optimization. Scenarios covering demand changes and electricity price fluctuations were investigated. The feasible operating window of the pilot plant was determined. Factors limiting plant dynamic performance were identified. Note that the dynamic performance obtained in this study is independent of the control structure

of the plant. Thus it can serve as a benchmark for identifying the best achievable plant performance.

In addition, for the numerical difficulties encountered in the project, several strategies are proposed. Methods for handling step-wise discontinuities, variable scaling and transformation, as well as constraint formulation are discussed.

1.3 Thesis overview

Chapter 2 – Literature Review

Four relevant topics are reviewed in this chapter:

- Air separation process: cryogenic air separation is discussed in detail.
- Distillation column modeling, including order reduction procedures.
- Dynamic optimization: general formulation and solutions strategies are reviewed.
- Differential algebraic equations: important aspects, including mathematical structure, index and solution methods are briefly outlined.

Chapter 3 – Mathematical Model

Mathematical models developed to represent a nitrogen plant are described in this chapter. The proposed integrated plant model consists of both first principles and empirical models. The general approach to model a distillation column is discussed in detail and a manual index reduction approach is proposed. Models for the integrated reboiler/condenser and column sump are also described. The primary heat exchanger (PHX) model is derived following a similar approach as Miller *et al.* [2008a]; however, the phase change in the air feed and pressure drop within the PHX are considered in our study. Compressor and turbine models are empirical, consisting systems of algebraic equations only. A parameter estimation procedure is performed to reconcile the integrated model with plant measurements. Dynamic simulations are conducted, and reasonable model predictions are obtained.

Chapter 4 – Optimization Formulation

The optimization problem formulation, including objective function, constraints and decision variables is outlined. Our proposed optimization approach follows a decomposition strategy: economic steady-state optimization followed by trajectory-tracking based dynamic optimization.

Chapter 5 – Case Studies

Optimization results following the proposed decomposition approach are presented in this chapter. A series of studies covering a variety market conditions (i.e. demand changes and electricity price fluctuations) without plant modifications are conducted. In addition, two sets of studies considering design alternations of (1) introducing external liquid nitrogen to the column, and (2) allowing a vent stream after the compressor on the dynamic performance of the system are investigated.

Chapter 6 – Conclusion and Recommendations

The final chapter of this thesis first highlights major accomplishments and results of this project. Then avenues for future studies are recommended.

Chapter 2

Literature Review

The intent of this chapter is to provide a brief review of some research topics relevant to this project. Topics covered in this chapter include: (1) air separation processes, specifically, cryogenic air separation; (2) distillation column modeling with more emphasis given to order reduction procedures; (3) dynamic optimization, including a general formulation and solutions strategies; (4) mathematical structure, index and solution methods for differential algebraic equations. More information is available from the references.

2.1 Air Separation Process

2.1.1 Process Description

Products of air separation processes play key roles in a variety of market sectors, such as petrochemical, metal, food processing and health care. The separation of air into oxygen, nitrogen and argon can be achieved by either cryogenic or noncryogenic processes (Sirdeshpande *et al.* [2005]). The cryogenic approach for air separation is based on low-temperature distillation and is capable of producing large quantities of high purity liquid and gas phase products. On the other hand, noncryogenic processes rely on adsorption and membrane

separation. In this project, we will focus on the cryogenic approach for air separation.

Descriptions of cryogenic air separation processes are outlined in many studies (e.g. Roffel *et al.* [2000], Zhu *et al.* [2001], Miller *et al.* [2008a]). Fig. 2.1 shows a typical plant setup for air separation units producing multiple products and Fig. 2.2 presents the process diagram of a N₂ plant. The major difference between the two plants is that the multi-product air separation plant has additional distillation columns (i.e. upper and super-staged argon columns in Fig. 2.1) to produce O₂ and Ar products. The lower column of the multi-product air separation plant and the distillation column in the N₂ plant operate at similar conditions; both of them are high pressure columns. Moreover, air separation plants of both multiple and N₂ only products have several heat integration units, such as the primary heat exchanger, utilizing low temperature waste and product streams to provide cooling for the warm air feed into the system. In this section, we will give more emphasis to the multi-product air separation plant. A detailed process description of a nitrogen plant is provided in Chapter 3.

An air separation plant producing multiple products usually has double or triple column arrangements, as in Fig. 2.1. These cryogenic distillation columns, operating at -170 to -190 °C, are the core of the air separation process (Zhu *et al.* [2001]). As in ordinary distillation processes, cryogenic distillation separates air components utilizing differences in component's boiling points. A air drawn from the atmosphere goes through compression and purification prior to being introduced at different locations to the upper and lower columns. The upper and lower columns of the cryogenic air separation unit operate at different pressures (i.e. at approximately 1.38×10^5 Pa and 5.86×10^5 Pa, respectively). Along the path, necessary refrigeration and expansion are provided according to the feed location. As N₂ is the most volatile component, it is concentrated in the overhead products of both the upper and lower columns. The oxygen product stream is drawn from the bottom of the upper column. The boiling point of Ar is between O₂ and N₂, and is recovered in the super-staged argon column. To achieve this, a vapor side stream is drawn from the upper column, close to the composition peak of argon, and is supplied to the super-staged argon

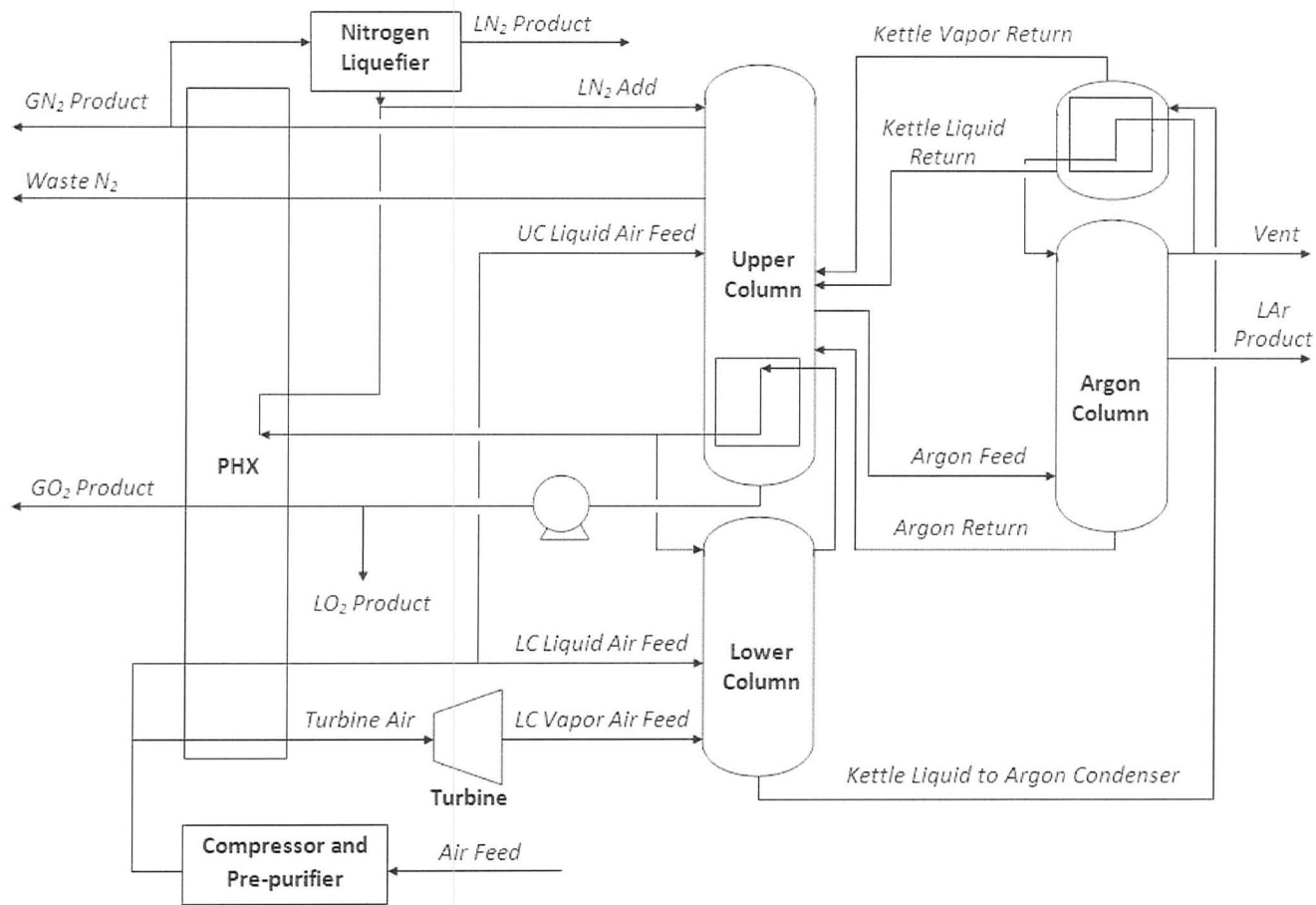


Figure 2.1: A cryogenic air separation plant that produces argon in addition to oxygen and nitrogen diagram, as depicted in Miller *et al.* [2008b]. LAr = Liquid Argon; LO₂ = Liquid Oxygen; GO₂ = Gas Oxygen; LN₂ = Liquid Nitrogen; GN₂ = Gas Nitrogen; PHX = Primary Heat Exchanger; LC = Lower Column; UC = Upper Column.

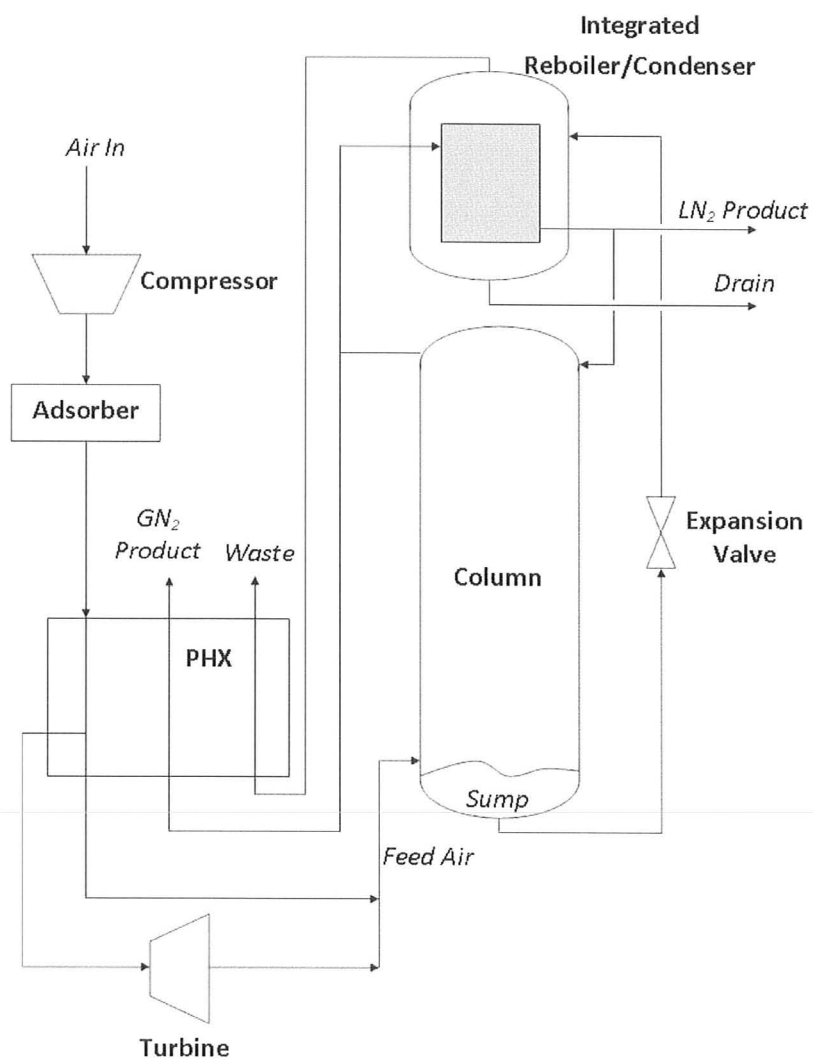


Figure 2.2: Nitrogen plant process diagram, as depicted in Zhu *et al.* [2001]. LN₂ = Liquid Nitrogen; GN₂ = Gas Nitrogen; PHX = Primary Heat Exchanger.

column. More details are available from Roffel *et al.* [2000] and Miller *et al.* [2008a].

Cryogenic air separation exhibits a high degree of integration of material and energy. There are many heat integration units in the process. The primary heat exchanger (PHX) utilizes the temperature differences between feed and products. The integrated reboiler/condensers (IRC) between the upper and lower columns and at the super-staged argon column accomplish heat transfer in accordance with different boiling points due to differences in operating pressures (Roffel *et al.* [2000], Miller *et al.* [2008a]). For illustration, consider the IRC located at the bottom of the upper column (Fig. 2.1). The top vapor stream from the lower column is at a higher pressure, hence, at a higher boiling point than the liquid mixture at the bottom of the upper column. In this IRC, the condensation of the top vapor from the lower column serves as the heat source for the energy transfer. The use of integrated reboiler/condensers is cost-effective, since obtaining a cooling medium for distillation columns at extreme low temperature is very expensive (Roffel *et al.* [2000]).

2.1.2 Modeling of Cryogenic Distillation Column

A typical stage-by-stage model for distillation columns consists of dynamic material and energy balances (i.e. differential equations), and algebraic equations to represent tray hydraulics, thermodynamic correlations and other physical properties. A stage-by-stage dynamic distillation model for a column of N_{tray} stages and N_{comp} components generally consists of $N_{tray} \times N_{comp}$ differential material equations and N_{tray} differential energy equations. More detail on rigorous stage-by-stage models is given in Chapter 3 of this thesis. The development of model order reduction methods has been an active research area. The reason for doing so is that the complexity of the full model imposes challenges in adopting optimization based strategies, such as the application of nonlinear model predictive control (NMPC) technology (Zhu *et al.* [2001], Bian *et al.* [2005b]). A nonlinear wave theory approach was used in Zhu *et al.* [2001], and compartmental modeling was followed in Bian *et al.* [2005b] in cryogenic distillation column applications.

Nonlinear Wave Theory

The fundamental principle underlying dynamic models for distillation columns based on nonlinear wave theory is that the concentration and/or temperature profile of a column can be approximated using constant shape wavefronts (Zhu *et al.* [2001], Kienle [2000]). One of the attractive aspects of the wave modeling approach is that the number of differential equations in the model can be one less than the number of components in the system. However, the constant wave pattern assumption is inadequate for non-ideal mixtures, and hence limits prediction accuracy (Kienle [2000], Zhu *et al.* [2001], Bian *et al.* [2005b]).

Compartmentalization

Order reduction following a compartmentalization approach is achieved by dividing a distillation column into a number of compartments, consisting of one or multiple trays. Differential equations are derived for each compartment with entering and leaving streams of the compartment to capture the dynamics of the column. Balance equations of trays within a compartment are simplified into pure algebraic equations as they have relatively faster dynamics (Bian *et al.* [2005b]). The model is still dynamic since modeling equations for the compartment are differential equations. To illustrate, consider a column compartment comprising five trays. Material and/or energy balances for the overall compartment are differential equations, but for each individual tray within the compartment, balances are algebraic (i.e. steady state balances). Detailed modeling equations are available in Bian *et al.* [2005b]. However, the prediction accuracy in dynamic simulations depends on the number of compartments selected. Moreover, the authors also observed that despite the reduced number of differential equations required in the model, it did not yield significant simulation time reduction.

2.1.3 Control of Cryogenic Air Separation Process

Typical measured variables for an air separation plant producing Ar in addition to N₂ and O₂ (Fig. 2.1) comprise:

- feed air flow rate to the system,
- air feed temperature prior to the PHX,
- turbine inlet and outlet temperatures,
- turbine air flow rate,
- purity of reflux for the lower column,
- nitrogen purity in the gas nitrogen and waste nitrogen streams,
- purity and flow rate of the gas oxygen product flow,
- purity and flow rate of the liquid oxygen product flow,
- argon column feed purity,
- as well as purity and flow rate of the argon product (Hanson [1993]).

The selection of controlled variables varies in research literature descriptions, such as pure oxygen flow rates (Huang *et al.* [2009]), product composition/purity (Bian *et al.* [2005a], Roffel *et al.* [2000]), as well as liquid levels at the column bottom and in the integrated reboiler/condenser (Roffel *et al.* [2000]). Manipulated variables that have been used in the study of advanced control procedures for air separation units of multiple products include flow rates of: total air feed, air feed to the upper column, reflux liquid nitrogen from the lower to the upper column (Roffel *et al.* [2000], Trierweiler and Engell [2000], Huang *et al.* [2009]).

Detailed control structures for air separation processes, producing multiple products, are not clearly defined in publications and may vary according to the particular plant configuration. For example, Canney [1996] controls nitrogen content in the argon product using cascade control procedure. Primary control loops for a N₂ plant (Fig. 2.2) are defined in Espie and Papageorgaki [1998]:

- column pressure is controlled by adjusting the flow rate of the waste stream;

- sump level is controlled by manipulating the flow rate of the LN₂ and drain streams;
- reboiler level is regulated using the flow rate of the stream flowing from the bottom sump to the reboiler;
- and the air feed flow rate is maintained by adjusting the inlet guide vane angle and the number of compressor stages running in the multistage compressor system.

To determine the control structure (control loop pairing), Roffel *et al.* [2000] follow the relative gain array approach, while Trierweiler and Engell [2000] introduced a robust performance number, which indicates the level of difficulty associated for a given plant to achieve a desired performance.

Besides the conventional proportional-integral-derivative (PID) control algorithm with gain scheduling, feed-forward and decoupling (Roffel *et al.* [2000]), advanced control strategies, such as model predictive control (Canney [1996]) and statistical process control (Hanson [1993]), have been applied in air separation processes. Currently, the dominating control practice in air separation processes is regulatory control in combination with linear model predictive control (MPC). Roffel *et al.* [2000] demonstrated the capability of multivariable MPC based on a linearized model on improving process dynamic performance for set point tracking (i.e. in selected product purities and liquid levels) and disturbance rejection (i.e. in selected product flow rates) up to 10 % changes compared with the conventional PI control algorithm. This study was conducted on the upper and lower columns of a multi-product air separation process. Linear control technology for air separation processes was traditionally found to be sufficient and successful as cryogenic plants experienced infrequent load changes. However, due to electricity price deregulation, frequent changes in production points are now expected. Consequently, processes nonlinearity is more noticeable and the performance of control procedures based on linear models becomes questionable (Zhu *et al.* [2001], Bian *et al.* [2005a]). This motivates the air separation processes switching to nonlinear model based control strategies, and efforts have been spent on developing nonlinear MPC for this process. Bian *et al.* [2005a] proposed nonlinear MPC (NMPC), incorporated with extended Kalman filtering, for a nitrogen purification column using the nonlinear wave

column model. The proposed controller shows promising results in rejecting disturbances in the feed flow rate. In the study of Huang *et al.* [2009], a proposed advanced step NMPC (asNMPC) following a sensitivity-based algorithm and incorporating a rigorous full column model was shown to be able to: (1) handle the nonlinear process dynamics over wide production rate changes, and (2) achieve performance close to that of a hypothetical ideal NMPC.

2.1.4 Optimization for Design and Operation of Air Separation Processes

Optimization approaches have been used in design and operational aspects for an air separation plant. Sirdeshpande *et al.* [2005] addressed the issue of determining optimal plant configurations through equipment selection (for the heat exchange, refrigeration, distillation and compression stages) and cycle flexibility analysis by solving mixed integer nonlinear programming problems. Zhu *et al.* [2010] followed a multi-scenario programming approach to obtain optimal design parameters (e.g. tray diameters of the columns and the heat transfer area of the integrated reboiler/condenser) under uniformly distributed uncertainties with steady state models. Zhu *et al.* [2006] demonstrated the usefulness of optimization approaches in improving productivity and profit of cryogenic distillation systems by operating at different operating points (e.g. production rates) with steady-state column models.

In addition to the studies discussed, there are several studies more directly related to electricity price deregulation. In the study by Miller *et al.* [2008b], effects of hourly variations in the electricity price on energy and capital cost of the plant were investigated through the use of thermodynamic ideal work, which is computed on the basis of changes in conditions between the feed and the products. An optimization approach for analyzing the switchability of an air separation column was proposed by White *et al.* [1996]. This study implemented a compartmental column model, with assumptions of constant molar overflow and constant relative volatility. Design modification of air separation processes in response to dynamic market conditions has also been evaluated. In particular, Miller *et al.* [2008a] illustrated the positive effects of introducing pre-collected liquid to the super-stage argon

column on reducing the start-up time of the plant.

2.2 Dynamic Optimization

Dynamic optimization or open-loop optimal control problems optimize dynamic system performance through obtaining optimal trajectories of a set of control variables (Feehery and Barton [1999]). Two unique characteristics of such problems in process engineering are: (1) the dynamic systems are typically represented by large sets of differential algebraic equations; (2) the problems contains path constraints, equality and/or inequality, that regulate the behavior of variables due to operation and economic considerations. In this section, we will review the general form and solution methods of dynamic optimization problems. Details on differential algebraic equations will be examined in a later section.

2.2.1 General Form

Dynamic optimization, as described by various authors (e.g. Feehery and Barton [1999] and Cervantes and Biegler [2009]), has the general form:

$$\min_{\mathbf{x}(t), \mathbf{y}(t), \mathbf{u}(t), t_f, \boldsymbol{\theta}} \phi(\mathbf{x}(t), \mathbf{y}(t), \mathbf{u}(t), t_f, \boldsymbol{\theta}) \quad (2.1)$$

subject to:

$$\dot{\mathbf{x}}(t) = \mathbf{f}(\mathbf{x}(t), \mathbf{y}(t), \mathbf{u}(t), t, \boldsymbol{\theta}) \quad (2.2)$$

$$\mathbf{h}(\mathbf{x}(t), \mathbf{y}(t), \mathbf{u}(t), t, \boldsymbol{\theta}) = \mathbf{0} \quad (2.3)$$

$$\mathbf{g}(\mathbf{x}(t), \mathbf{y}(t), \mathbf{u}(t), t, \boldsymbol{\theta}) \leq \mathbf{0} \quad (2.4)$$

with initial conditions:

$$\mathbf{x}(t_0) = \mathbf{x}_0 \quad (2.5)$$

as well as upper and/or lower bounds on the variables and point conditions when necessary. In above equations, ϕ is the objective function; \mathbf{x} and \mathbf{y} are time-dependent differential and algebraic variables; \mathbf{u} is the vector of control variables; and $\boldsymbol{\theta}$ comprises time-invariant parameters.

2.2.2 Solution Strategies

Dynamic optimization problems can be solved either by variational/indirect methods or direct methods, which require certain levels of discretization and application of nonlinear programming solvers (Biegler *et al.* [2002]). Based on the level of discretization, the direct methods can be further divided into several sub-categories. A common way to classify the direct methods are: direct simultaneous method, direct sequential method and multiple shooting (Biegler and Grossmann [2004]).

The theory for indirect/variational methods was initially developed as early as late 1600s to mid 1700s, with a major development in 1962 – Pontryagin’s maximum principle (Cervantes and Biegler [2009]). This approach solves first-order necessary conditions for optimality. According to Biegler and Grossmann [2004] and Cervantes and Biegler [2009], obtaining solutions following this approach is troublesome and prohibitively expensive as it leads to systems of differential equations with split boundary conditions (two-point boundary value problems). Single shooting, invariant embedding and so forth are strategies that can be used to solve such boundary value problems. Details are available in many studies (e.g. Cervantes and Biegler [2009]). In addition to the solution challenges of the resulting boundary problem, another drawback of this approach is that it is inefficient for constrained problems, especially in handling active inequality constraints (Biegler [2007], Cervantes and Biegler [2009]).

Direct methods for dynamic optimization have been successfully employed in many complex applications, and are capable of handling models of ordinary differential equations (ODEs), differential algebraic equations (DAEs) and partial differential algebraic equations (Chachuat [2009]). Regardless the exact procedure, control vector parameterization (CVP) is required in all the direct approaches. The principle of CVP involves subdividing the optimization horizon into a number of control stages, and approximating control variable profiles by functions of specified structure characterized by a finite number of parameters such as piecewise constant, piecewise linear or polynomial functions (Biegler and Grossmann

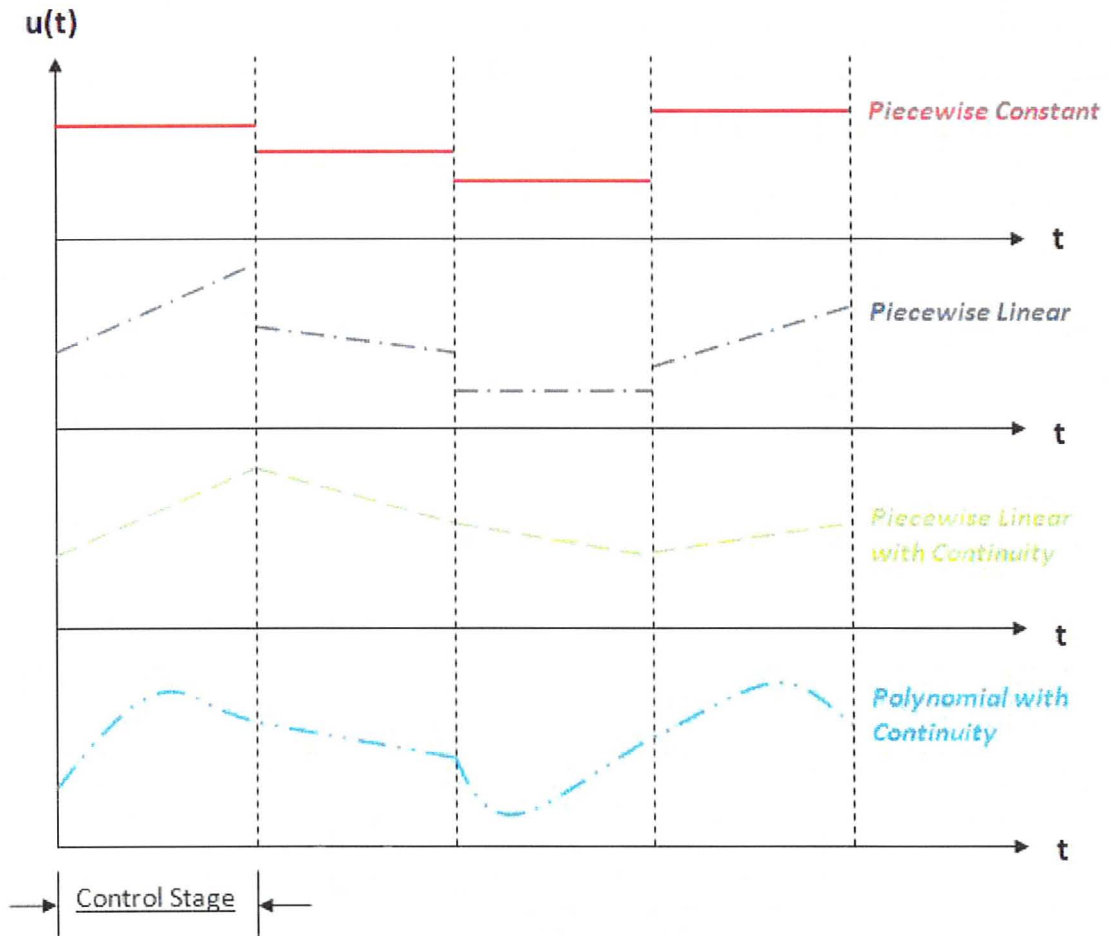


Figure 2.3: Example control variable profiles for control vector parameterization, adapted from Chachuat [2009] and Biegler [2007].

[2004], Chachuat [2009]). Some control vector parameterization examples are presented in Fig. 2.3. Control bounds and control continuity among stages can be enforced as well. The main difference among subgroups of the direct method is in terms of handling the ordinary differential equations.

Direct Simultaneous Methods

Direct simultaneous, also known as full discretization methods, reformulate the problem into a finite-dimensional nonlinear programming (NLP) problem through not only CVP,

but also discretization of state variables (Biegler and Grossmann [2004]). For illustration, application of the implicit (backward) Euler method to the ODE:

$$\frac{dx(t)}{dt} = f(x(t)) \quad (2.6)$$

gives

$$\frac{x(t_j) - x(t_{j-1})}{\delta} = f(x(t_j)), \quad j = 1, \dots, N \quad (2.7)$$

where δ is the time discretization interval; the set of t_j are discretization points. Following this approach, the original DAE problem is transformed into a system of algebraic equations only.

Another alternative is using the collocation method. The collocation method is derived based on the principle of approximating dependent variables with functions of specified structures (typically polynomials) in the independent variable, and requiring that the model equations be satisfied at selected collocation points. The trajectory is represented by a family of polynomials. To illustrate, Fig 2.4 shows the profile of dependent variable x that solves the ODE,

$$\frac{dx}{dt} = f(x(t)), \quad x(0) = x_0. \quad (2.8)$$

The trajectory in the first discretization stage can be approximated using a polynomial of degree n , using the independent variable t ,

$$\hat{x} = x_0 + a_1 t + a_2 t^2 + \dots + a_n t^n \quad (2.9)$$

This polynomial has zero or negligible errors at the collocation points, t_1^1, \dots, t_n^1 (Huss and Westerberg [1996]).

Discretizations of control and state variables do not need to be at the same accuracy level, as show in Fig. 2.3. Basic characteristics of direct simultaneous methods are (1) the model solution and optimization are executed at the same time, and the DAE system is solved only once, at the optimum; (2) path constraints are only enforced directly at each collocation point (Biegler and Grossmann [2004], Biegler [2007], Cervantes and Biegler [2009]).

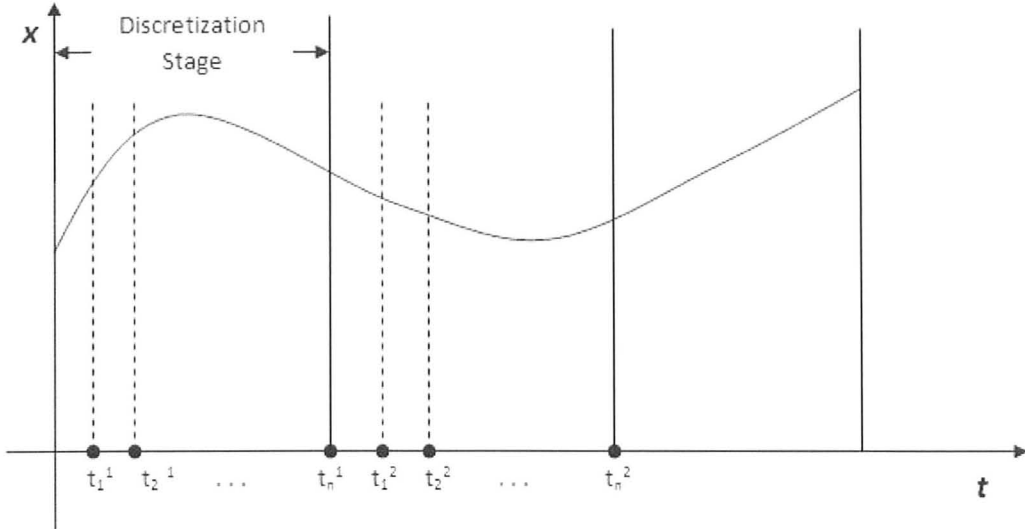


Figure 2.4: Example collocation, as depicted in Biegler [2007]. Black dots denote the collocation points.

Direct Sequential Methods

Direct sequential methods discretize only the control variables while maintaining the set of ordinary differential equations. Hence, they are also referred to as “single shooting” or partial discretization methods (Biegler and Grossmann [2004], Cervantes and Biegler [2009]). In contrast to the simultaneous approach, direct sequential methods are feasible path methods. This means that given the initial conditions and a control input profile, the DAE system is solved at each iteration with a differential algebraic equation solver. Based on the resulting objective function value, the NLP solver determines the optimal values of the control parameters. In other words, the sequential methods follow the repeated routine of integration and optimization until the solution converges. The necessary gradient information for NLP solvers can be obtained from evaluating sensitivity equations or adopting an adjoint method (Biegler and Grossmann [2004]). Path constraints may be handled indirectly by defining dummy variables to track accumulated constraint violations over the entire horizon, and then regulating the final value of the dummy variable through end-point inequality constraints or penalization in the objective function (Biegler and Grossmann [2004]).

Multiple Shooting

Multiple shooting is a combination of direct simultaneous and direct sequential methods. This method discretizes only the control variables, but discontinuities in state variables are allowed at each stage time. Instead of integrating over the entire optimization horizon, the DAE system is integrated separately in each control stage at each iteration. Initial conditions of state variables at each stage time together with the control parameters define the complete decision variable space (Biegler and Grossmann [2004], Biegler [2007]). To ensure that the final solution satisfies the original DAE system, continuity of state variables between conjoint control stages is enforced through imposing equality constraints at each stage boundary time. Gradient information and path constraints are handled in the same way as with the sequential methods.

Table 2.1 summarizes the advantages and disadvantages of the different solution methods.

2.3 Differential Algebraic Equations

As described in many publications, dynamic models of chemical processes often give rise to sets of differential algebraic equations (DAEs): differential equations typically originate from dynamic material, energy and momentum balances, while algebraic equations arise from thermodynamic correlations, kinetic relations and such (e.g. Gani and Cameron [1992], Unger *et al.* [1995], Feehery and Barton [1999]). Hence, it is important to have a brief understanding about the mathematical structure and numerical solution of DAE systems. We will start with a discussion of ordinary differential equations (ODEs).

2.3.1 Ordinary Differential Equations

Heath [2002] defines an ODE as a relation that has only one independent variable (e.g. time) and contains derivatives of dependent variables with respect to that independent variable

Table 2.1: Advantages and disadvantages of direct solution methods (Biegler and Grossmann [2004], Cervantes and Biegler [2009], Chachuat [2009]).

	Direct Simultaneous	Direct Sequential	Multiple Shooting
Pros	<ul style="list-style-type: none"> • infeasible path method: (1) suitable for unstable system; (2) avoids nonexistent or computationally expensive intermediate solutions — save computation effort • directly handles constraints • duration time of subintervals can be optimized 	<ul style="list-style-type: none"> • relatively low dimension nonlinear programming (NLP) problems • accurate solutions for the differential equations • duration time of subintervals can be optimized 	<ul style="list-style-type: none"> • intermediate size NLP • sequential infeasible path method: reliable for optimization of unstable systems and efficient error control • permits parallelization
Cons	<ul style="list-style-type: none"> • very large scale NLP problems • constraints are enforced only at collocation points • placement of the finite elements and the collocation points affects solution and has to be pre-determined 	<ul style="list-style-type: none"> • difficult to handle path constraints • computationally demanding due to integration at each iteration • for unstable systems, finding feasible solutions is challenging 	<ul style="list-style-type: none"> • difficult to handle path constraints

such as:

$$x' = x \quad (2.10)$$

The solution of an initial value problem such as:

$$x' = x, \quad x(0) = 1 \quad (2.11)$$

can be approximated by different numerical methods. According to Ascher and Petzold [1998], these methods are classified as:

- basic methods, where approximate solutions have relatively low accuracies. Examples are
 - Euler method: forward Euler and backward Euler
 - Trapezoidal method
- high-order methods
 - one step methods: Taylor series method and Runge-Kutta method
 - linear multi-step methods: Adams method family and backward differentiation formulas (BDF)

The classic Runge-Kutta method for

$$x' = f(t, x), \quad x(t_0) = x_0 \quad (2.12)$$

has the form of

$$x_{n+1} = x_n + \frac{1}{6}h(k_1 + 2k_2 + 2k_3 + k_4), \quad t_{n+1} = t_n + h \quad (2.13)$$

where

$$k_1 = f(t_n, x_n) \quad (2.14)$$

$$k_2 = f\left(t_n + \frac{1}{2}h, x_n + \frac{1}{2}hk_1\right) \quad (2.15)$$

$$k_3 = f\left(t_n + \frac{1}{2}h, x_n + \frac{1}{2}hk_2\right) \quad (2.16)$$

$$k_4 = f(t_n + h, x_n + hk_3) \quad (2.17)$$

The example in Eqn. 2.11 solved with the classic Runge-Kutta method, with a step size of 1 for $t = 1$ gives:

$$x(1) = 1 + \frac{1}{6}[1 + 2(1.5) + 2(1.75) + 2.75] = 2.708$$

Exact forms of other solution methods can be found in texts such as Ascher and Petzold [1998] and Heath [2002].

2.3.2 Mathematical Structure and Index of Differential Algebraic Equations

A DAE system differs from an ODE system due to the presence of algebraic equations, and can be described as:

$$\mathbf{x}' = \mathbf{f}(\mathbf{x}, \mathbf{y}, t) \quad (2.18)$$

$$\mathbf{0} = \mathbf{g}(\mathbf{x}, \mathbf{y}, t) \quad (2.19)$$

A typical way to classify a DAE system is based on its index, which is commonly defined as the minimum number of differentiations of the algebraic equations undertaken to transform a DAE system to a system of ODEs (Ascher and Petzold [1998], Hangos and Cameron [2001]). The index may also be considered to indicate the level of difficulty to obtain the numerical solution for a DAE system. Using an example in Hangos and Cameron [2001]:

$$x_1' = x_1 + x_2 + y_1$$

$$x_2' = x_1 - x_2 - y_1$$

$$y_1 = x_1 + 2x_2$$

the expression of y_1' can be obtained by simply differentiating the algebraic equation

$$y_1' = x_1' + 2x_2' = 3x_1 - x_2 - y_1$$

Only one differentiation is required to transform the system to a set of ODEs, so the system is index 1. However, if we replace the algebraic equation in the above example using

$$0 = x_1 + 2x_2$$

differentiating this expression one time gives:

$$0 = x'_1 + 2x'_2 = 3x_1 - x_2 - y_1$$

Note that the system is still in the form of a set of DAEs, hence, we need to differentiate it again

$$0 = 3x'_1 - x'_2 - y'_1 \Rightarrow y'_1 = 2x_1 + 4x_2 + 4y_1$$

This implies that the index of the modified system is 2. High-index systems typically refer to sets of DAEs having index greater than 1. For a DAE system to be index 1, we require the Jacobian of the algebraic set to be full rank (Hangos and Cameron [2001]). In other words,

$$\mathbf{g}_y = \left(\frac{\partial \mathbf{g}}{\partial \mathbf{y}} \right) \quad (2.20)$$

has to be non-singular, since then we can then differentiate Eqn. 2.19 and solve for y' as

$$\mathbf{y}' = -\mathbf{g}_y^{-1} \mathbf{g}_x \mathbf{f}(\mathbf{x}, \mathbf{y}, t) \quad (2.21)$$

Returning to the example shown previously, the Jacobian of the algebraic expression for the original and modified systems are

$$J_1 = [-1], \quad J_2 = [0]$$

Gani and Cameron [1992] identified three factors leading to high-index problems in process modeling:

- choice of specified (design) variables,
- use of forcing functions, and
- modeling issues.

They concluded that satisfying the overall degrees of freedom of the system does not guarantee consistent modeling and avoiding high-index problems. Furthermore, in this study, the use of the structure incidence matrix of a DAE system was proposed to aid specification selections and detect the presence of high-index problems. An incidence matrix is a matrix

that shows that the relation between equations and unknowns, and consists of one row for each equation and one column for every unknown. More detail can be found in Gani and Cameron [1992] and Hantos and Cameron [2001].

2.3.3 Numerical Solution

In general, high-index DAEs are more challenging to solve due to hidden constraints, resulting from algebraic equation differentiations (Costa Jr. *et al.* [2003]). Also, analysis in Ascher and Petzold [1998] illustrates that high-index systems (i.e. index > 1) have many practical problems such as stability restrictions and determining a consistent set of initial conditions. Numerical methods for handling index-1 DAE systems are well-established, but not for high-index systems (Gani and Cameron [1992]). Conventional ODE methods can be employed generally to solve index-1 systems; however, applying these method to a high-index system may result in poor convergence, convergence failure or converging to wrong solutions (Unger *et al.* [1995], Hantos and Cameron [2001]). Ascher and Petzold [1998] classified solution strategies for high-index systems into two categories:

Index Reduction by Reformulation

This method requires performing symbolic manipulations to reduce the index to 1 or ODEs prior to solving the problem numerically (Unger *et al.* [1995] provide more detail on this approach). The major drawback of this approach is that depending on the size and complexity of the original high-index problem, performing the reformulation can be very costly. An index reduction procedure for an index-2 distillation model can be found in Chapter 3 of this thesis.

Direct Approach

Methods such as Backward differentiation formulas, Runge-Kutta and extrapolation methods belong to the direct approach category. Unger *et al.* [1995] and Ascher and Petzold [1998] point out that applications of these methods are limited to high-index systems of certain structures.

Chapter 3

Mathematical Model

This chapter will outline the mathematical model developed for a nitrogen plant. Fig. 2.2 shows a simplified schematic of major process equipment in a typical nitrogen plant. Espie and Papageorgaki [1998] and Zhu *et al.* [2001] provide a detailed process description. The intake air from the atmosphere is first compressed through a multi-stage compressor and then introduced to an adsorber or other purification units to remove impurities such as carbon dioxide and water. The treated air feed is cooled against the returning gas product stream and waste stream from the distillation column in a multi-path heat exchanger. A portion of the air feed is withdrawn at an intermediate point of the heat exchanger and goes through a turbine for additional cooling prior to being introduced to the column. The air feed, entering at the bottom of the column, is distilled into a high purity nitrogen stream, which leaves at the top, and the liquid crude oxygen stream, which accumulates at the bottom. A portion of the overhead stream is withdrawn as the gas product while the rest is sent to the integrated reboiler/condenser to exchange heat with the crude oxygen stream drawn from the bottom to produce the reflux stream and the liquid nitrogen product.

The integrated plant model presented comprises both first principles and empirical models. Models for the cryogenic distillation column with integrated reboiler/condenser and the primary heat exchanger are systems of differential algebraic equations (DAEs). Man-

ual index reduction was performed to reduce the high index column model to an index-1 DAE system. The compressor and turbine models are empirical and are based on available compressor maps and plant data. To improve the model robustness when solving with gPROMS, necessary equation scaling was performed after investigating the problem report generated by gPROMS. Then, individual unit models were assembled in accordance with the plant configuration. Parameter estimation was performed using gPROMS with the integrated plant model to obtain values of unknown model parameters and reconcile the model with available plant measurements.

3.1 Physical Property Estimation

This section documents important correlations used to estimate physical properties. The vapor-liquid phase equilibrium correlation is used primarily in the distillation model to represent the phase equilibrium at each column tray and the reboiler side of the integrated reboiler/condenser. The correlation for approximating the vapor phase molar density is used in every individual unit model of the integrated plant. Estimations of the vapor compressibility factor are required in the compressor and the turbine model. In the primary heat exchanger (PHX) model, as well as the column model, the liquid phase molar density has to be computed. The value of liquid surface tension has to be obtained for each column tray, and is used to compute the flooding velocity.

3.1.1 Vapor-Liquid Phase Equilibrium (VLE)

Vapor-liquid phase equilibrium is captured by the modified Raoult's Law and the Antoine equation (Smith *et al.* [2005]):

$$y_i = K_i x_i \quad (3.1)$$

$$K_i = \frac{\gamma_i P_i^{sat}}{P} \quad (3.2)$$

$$\ln(P_i^{sat}) = A_i + \frac{B_i}{T + C_i} \quad (3.3)$$

The non-idealities in the thermodynamics can be accurately represented using non-ideal physical property models, such as the Wilson equation and the modified Margules equation for component activity coefficients (Bansal *et al.* [2000], Georgiadis *et al.* [2002]). In this model, the two-suffix Margules equation for multicomponent systems is used (Reid *et al.* [1977]). For a system with NC components:

$$R_{gas}T \ln(\gamma_i) = \sum_{j=1}^{NC} \sum_{k=1}^{NC} \left(A_{ji}^{Margules} - \frac{1}{2} A_{jk}^{Margules} \right) x_j x_k \quad (3.4)$$

In the above equations:

K_i = vapor/liquid equilibrium ratio for component i

y_i, x_i = mole fraction of component i in vapor and liquid phases

P = pressure

T = temperature

R_{gas} = universal gas constant

P_i^{sat} = saturated vapor pressure of component i at temperature T

γ_i = activity coefficient of component i

A_i, B_i, C_i = Antoine parameters for component i

$A_{ij}^{Margules}$ = Margules interaction parameters between components i and j .

Note that values of $A_{ij}^{Margules}$ and $A_{ji}^{Margules}$ are identical, and $A_{ii}^{Margules}$ is zero. Values of these parameters should be applicable to the system under consideration. In this case, they were supplied by Praxair, Inc.

3.1.2 Vapor Phase Compressibility Factor and Molar Density

In order to obtain accurate approximations for vapor phase compressibility and molar density of a gas mixture, the Peng-Robinson equation of state is used (Peng and Robinson [1976], Infochem Computer Services Ltd [2008]):

$$P = \frac{R_{gas}T}{V_m - b} - \frac{a}{V_m(V_m + b) + b(V_m - b)} \quad (3.5)$$

with

$$b = \sum_{i=1}^{NC} x_i b_i \quad (3.6)$$

$$b_i = \frac{0.0778 R_{gas} T_i^c}{P_i^c} \quad (3.7)$$

$$a = \sum_{i=1}^{NC} \sum_{j=1}^{NC} x_i x_j (a_i a_j)^{1/2} (1 - k_{ij}) \quad (3.8)$$

$$a_i = \frac{R_{gas}^2 (T_i^c)^2}{P_i^c} \left\{ 1 + f(\omega_i) \left[1 - \left(\frac{T}{T_i^c} \right)^{1/2} \right] \right\}^2 \quad (3.9)$$

$$f(\omega_i) = 0.37464 + 1.54226\omega_i - 0.26992\omega_i^2 \quad (3.10)$$

where:

V_m = molar volume

k_{ij} = binary interaction parameters between components i and j

ω_i = acentric parameter of component i

P_i^c, T_i^c = critical pressure and temperature of component i

Note that x_i denotes the mole fraction of component i in the mixture, which in this case corresponds to the vapor phase mole fraction. Then, with the molar volume computed from Eqn. 3.5, the compressibility factor, Z , and the molar density of the gas mixture are estimated

$$Z = \frac{PV_m}{R_{gas}T} \quad (3.11)$$

$$\rho = \frac{1}{V_m} \quad (3.12)$$

Values of k_{ij} , ω_i , P_i^c and T_i^c were supplied by Praxair, Inc.

3.1.3 Liquid Phase Molar Density

The liquid mixture molar density, ρ^{liq} , is approximated using a simple and precise correlation, the Rackett equation (described in Green *et al.* [1997]), to reduce the complexity of

the model.

$$\ln\left(\frac{1}{\rho_i^{liq}}\right) = \ln\left(\frac{R_{gas}T_i^c}{P_i^c}\right) + \left[1 + \left(1 + \frac{T}{T_i^c}\right)^{2/7}\right] \ln(Z_i^{Ra}) \quad (3.13)$$

$$\rho^{liq} = \sum_{i=1}^{NC} x_i \rho_i^{liq} \quad (3.14)$$

where Z_i^{Ra} is Rackett compressibility factor of component i and is a constant in the system. The value of Z_i^{Ra} was obtained from Green *et al.* [1997]. Predictions from the Rackett equation have been compared with results from simulation software. As no or negligible differences were observed, it was concluded that the predictions are sufficiently accurate.

3.1.4 Liquid Phase Surface Tension

As documented in Reid *et al.* [1977] and Infochem Computer Services Ltd [2008], the surface tension of a liquid mixture can be computed from the pure component parachors using the Macleod-Sugden correlation:

$$\sigma^{1/4} = \sum_i^{NC} [P_i](\rho^{liq}x_i - \rho^{vap}y_i) \quad (3.15)$$

where σ is surface tension of a liquid mixture and $[P_i]$ is the parachor of component i . Values of the component parachors were obtained from the pure component databank of Multiflash 3.8 for gPROMS.

3.2 Distillation Column Tray

In this section, we will describe the dynamic distillation model under assumptions:

- Ternary column with components: nitrogen, oxygen and argon.
- Negligible vapor holdup. Roffel *et al.* [2000] showed that in low temperature, high pressure columns, vapor holdups do not have a significant impact on the process dynamics.

- Perfect mixing and saturated liquid on each tray.
- Sieve tray. No packing.
- Vapor and liquid air feed to the column are introduced at different locations.
- Heat leakage between the cold box and the ambient surrounding occurs at each column tray. Values of the product of heat transfer coefficient and effective heat transfer area for heat leakage, $UA_{leakage}$, at each tray are identical and constant.

3.2.1 General Approach

General approaches of modeling distillation columns are outlined by various authors, such as Roffel *et al.* [2000], Bansal *et al.* [2002] and Miller *et al.* [2008a]. Each of these studies has different emphases on or assumptions made for different aspects of the column. In this study, component and energy balances are expressed as differential equations at each tray. Vapor-liquid phase equilibrium, thermodynamics and hydraulic models are in the form of algebraic equations. This results in the general column model being formulated as a differential algebraic equation (DAE) system. A schematic representation of a general column tray n is shown in Fig. 3.1. The tray number is assigned from the bottom of the column.

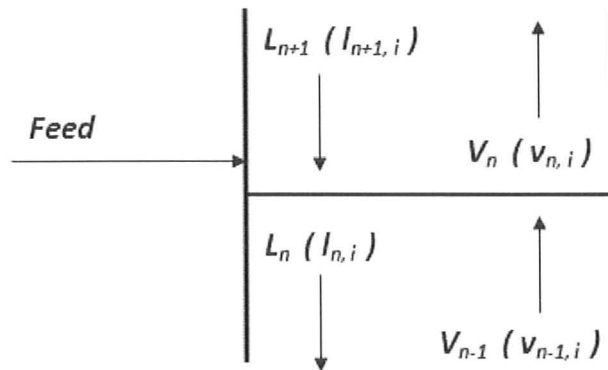


Figure 3.1: Schematic representation of a column tray.

Material Balances

At column tray n ($1 \leq n \leq N_{tray}$), for each component i :

$$\frac{dm_{n,i}}{dt} = l_{n+1,i} + v_{n-1,i} - l_{n,i} - v_{n,i} + \begin{cases} z_i F_{vap}, & \text{vapor feed tray;} \\ z_i F_{liq}, & \text{liquid feed tray;} \\ x_i^{cond} F_{reflux}, & \text{reflux tray;} \\ 0, & \text{other column tray;} \end{cases} \quad (3.16)$$

where:

$m_{n,i}$ = molar holdup of component i at tray n

$l_{n,i}, v_{n,i}$ = liquid and vapor molar flow rates of component i leaving tray n

z_i = mole fraction of component i in the feed

$F_{vap}, F_{liq}, F_{reflux}$ = molar flow rate of the vapor and the liquid feed and reflux

x_i^{cond} = mole fraction of component i in the reflux

Note that $v_{0,i}$ and $l_{N_{tray}+1,i}$ are outside the range and take values of zero.

Energy Balances

At column tray n ($1 \leq n \leq N_{tray}$):

$$\frac{dE_n}{dt} = H_{n+1}^{liq} + H_{n-1}^{vap} - H_n^{liq} - H_n^{vap} + Q_n^{leakage} + \begin{cases} H_{feed}^{vap}, & \text{vapor feed tray;} \\ H_{feed}^{liq}, & \text{liquid feed tray;} \\ H_{reflux}, & \text{reflux tray;} \\ 0, & \text{other column tray;} \end{cases} \quad (3.17)$$

with

$$E_n = M_n h_n^{liq \text{ mix}} \quad (3.18)$$

$$H_n^{liq} = L_n h_n^{liq \text{ mix}} \quad (3.19)$$

$$H_n^{vap} = V_n h_n^{vap \text{ mix}} \quad (3.20)$$

$$Q_n^{leakage} = U A_{leakage} (T_{ambient} - T_n) \quad (3.21)$$

$$H_{reflux} = F_{reflux} h_{reflux}^{liq\ mix} \quad (3.22)$$

$$H_{feed}^{vap} = F_{vap} h_{feed}^{vap\ mix} \quad (3.23)$$

$$H_{feed}^{liq} = F_{liq} h_{feed}^{liq\ mix} \quad (3.24)$$

$$h_{-}^{liq\ mix} = \sum_{i=1}^{NC} x_{-,i} h_{-,i}^{liq} \quad (3.25)$$

$$h_{-}^{vap\ mix} = \sum_{i=1}^{NC} y_{-,i} h_{-,i}^{vap} \quad (3.26)$$

In the above equations:

E_n = total energy holdup at tray n

M_n = total molar holdup at tray n

H_n^{liq} , H_n^{vap} = total enthalpy in the liquid and vapor flows leaving tray n

L_n , V_n = total molar flow rate of liquid and vapor phase streams leaving tray n

$Q_n^{leakage}$ = heat transferred between the ambient and the tray

H_{feed}^{liq} , H_{feed}^{vap} = molar flow rate of the liquid and the vapor feed

H_{reflux} = total enthalpy of the reflux stream

$UA_{leakage}$ is the product of heat transfer coefficient and effective heat transfer area for heat leakage. Note that H_0^{vap} and $H_{N_{tray}+1}^{liq}$ are outside the range and take values of zero. Also, in the feed, reflux or at tray n :

$x_{-,i}$, $y_{-,i}$ = mole fraction of component i in liquid and vapor phase

$h_{-}^{liq\ mix}$ and $h_{-}^{vap\ mix}$ = the molar enthalpy of liquid and vapor mixtures

$h_{-,i}^{liq}$ and $h_{-,i}^{vap}$ = the component liquid and vapor phase molar enthalpy

In the feed stream, we have $x_{feed,i} = y_{feed,i} = z_i$.

The vapor phase component molar enthalpy is temperature and pressure dependent. For pressure within a range (P_{j-1} , P_j], the vapor phase molar enthalpy for component i can be approximated as:

$$h_{-,i}^{vap} = a_{j,i}^{vap} + b_{j,i}^{vap} T_- \quad (3.27)$$

Procedures taken for handling this discontinuity are discussed in detail in Appendix A. The liquid phase component molar enthalpy is mainly temperature dependent and is approximated as linear functions of temperature:

$$h_{-,i}^{liq} = a_i^{liq} + b_i^{liq}T_- \quad (3.28)$$

The coefficients $a_{j,i}^{vap}$, a_i^{liq} , $b_{j,i}^{vap}$ and b_i^{liq} in the above equations are provided by our industrial partner. In the component molar enthalpy calculation, T_- denotes the temperature in the feed, reflux or at column tray n , etc.

Mole Fractions Normalization

At column tray n ($1 \leq n \leq N_{tray}$):

$$\sum_{i=1}^{NC} x_{n,i} = \sum_{i=1}^{NC} y_{n,i} = 1 \quad (3.29)$$

$$l_{n,i} = x_{n,i}L_n \quad (3.30)$$

$$v_{n,i} = y_{n,i}V_n \quad (3.31)$$

$$\frac{m_{n,i}}{M_n} = \frac{l_{n,i}}{L_n} \quad (3.32)$$

Tray Hydraulics

The Francis Weir equation of the form

$$M_n = A_s \rho_n^{liq} \left[H_{weir} + 1.41 \left(\frac{L_n}{\sqrt{g} \rho_n^{liq} L_{weir}} \right)^{2/3} \right] \quad (3.33)$$

is used to represent the tray hydraulics (Prokopakis and Seider [1983], Cho and Joseph [1983]). A_s is the cross-sectional area of the tray, H_{weir} and L_{weir} are the height and the length of the weir and g is the gravitational constant.

Vapor-Liquid Phase Equilibrium

As discussed in Section 3.1.1, the vapor-liquid phase equilibrium in this study is captured by the modified Raoult's Law

$$y_{n,i}^{equil} = K_{n,i}x_{n,i}$$

The vapor pressure of each component is approximated using the Antoine equation (Eqn. 3.3) and the activity coefficient approximated using the Margules equation (Eqn. 3.4) with the temperature of tray n . $y_{n,i}^{equil}$ is the vapor phase equilibrium molar fraction of component i at tray n . Use of the Murphree tray efficiency gives

$$y_{n,i} = y_{n-1,i} + \eta_n(y_{n,i}^{equil} - y_{n-1,i}) \quad (3.34)$$

where η_n is the Murphree efficiency of tray n . The Murphree tray efficiency is introduced to account for the tray nonideality (Lockett [1986], Georgiadis *et al.* [2002], Bansal *et al.* [2002]). Since there is no vapor stream flow to the bottom tray from below, the vapor and liquid at bottom tray are assumed to be at equilibrium. This implies $\eta_1 = 1$ ($y_{0,i}$ does not exist). For the remainder of the column, it was assumed that η_n equals to η_{spec} . In this study, η_{spec} is selected so that the impurity level predicted by the model matches the measured value.

Pressure Profile

It was assumed that the top tray pressure is the same as that on the condenser side of the integrated reboiler/condenser (i.e. P_{cond}). Also, the pressure drop across each tray, ΔP , is assumed to be uniform and a function of the flow rate of the vapor air to the column, F_{vap} .

$$P_{Ntray} = P_{cond} \quad (3.35)$$

$$P_n = P_{n-1} + \Delta P, \quad n = 1, \dots, N_{tray} - 1 \quad (3.36)$$

$$\Delta P = f(F_{vap}) \quad (3.37)$$

Vapor Velocity

The vapor velocity at each tray can be calculated using the vapor molar flow rate and molar density of the vapor mixture at each tray (Bansal *et al.* [2002]):

$$vel_n = \frac{V_n}{\rho_n^{vap} A_a} \quad (3.38)$$

where vel_n is the vapor velocity at tray n and A_a is the active area of a tray. ρ_n^{vap} is the vapor phase molar density at tray n , which is approximated using Peng-Robinson equation

of state (Eqn. 3.5).

Flooding Velocity

When vapor flow relative to the liquid load exceeds the column capacity, flooding will occur. This phenomenon imposes a critical restriction on the column performance (Lockett [1986]). In this study, the flooding velocity for each tray is calculated following the procedure summarized in Lockett [1986]:

$$vel_n^{flooding} = CF_n' \left[\frac{\tilde{\rho}_n^{liq} - \tilde{\rho}_n^{vap}}{\tilde{\rho}_n^{vap}} \right]^{0.5} \quad (3.39)$$

where

$$CF_n' = CF_n'' \left(\frac{\sigma_n}{20 \times 10^{-3}} \right)^{0.2} \left(\frac{\phi}{0.1} \right)^{0.44} \quad (3.40)$$

$$CF_n'' = (0.0744T_s + 0.0117) (\log FP_n^{-1}) + 0.0304T_s + 0.0153 \quad (3.41)$$

$$FP_n = \frac{\tilde{M}_n^{liq}}{\tilde{M}_n^{vap}} \left(\frac{\tilde{\rho}_n^{vap}}{\tilde{\rho}_n^{liq}} \right)^{0.5} \quad (3.42)$$

where the variables and corresponding units are defined as

$vel_n^{flooding}$ = flooding velocity (m/s)

CF_n', CF_n'' = capacity factors (m/s)

σ_n = surface tension of the liquid mixture (N/m)

FP_n = flow parameter

$\tilde{\rho}_n^{liq}, \tilde{\rho}_n^{vap}$ = mass density of liquid and vapor mixtures (kg/m³)

$\tilde{M}_n^{liq}, \tilde{M}_n^{vap}$ = liquid and vapor mass flow rate (kg/s)

T_s = tray spacing (m)

ϕ = fractional perforated tray area

The correction factor for fractional tray open area $\left(\frac{\phi}{0.1} \right)^{0.44}$ in Equation 3.40 is only required when $\phi < 0.1$. Also, if the value of FP_n is calculated to be less than 0.1, it is assigned to the value of 0.1 (Lockett [1986]). The surface tension of a liquid mixture is approximated with the pure component parachors using the Macleod-Sugden correlation (Eqn. 3.15). The liquid density can be computed from the Rackett equation (Eqn. 3.13 and Eqn. 3.14).

For tracking the flooding in the column, fractional flooding is computed at each tray:

$$\alpha_n^{flooding} = \frac{vel'_n}{vel_n^{flooding}} \quad (3.43)$$

where vel'_n is the vapor velocity in the same units as $vel_n^{flooding}$. If there is no flooding at tray n , $\alpha_n^{flooding} < 1$.

3.2.2 Index Reduction

The index of a DAE system indicates how many times the system has to be differentiated with respect to time to convert it to a set of ordinary differential equations as defined earlier in Section 2.3. High-index DAE systems are more challenging to solve and require specific methods. Such systems tend to be very sensitive to input changes; according to Fikar *et al.* [1999], only those only inputs having continuous time derivatives can be accepted. In addition, high-index DAEs have hidden constraints as shown previously by the example in Section 2.3. These issues are problematic not only during initialization but also while integrating over time. A common approach to handling high-index DAE systems is to reformulate them as index-1 DAE problems (Fikar *et al.* [1999], Costa Jr. *et al.* [2003]).

The dynamic distillation model formulation described in Section 3.2.1 constitutes a high-index DAE system. This is known to be mainly due to the assumption of negligible vapor holdup, so that the vapor phase molar flow rate, V_n , cannot be determined directly from the set of equations summarized in Section 3.2.1 (Biegler [2000], Raghunathan *et al.* [2004], Huang *et al.* [2009]). The structural analysis in gPROMS indicates that the index of the system is 2. Our experience with the model in this high-index form is consistent with expectations: (1) difficult initialization; (2) low model robustness.

In order to reduce the index of the system, model reformulation was performed. The general idea is to derive a mathematically equivalent algebraic expression for the left hand side of the energy balance (i.e. $\frac{dE_n}{dt}$ in Eqn. 3.17). Key equations involved in the index reduction procedure are the VLE correlations. A similar approach has been adopted in other

studies involving distillation column modeling (Ballard *et al.* [1978], Raghunathan *et al.* [2004], Huang *et al.* [2009]).

Recall that the total energy holdup at tray n , E_n , in $\frac{dE_n}{dt}$ is defined in Eqn. 3.18 as

$$E_n = M_n h_n^{liq\ mix}$$

Differentiating and applying the chain rule gives:

$$\frac{dE_n}{dt} = M_n \left[\frac{\partial h_n^{liq\ mix}}{\partial T_n} \cdot \frac{dT_n}{dt} + \sum_{i=1}^{NC} \left(\frac{\partial h_n^{liq\ mix}}{\partial x_{n,i}} \cdot \frac{dx_{n,i}}{dt} \right) \right] + h_n^{liq} \cdot \frac{dM_n}{dt} \quad (3.44)$$

Hence, to obtain an equivalent algebraic expressions for $\frac{dE_n}{dt}$, we need to derive expressions for $\frac{dT_n}{dt}$, $\frac{dx_{n,i}}{dt}$ and $\frac{dM_n}{dt}$.

Derivations of Temperature Time Derivative Expressions

To determine the expression for $\frac{dT_n}{dt}$, we need to revisit the VLE model (Section 3.1.1). At each tray, differentiating and applying the chain rule to

$$\sum_{i=1}^{NC} K_{n,i} x_{n,i} = 1$$

results in

$$\sum_{i=1}^{NC} \left(\frac{dK_{n,i}}{dt} x_{n,i} + \frac{dx_{n,i}}{dt} K_{n,i} \right) = 0 \quad (3.45)$$

In this study (pressure profile description in Section 3.2.1), P_n is defined by the condition of the IRC and the feed flow rate, rather than T_n . From the Modified Raoult's Law and Antoine equation, we have that:

$$\frac{dK_{n,i}}{dt} = \frac{\gamma_{n,i}}{P_n} \frac{\partial P_{n,i}^{sat}}{\partial T_n} \frac{dT_n}{dt} + \frac{P_{n,i}^{sat}}{P_n} \left(\frac{\partial \gamma_{n,i}}{\partial T_n} \frac{dT_n}{dt} + \sum_{j=1}^{NC} \frac{\partial \gamma_{n,i}}{\partial x_{n,j}} \frac{dx_{n,j}}{dt} \right) + \left(-\frac{\gamma_{n,i} P_{n,i}^{sat}}{P_n^2} \right) \frac{dP_n}{dt} \quad (3.46)$$

Expressions of $\frac{\partial P_{n,i}^{sat}}{\partial T_n}$, $\frac{\partial \gamma_{n,i}}{\partial T_n}$ and $\frac{\partial \gamma_{n,i}}{\partial x_{n,j}}$ can be derived from the Antoine and Margules equations. After rearranging terms in Eqn. 3.46, an expression of $\frac{dT_n}{dt}$ can be obtained:

$$\begin{aligned}
 f_T = \frac{dT_n}{dt} &= \frac{\sum_{i=1}^{NC} \left[K_{n,i} \frac{dx_{n,i}}{dt} + x_{n,i} \frac{P_{n,i}^{sat}}{P_n} \left(\sum_{j=1}^{NC} \frac{\partial \gamma_{n,i}}{\partial x_{n,j}} \frac{dx_{n,j}}{dt} \right) - x_{n,i} \frac{\gamma_{n,i} P_{n,i}^{sat}}{P_n^2} \frac{dP_n}{dt} \right]}{\sum_{i=1}^{NC} \left[- \left(\frac{\gamma_{n,i}}{P_n} \frac{\partial P_{n,i}^{sat}}{\partial T_n} + \frac{P_{n,i}^{sat}}{P_n} \frac{\partial \gamma_{n,i}}{\partial T_n} \right) x_{n,i} \right]} \\
 &= \frac{\sum_{i=1}^{NC} \left\{ K_{n,i} \frac{dx_{n,i}}{dt} + x_{n,i} P_{n,i}^{sat} \gamma_{n,i} \left[\left(\frac{1}{P_n R_{gas} T_n} \sum_{j=1}^{NC} \frac{\partial g_{n,i}}{\partial x_{n,j}} \frac{dx_{n,j}}{dt} \right) - \frac{1}{P_n^2} \frac{dP_n}{dt} \right] \right\}}{\sum_{i=1}^{NC} \left\{ \frac{P_{n,i}^{sat}}{P_n} \gamma_{n,i} \left[\frac{B_i}{(T_n + C_i)^2} + \frac{g_{n,i}}{R_{gas} T_n^2} \right] x_{n,i} \right\}}
 \end{aligned} \tag{3.47}$$

with

$$g_{n,i} = \sum_{j=1}^{NC} \sum_{k=1}^{NC} \left(A_{ji}^{Margules} - \frac{1}{2} A_{jk}^{Margules} \right) x_{n,j} x_{n,k} \tag{3.48}$$

Details of the derivation are provided in Appendix B.

Derivations of Composition and Holdup Time Derivative Expressions

As at each tray

$$\frac{m_{n,i}}{M_n} = \frac{l_{n,i}}{L_n} = x_{n,i} \quad \Rightarrow \quad m_{n,i} = M_n x_{n,i} \quad \text{and} \quad \sum_{i=1}^{NC} m_{n,i} = M_n$$

it can be shown that, for a common column tray n ($1 \leq n \leq N_{tray}$, $n \neq N_{feed}, N_{tray}$), following expressions hold

$$\frac{dx_{n,i}}{dt} = \frac{1}{M_n} \left[\frac{dm_{n,i}}{dt} - x_{n,i} \frac{dM_n}{dt} \right] \tag{3.49}$$

$$\frac{dM_n}{dt} = L_{n+1} + V_{n-1} - L_n - V_n \tag{3.50}$$

For the feed tray and the reflux tray, there are additional terms in Eqn. 3.50.

Final Energy Balance Expression and Distillation Model

Substituting Eqn. 3.47, Eqn. 3.49 and Eqn. 3.50 into Eqn. 3.44 gives

$$\begin{aligned} \frac{dE_n}{dt} = & M_n \left(\sum_{i=1}^{NC} x_{n,i} b_i^{liq} \right) f_T \\ & + \sum_{i=1}^{NC} \left\{ h_{n,i}^{liq} \left[\frac{dm_{n,i}}{dt} - x_{n,i} (L_{n+1} + V_{n-1} - V_n - L_n) \right] \right\} \\ & + h_n^{liq} (L_{n+1} + V_{n-1} - V_n - L_n) \end{aligned} \quad (3.51)$$

The reformulated dynamic distillation model after index reduction thus consists of the original material balances and the revised energy balances. For a general non-feed/reflux tray n , the component material balances are

$$\frac{dm_{n,i}}{dt} = l_{n+1,i} + v_{n-1,i} - l_{n,i} - v_{n,i}, \quad i = 1, \dots, NC$$

Substituting Eqn. 3.51 into Eqn. 3.17, the energy balance in Section 3.2.1 is now replaced by

$$\begin{aligned} & M_n \left(\sum_{i=1}^{NC} x_{n,i} b_i^{liq} \right) f_T \\ & + \sum_{i=1}^{NC} \left\{ h_{n,i}^{liq} \left[\frac{dm_{n,i}}{dt} - x_{n,i} (L_{n+1} + V_{n-1} - V_n - L_n) \right] \right\} \\ & + h_n^{liq} (L_{n+1} + V_{n-1} - V_n - L_n) \\ & = H_{n+1,i}^{liq} + H_{n-1,i}^{vap} - H_{n,i}^{liq} - H_{n,i}^{vap} \end{aligned} \quad (3.52)$$

All the algebraic equations of the model are the same as in those in Section 3.2.1. Note that the true differential variables after completing all the substitutions are $m_{n,i}$.

3.3 Integrated Reboiler/Condenser (IRC)

The model for IRC comprises two sub-models: one for the condenser side and another for the reboiler side. A schematic of the IRC is shown in Fig. 3.2.

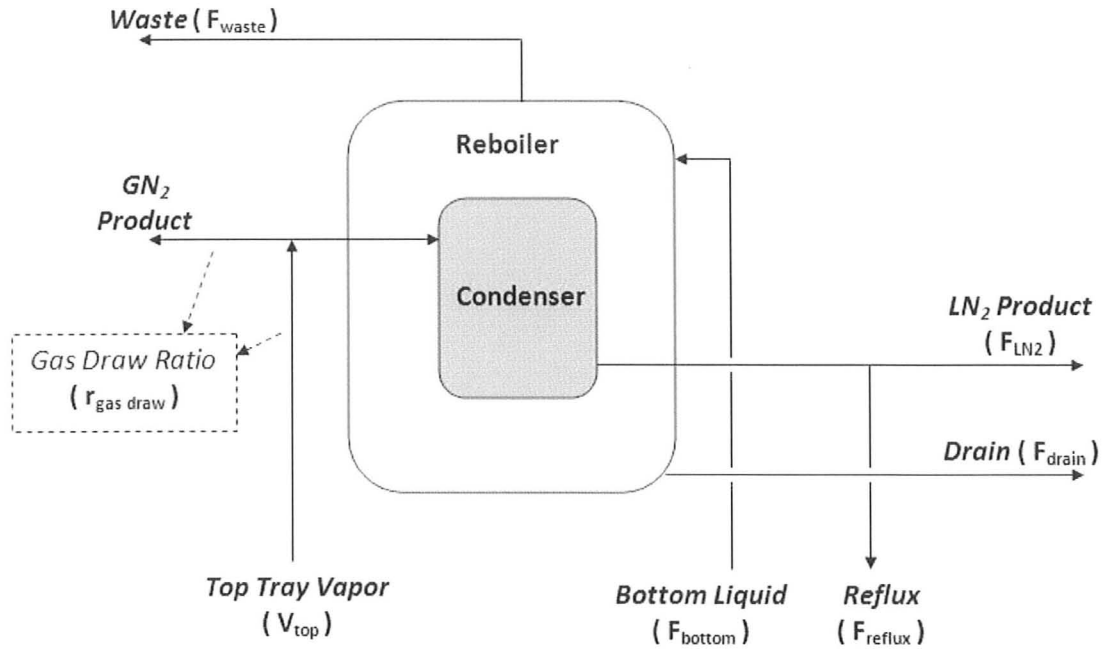


Figure 3.2: Schematic representation of the integrated reboiler/condenser.

3.3.1 Condenser Side Model

The condenser side is assumed to have negligible material and energy holdup. The same assumption was also applied in studies conducted by Zhu *et al.* [2001] and Roffel *et al.* [2000] on air separation units. Following Zhu *et al.* [2001], the portion of top tray vapor drawn into the condenser goes through a phase change and leaves the condenser as a saturated liquid. Hence, the material and energy balances on the condenser side are steady state equations:

$$0 = V_{top} (1 - r_{gas\ draw}) - (F_{LN_2} + F_{reflux}) \quad (3.53)$$

$$0 = V_{top} (1 - r_{gas\ draw}) h_{top}^{vap\ mix} - (F_{LN_2} + F_{reflux}) h_{cond}^{liq\ mix} - Q_{cond} \quad (3.54)$$

where

Q_{cond} = heat extracted from vapor condensation

V_{top} = vapor molar flow rate from the top column tray

$r_{gas\ draw}$ = gas draw fraction (the fraction of V_{top} drawn to the heat exchanger)

F_{LN_2} = LN₂ production rate

F_{reflux} = reflux flow rate

$h_{top}^{vap\ mix}$ = molar enthalpy of the top tray vapor

$h_{cond}^{liq\ mix}$ = molar enthalpy of the liquid leaving the condenser

Variable assignments are indicated in Fig. 3.2. The composition of the liquid stream leaving the condenser ($x_{cond,i}$) is the same as the composition of the top tray vapor ($y_{top,i}$):

$$x_{cond,i} = y_{top,i}, \quad i = 1, \dots, NC \quad (3.55)$$

Under the assumption of saturated liquid on the condenser side, the condenser side pressure is approximated using

$$P_{cond} = \sum_{i=1}^{NC} x_{cond,i} P_{cond,i}^{sat} \quad (3.56)$$

with component saturated pressure evaluated at the condenser side temperature using the Antoine equation (Eqn. 3.3). Note that P_{cond} corresponds to the bubble point pressure under the assumption that Raoult's law applies (Smith *et al.* [2005]). In this study, the condenser pressure is treated as a modeling specification, and is assigned in accordance with plant measurements.

In order to ensure that a temperature difference remains between the reboiler and the condenser side of the IRC, a tracking variable is introduced and defined as

$$\Delta T_{IRC} = T_{cond} - T_{reb} \quad (3.57)$$

where ΔT_{IRC} is the temperature difference between the reboiler and the condenser. ΔT_{IRC} should be nonnegative for the correct direction of the heat transfer in the IRC. In dynamic simulations, it can be detected by investigating the variable trajectories. In optimizations, constraints are imposed to enforce satisfactions of this condition. More detail will be presented in Chapter 4 of this thesis.

3.3.2 Reboiler Side Model

The reboiler side model is similar to the column tray model except that a static energy balance is used. As there is no material or energy accumulation in the expansion valve, the expansion valve in Fig. 2.2 and the reboiler are lumped together for simplicity. Modeling equations for the reboiler side include dynamic component balances:

$$\frac{dm_{reb,i}}{dt} = F_{bottom}x_{bottom,i} - F_{waste}y_{reb,i} - F_{drain}x_{reb,i}, \quad i = 1, \dots, NC \quad (3.58)$$

with composition relations

$$x_{reb,i}M_{reb} = m_{reb,i}, \quad i = 1, \dots, NC \quad (3.59)$$

$$M_{reb} = \sum_{i=1}^{NC} m_{reb,i} \quad (3.60)$$

and a static energy balance, derived in the same manner as in Roffel *et al.* [2000]:

$$F_{waste} = \frac{F_{bottom}(h_{bottom}^{liq\ mix} - h_{reb}^{liq\ mix}) + Q_{reb}}{h_{reb}^{vap\ mix} - h_{reb}^{liq\ mix}} \quad (3.61)$$

In the above equations:

$m_{reb,i}$ = component liquid molar holdup in the reboiler

M_{reb} = total liquid molar holdup in the reboiler

F_{bottom} = molar flow rate of the liquid flow drawn from the bottom of the column

F_{waste} = vapor molar flow leaving the reboiler

F_{drain} = liquid molar flow leaving the reboiler

$x_{bottom,i}$ = mole fraction of the bottom liquid stream

$x_{reb,i}$ = liquid phase mole fraction of component i in the reboiler

$y_{reb,i}$ = vapor phase mole fraction of component i in the reboiler

$h_{bottom}^{liq\ mix}$ = molar enthalpy of the bottom liquid stream

$h_{reb}^{liq\ mix}$, $h_{reb}^{vap\ mix}$ = liquid and vapor phase molar enthalpy in the reboiler

Q_{reb} = heat supplied to the reboiler

The value of molar enthalpy is computed as in the general column model (Eqn. 3.27 and Eqn. 3.28). Assuming there is no heat loss between the reboiler and the condenser gives:

$$Q_{cond} = Q_{reb} \quad (3.62)$$

As with a column tray, vapor-liquid phase equilibrium in the reboiler is represented using the modified Raoult's Law and the Antoine equation with the Margules equation for determining the component activity coefficient (Section 3.1.1). The liquid level in the reboiler, in percentage of the full tank level, is predicted as:

$$l_{reb} = 100 \left(\frac{M_{reb}}{\rho_{reb}^{liq}} \frac{1}{V_{reb}} \right) \quad (3.63)$$

with liquid phase density ρ_{reb}^{liq} approximated using the Rackett equation. The liquid level in the reboiler is regulated by manipulating the flow rate of the drain stream following a proportional-integral control algorithm:

$$F_{drain} = F_{drain}^{ss} + K_c^{reb}(l_{reb} - l_{reb}^{ss}) + \frac{K_c^{reb}}{\tau_I^{reb}} I_{reb} \quad (3.64)$$

$$\frac{dI_{reb}}{dt} = l_{reb} - l_{reb}^{ss} \quad (3.65)$$

where K_c^{reb} and τ_I^{reb} are controller tuning parameters. The superscript *ss* denotes steady state conditions.

3.4 Sump at the Column Bottom

The sump at the bottom of the column acts as a buffer tank. It is assumed the temperature of the sump is at the temperature of the liquid flow of the bottom tray. At the sump, liquids are blended, with dynamic expressions given by

$$\frac{dm_{sump,i}}{dt} = l_{1,i} - F_{bottom}x_{sump,i}, \quad i = 1, \dots, NC \quad (3.66)$$

and composition relations

$$x_{sump,i}M_{sump} = m_{sump,i}, \quad i = 1, \dots, NC \quad (3.67)$$

$$M_{sump} = \sum_{i=1}^{NC} m_{sump,i} \quad (3.68)$$

In the above expressions, $m_{sump,i}$ and M_{sump} are component and total molar holdups; $l_{1,i}$ is the molar flow rate of component i from the bottom column tray; $x_{sump,i}$ is the component molar fraction. As no separation occurs in the sump, no VLE correlations are required.

The liquid level at the bottom of the column, l_{sump} , can be calculated in the same way as that in the reboiler

$$l_{sump} = 100 \left(\frac{M_{sump}}{\rho_{sump}^{liq}} \frac{1}{V_{sump}} \right) \quad (3.69)$$

A PI controller is used control the liquid level

$$F_{bottom} = F_{bottom}^{ss} + K_c^{sump}(l_{sump} - l_{sump}^{ss}) + \frac{K_c^{sump}}{\tau_I^{sump}} I_{sump} \quad (3.70)$$

with

$$\frac{dI_{sump}}{dt} = l_{sump} - l_{sump}^{ss} \quad (3.71)$$

In above equations, ss denotes steady state conditions; ρ_{sump}^{liq} is the density of the liquid mixture; V_{sump} is the volume of the column below the bottom tray; K_c^{sump} and τ_I^{sump} are controller tuning parameters.

3.5 Primary Heat Exchanger (PHX)

The primary heat exchanger is a brazed aluminium plate-fin heat exchanger. Described by ALPEMA [2000], such heat exchangers consist of stacked layers of fins with parting sheets used to separate different layers. Different fluids would be distributed into different layers and each layer carries the same fluid (ALPEMA [2000], Averous *et al.* [1999]). A simplified illustration of the plate-fin heat exchanger used in this study is shown in Fig. 3.3.

The model outlined here consists of differential and algebraic equations. Changes in metal wall temperature as well as the process stream temperatures with respect to time are captured using differential equations. Algebraic equations are used for calculating the thermal properties of the stream. The PHX is modelled following a similar approach used

in Miller *et al.* [2008a]; however, in this study, there are three counter-current processing streams instead of two. As shown in Fig. 3.4, the two cold streams flow counter-currently with the hot air feed.

At the vapor air withdraw point, the PHX is partitioned into two zones with the assumption that there is no phase change in zone 1, but a phase change occurs in the air stream in zone 2. The following assumptions are invoked for the PHX to reduce the model complexity:

- The metal temperature at any axial position is uniform ; however, the metal temperature varies along the length of the PHX.
- The product of the heat transfer coefficient (between the metal wall and the processing streams) and the heat exchange area, UA , is constant in each zone, but different for each stream. In other words, there are three UA values in each zone.
- The liquid air leaving the PHX from zone 2 is saturated.
- The pressure drop of the processing streams in each zone is approximated as a function of the flow rate of that stream.
- The specific heat capacity of the metal is constant.
- Three processing streams ($NS = 3$) alternate from the top to the bottom layer with each stream exchanging heat with the other two streams across a metal wall. 1 and 2 denote the cold streams.

3.5.1 Volume Calculation

Before describing the dynamic model for the PHX, the approach of estimating the volume information required is described.

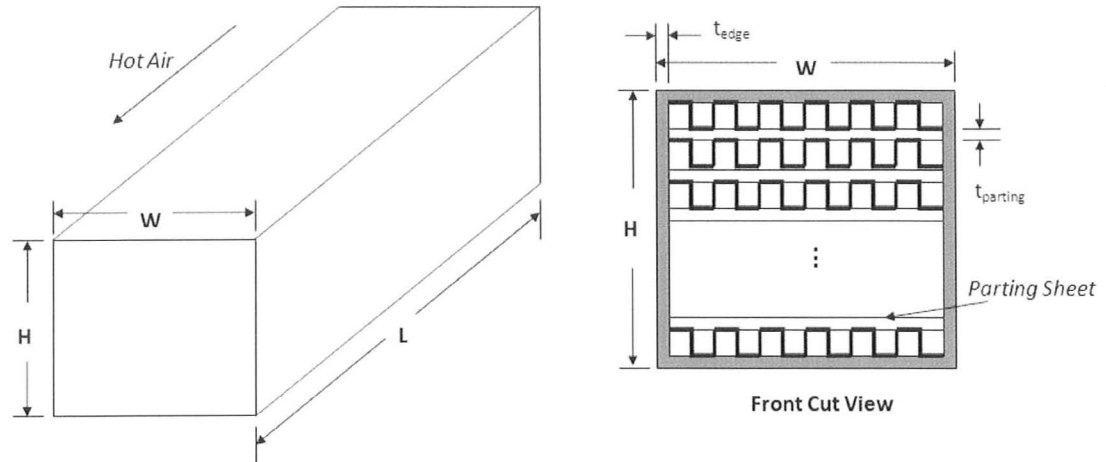


Figure 3.3: Simplified illustration of a brazed aluminium plate-fin heat exchanger used in air separation processes, modified from ALPEMA [2000]. A detailed illustration of a brazed aluminium plate-fin heat exchanger is available in ALPEMA [2000].

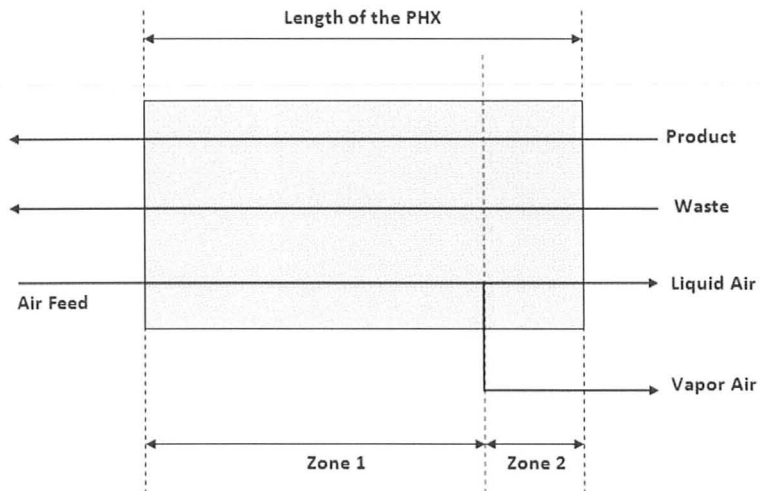


Figure 3.4: Sectional view of the primary heat exchanger, as modelled.

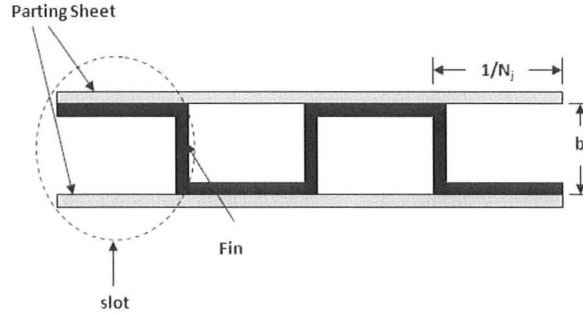


Figure 3.5: Schematic of each layer of the primary heat exchanger. Modified from ALPEMA [2000].

Volume Occupied by Each Stream

Neglecting the heads of the heat exchanger, the entire PHX can be simplified to a rectangular cuboid (Fig. 3.3). The total volume occupied by stream j in the heat exchanger can be calculated via following procedures. For each slot (Fig. 3.5) in the PHX:

$$V_j^{slot} = \left\{ \left(\frac{1}{N_j} \right) b_j - \left[b_j t_j + \left(\frac{1}{N_j} - t_j \right) t_j \right] \right\} (L - 2t_{edge}) \quad (3.72)$$

where

V_j^{slot} = the volume occupied by stream j in each slot

b_j = the distance between parting sheets for sections of stream j

t_j = the fin thickness for sections of stream j

N_j = the number of fins per unit width of the PHX for layers of stream j

t_{edge} = the heat exchanger wall thickness

In Eqn. 3.72, $\frac{1}{N_j}$ corresponds to the width of a single slot, and $\left(\frac{1}{N_j} \right) b_j$ denotes the cross-sectional area of the slot. In the term in the square brackets, we subtract the area of the slot that is occupied by the metal thickness. For each layer:

$$V_j^{layer} = (W - 2t_{edge}) (N_j V_j^{slot}) \quad (3.73)$$

where V_j^{layer} is the volume occupied by stream j in each layer; W is the heat exchanger width. The total volume occupied by stream j in the heat exchanger, neglecting the heads,

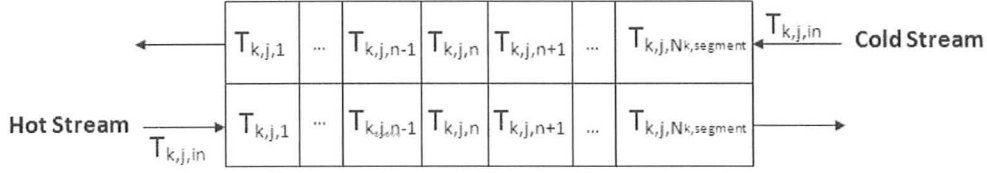


Figure 3.6: Segment division and numbering in each zone.

can then be estimated as:

$$V_j = V_j^{layer} n_j \quad (3.74)$$

where n_j is number of layers in the heat exchanger for stream j (i.e. hot air, cold product and cold waste).

Mass of Metal

Once of the total volume of the processing streams is determined, the calculation of the mass of the metal wall is straightforward:

$$m_{metal} = \rho_{metal} \left(WLH - \sum_{j=1}^{NS} V_j \right) \quad (3.75)$$

where ρ_{metal} is the metal density, and W , L and H are the dimensions of the heat exchanger, as shown in Fig. 3.3.

3.5.2 Dynamic Heat Exchanger Model

The dynamic equations for the PHX are energy balances. Zone 1 is partitioned into segments with the assumption that the fluids are well mixed in each segment; however, zone 2 is treated as one single segment in order to reasonably capture the phase change without complicating the model. The segment number is assigned in the direction of the hot air flows as shown in Fig. 3.6

Even though modeling approaches are slightly different for the two zones, there are some correlations common to both. The overall UA values in each zone are estimated from the

stream flow rate and base case conditions, as in Roffel *et al.* [2000]:

$$UA_{k,j} = UA_{k,j}^{base} \left(\frac{F_{k,j}}{F_{k,j}^{base}} \right)^{0.8} \quad (3.76)$$

where $F_{k,j}$ and $UA_{k,j}$ are the flow rate and overall UA value of stream j in zone k . The superscript *base* denotes the selected base case conditions. A constant segment UA value is assumed to hold in each zone as the segments are equally spaced. Thus, for each segment:

$$UA_{k,j,n} = UA_{k,j} \frac{1}{N_{k,segment}}, \quad n = 1, \dots, N_{k,segment} \quad (3.77)$$

where $N_{k,segment}$ represents the number of segments in zone k . Note that $N_{2,segment} = 1$.

The mass of metal allocated in each segment is

$$m_{k,n} = \frac{r_k m_{metal}}{N_{k,segment}}, \quad n = 1, \dots, N_{k,segment} \quad (3.78)$$

where r_k is the fraction of the heat exchanger that is in zone k . Similarly, the volume occupied by stream j in segment n can be approximated as

$$V_{k,j,n} = \frac{r_k V_j}{N_{k,segment}}, \quad n = 1, \dots, N_{k,segment} \quad (3.79)$$

With the assumption of constant pressure drop in each segment:

$$P_{k,j,n} = P_{k,j,in} + \Delta P_{k,j} \frac{n}{N_{k,segment}}, \quad n = 1, \dots, N_{k,segment} \quad (3.80)$$

$$\Delta P_{k,j} = f(F_{k,j}) \quad (3.81)$$

In Eqn. 3.80, $P_{k,j,in}$ is the pressure of stream j entering zone k . $\Delta P_{k,j}$ is positive for the cold streams and negative for the hot streams.

Before the Air Withdrawal (Zone 1)

Before the air stream withdrawal, the PHX is subdivided into equally spaced segments along the length of the heat exchanger. In each small segment, the fluid is assumed to be well mixed. This means that the temperature of the stream leaving each segment is at the same temperature as the fluid within that segment. Also, the metal wall temperature is assumed to be uniform within each segment. The number of segments chosen has to be large enough to avoid the occurrence of temperature crossover.

The dynamic behavior of the metal wall temperature of each segment in zone 1 (i.e. $k = 1$) is described as:

$$m_{k,n} C_{p_m} \frac{dT_{k,n}^m}{dt} = \sum_{j=1}^{NS} U A_{k,j,n} (T_{k,j,n} - T_{k,n}^m), \quad n = 1, \dots, N_{k,segment} \quad (3.82)$$

where C_{p_m} is the specific heat capacity of the metal; $T_{k,j,n}$ and $T_{k,n}^m$ are temperatures of the processing stream j and metal wall in segment n in zone k , respectively.

Dynamic behavior of energy holdups in each segment for the cold streams ($j = 1, 2$) in Zone 1 ($k = 1$) are now represented by:

$$\frac{dE_{k,j,n}}{dt} = F_{k,j} (h_{k,j,n+1}^{vap} - h_{k,j,n}^{vap}) + U A_{k,j,n} (T_{k,n}^m - T_{k,j,n}), \quad n = 1, \dots, N_{k,segment} \quad (3.83)$$

Note that when $n = N_{k,segment}$, $h_{k,j,n+1}^{vap}$ in Eqn. 3.83 is out of range and assigned the value of $h_{k,j,in}^{vap}$. Similarly, for the hot stream, we have:

$$\frac{dE_{k,3,n}}{dt} = F_{k,3} (h_{k,3,n-1}^{vap} - h_{k,3,n}^{vap}) + U A_{k,3,n} (T_{k,n}^m - T_{k,3,n}), \quad n = 1, \dots, N_{k,segment} \quad (3.84)$$

Note that when $n = 1$, $h_{k,3,0}^{vap}$ in Eqn. 3.84 is out of range and is assigned the value of $h_{k,3,in}^{vap}$.

The energy holdup in Eqns. 3.83 and 3.84 is defined as

$$E_{k,j,n} = h_{k,j,n}^{vap} V_{k,j,n} \rho_{k,j,n}^{vap} \quad (3.85)$$

where the vapor molar densities, $\rho_{k,j,n}^{vap}$ are estimated using Peng-Robinson equation of state (Eqn. 3.5) and the vapor phase molar enthalpy $h_{k,j,n}^{vap}$ is a function of temperature and pressure corresponding to the operating condition of the PHX.

After the Air Withdrawal (Zone 2)

For the section after the air withdrawal, an average temperature approach is followed, bearing in mind that there is only one segment in zone 2 (i.e. $N_{2,segment} = 1$). Changes in the metal wall temperature with respect to time are still captured using Eqn. 3.82. However, the average of the inlet and outlet temperatures is used in the corresponding calculations. $T_{2,j,n}$ is defined as:

$$T_{2,j,n} = \frac{1}{2} (T_{2,j,in} + T_{2,j,out}), \quad j = 1, \dots, NS, \quad n = 1 = N_{2,segment} \quad (3.86)$$

Note that for the cold streams (i.e. $j = 1, 2$), the temperature of the outlet stream from zone 2, $T_{2,j,out}$, is simply the inlet stream temperature in zone 1:

$$T_{2,j,out} = T_{1,j,in}, \quad j = 1, 2$$

and the inlet temperature of the hot air stream in zone 2 is identical to the temperature of the air stream leaving zone 1:

$$T_{2,3,in} = T_{1,3,N_{1,segment}}$$

Also, note that for the flow rate of the air stream, we have

$$F_{1,3} = F_{2,3} + F_{air \text{ withdrawal}}$$

Differential equations for the processing streams in Zone 2 are

$$\frac{dE_{2,j,n}}{dt} = F_{2,j}(h_{2,j,in}^{vap} - h_{2,j,out}^{vap}) + UA_{2,j,n}(T_{2,n}^m - T_{2,j,n}), \quad j = 1, 2, \quad n = 1 = N_{2,segment} \quad (3.87)$$

$$\frac{dE_{2,3,n}}{dt} = F_{2,3}(h_{2,3,in}^{vap} - h_{2,3,out}^{liq}) + UA_j(T_{2,n}^m - T_{2,3,n}), \quad n = 1 = N_{2,segment} \quad (3.88)$$

with

$$E_{2,j,n} = h_{2,j,n}^{vap} V_{2,j,n} \rho_{2,j,n}^{vap}, \quad j = 1, 2, \quad n = 1 = N_{2,segment} \quad (3.89)$$

$$E_{2,3,n} = h_{2,3,n}^{liq} V_{2,3,n} \rho_{2,3,n}^{liq}, \quad n = 1 = N_{2,segment} \quad (3.90)$$

with the liquid molar enthalpy as a function of temperature. Gas phase and liquid phase molar densities are estimated using Peng-Robinson equation of state and the Rackett equation as in Section 3.1 at temperature $T_{2,j,n}$, respectively.

In order to ensure that the air feed at the air stream withdrawal point is in the vapor phase and the exiting air from Zone 2 of the PHX is in the liquid phase, pressures at these points are compared with the corresponding limiting pressures. In other words, the pressure at the air withdrawal point has to be less than the corresponding dew point pressure, and the the pressure at the air outlet from Zone 2 must be above the corresponding bubble point pressure. In dynamic simulations, it can be detected by investigating the variable trajectories. In dynamic optimizations, constraints are imposed to enforce satisfactions of these conditions. More detail will be outline in Chapter 4 of this thesis.

3.6 Compressor

The model of the multi-stage compressor is a system comprised of entirely algebraic equations, and is derived based on Brown [2005] with the aid of available compressor maps. As stated earlier in Section 2.1, the air feed flow rate can be maintained by adjusting the inlet guide vane angle (IGVA) and the number of compressor stages running (Espie and Papa-georgaki [1998]). This means that if the number of compressor stages running is fixed, the discharge conditions of the compressor will be affected by the IGVA. This is consistent with the compressor maps provided by our industrial collaborator. To incorporate the effect of the IGVA in the model, compressor maps, derived from available compressor maps, for our pilot plant must be obtained.

Available compressor maps show that the discharge pressure and the power consumption of the compressor are determined by the standard volumetric flow rate and the IGVA. As the available maps are for a larger plant, scaling would be required. In this case, scaling was performed to fit the pressure map to the operating pressure range of the pilot plant. Due to lack of information on the actual power consumption of the compressor in the pilot plant, scaling of the power map is not that attractive. Instead, the power requirement of the compressor is estimated from theoretical correlations using the polytropic head of the compressor. More detail is provided in the following section.

3.6.1 Modeling Equations

Assumptions made in the compressor model are:

- The inlet of the compressor is ambient air.
- Values of the polytropic exponent and the polytropic efficiency are constant.
- No pressure drop during intercooling.
- The cooler return gas has the same temperature as the feed to the first stage of the

compressor.

- The compressor has no mechanical losses.

Based on the compressor maps, the compressor outlet pressure is a function of the standard volumetric flow rate of the feed to the system, and the IGVA:

$$P_{discharge} = f(\dot{V}_{std}, \alpha) \quad (3.91)$$

where \dot{V}_{std} is the volumetric flow rates in cubic feet per hour at standard conditions (i.e. 14.7 psia, 70 °F and 0 percent relative humidity); α is the IGVA. Procedures for obtaining this expression are detailed in Section 3.6.2. Conversions would be required to convert the inlet volumetric flow rate to that at the standard condition.

$$\dot{V}_{std} = \dot{V} \frac{\rho_{air\ in}}{\rho_{air\ in}^{std}} \quad (3.92)$$

with \dot{V} is the actual volumetric flow rate of the air into the compressor; $\rho_{air\ in}$ is the vapor phase molar density; *std* denotes standard conditions.

Due to lack of information for performing scaling to the power map, the power consumption is calculated following a theoretical approach. Explained in Brown [2005], for a compressor system of N_{stage} stages and $N_{stage} - 1$ intercooling steps, assuming the compressor system of the plant has the most efficient division of work to achieve a minimum power consumption, the ratio of compression at each stage is:

$$r_P = \left(\frac{P_{discharge}}{P_{suction}} \right)^\xi \quad (3.93)$$

$$\xi = \frac{1}{N_{stage}} \quad (3.94)$$

The discharge temperature from the final stage is calculated as (Brown [2005], Neerken [1984]):

$$\frac{T_{discharge}}{T_{suction}} = r_P^{\left(\frac{n_{poly}-1}{n_{poly}} \right)} \quad (3.95)$$

where n_{poly} is the polytropic exponent; the subscript *discharge* and *suction* denote the discharge and inlet conditions, respectively.

The overall theoretical power of compressor system with intercooling defined in Brown [2005] is:

$$W_{poly} = \left(\frac{w_{flow} H_{poly}}{33000 \eta_{poly}} + \text{mech losses} \right) N_{stage} \quad (3.96)$$

with the corresponding polytropic head:

$$H_{poly} = Z_{avg} R_{spec} T_{suction} \frac{n_{poly}}{n_{poly} - 1} \left[r_P^{\left(\frac{n_{poly} - 1}{n_{poly}} \right)} - 1 \right] \quad (3.97)$$

where

$$Z_{avg} = \frac{1}{2} (Z_{suction} + Z_{discharge}) \quad (3.98)$$

$$R_{spec} = \frac{1545.349}{M_w} \quad (3.99)$$

$$\eta_{poly} = \left(\frac{n_{poly}}{n_{poly} - 1} \right) \frac{k - 1}{k} \quad (3.100)$$

Variables in Eqn. 3.96 to Eqn. 3.100 and their corresponding units are defined as:

W_p = shaft work (hp)

w_{flow} = weight flow (lb/min)

H_p = compressor head (ft-lb/lb)

η_p = polytropic efficiency

mech losses = mechanical losses (hp)

$Z_{discharge}$, $Z_{suction}$ = vapor compressibility factor

R_{spec} = specific gas constant (ft-lb/lb · R)

M_w = molecular weight of the vapor mixture

k = ratio of specific heats, C_p/C_v

The constant 33000 in Eqn. 3.96 accounts for the unit conversion; 1545.349 in Eqn. 3.99 is the gas constant in ft-lbR⁻¹lbmol⁻¹. Physical properties required in the model are calculated as in Section 3.1. For a single stage compressor without intercooling, equations documented in this section are still applicable with $N_{stage} = 1$. The value of the polytropic exponent is estimated from information given by the compressor maps. Knowing the inlet

and discharge conditions, ratio of specific heats, k , and the adiabatic efficiency, η_{ad} , the polytropic exponent can be approximated according to Neerken [1984] as:

$$\eta_{ad} = \frac{r_p^{(k-1)/k} - 1}{r_p^{(n_{poly}-1)/n_{poly}} - 1}. \quad (3.101)$$

Once the polytropic exponent is known, the polytropic efficiency is obtained as described in Eqn. 3.100. It is assumed that all stages have the identical polytropic exponent and efficiency. Thus, for a set of specifications (i.e. $T_{suction}$, $P_{suction}$, IGVA and $P_{discharge}$ in this study), the power consumption can be approximated via Eqns. 3.91 to 3.100.

While modeling the compressor, it is essential to consider the compressor surge. As explained by Brown [2005] and Neerken [1984], when the flow rate of the processing stream decreases below to a critical value, unstable operation, such as sudden failures and shut-downs, might result due to excessive vibrations of the compressor. These are undesirable for plant operations. To prevent surging, the compressor should not operate close to the surge line (Fig. 3.7). According to the given compressor map, critical values of the volumetric flow rate are a function of discharge pressures:

$$\dot{V}_{critical} = f(P_{discharge}) \quad (3.102)$$

To maintain safe operations, the inlet volumetric flow rate at the standard conditions should remain above this critical value.

3.6.2 Obtaining Surface Fits for Compressor Maps

In this section, the generation of compressor maps that are utilized in the proposed compressor model is described.

Original Compressor Maps

The available discharge pressure map has the standard volumetric flow rate on the x-axis and discharge pressure on the y-axis. 5 performance curves are plotted, each corresponding to a different IGVA. A considerable amount of effort was taken to obtain good surface fits

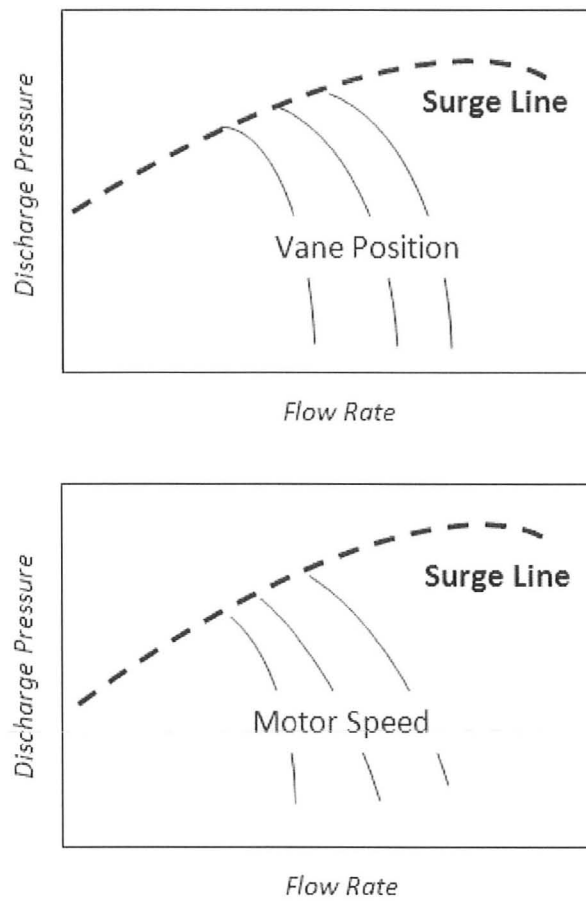


Figure 3.7: Example compressor maps of inlet guide vane angle and rotation speed effects with surge lines shown (Brown [2005], Neerken [1984]).

for the compressor map. The problem was posed as an optimization problem to minimize the sum of squared errors between the surface predictions and the corresponding points on the map. Microsoft Excel and AMPL were used to solve the problem. 4 curves (i.e. for inlet guide vane angles (IGVA) 0, 20, 40 and 60) for the pressure map were used to generate the fit and the fifth one was used to test the prediction accuracy. More than 20 points were collected from the map for each curve using a software program called *engage*.

The discharge pressure map was found to be well fitted by a third order polynomial with respect to the transformed volumetric flow rate, \dot{V}'_P ,

$$P_{discharge} = a_P \left(\dot{V}'_P\right)^3 + b_P \left(\dot{V}'_P\right)^2 + c_P \dot{V}'_P + d_P \quad (3.103)$$

with the transformed flow rate for the pressure map as an exponential function of the standard volumetric flow rate:

$$\dot{V}'_P = f(\dot{V}_{std}) \quad (3.104)$$

The subscript P in above equations denotes the pressure map. a , b , c , d and e in Eqn. 3.103 are the polynomial coefficients. These coefficients (i.e. in Eqn. 3.103) are highly nonlinear functions of the IGVA, α :

$$\ln(\text{coefficient}) = a_c \left(\frac{\alpha}{d_c}\right)^2 + b_c \left(\frac{\alpha}{d_c}\right) + c_c \quad (3.105)$$

As shown in Fig. 3.8, the resulting surface fits the data points well. The average absolute percent error between model predictions and map readings (obtained using *engage*) is less than 2 percent.

Compressor Map Scaling

The range of the volumetric flow rate of the available compressor map is greater than the plant operating range by a factor of 100, while the range of the discharge pressure of the map is about 1.25 times greater than the operating range of the plant compressor. As suggested by the industrial partner, scaling was performed with the available compressor map to get it to fit the operating conditions of the pilot plant. According to Brown [2005],

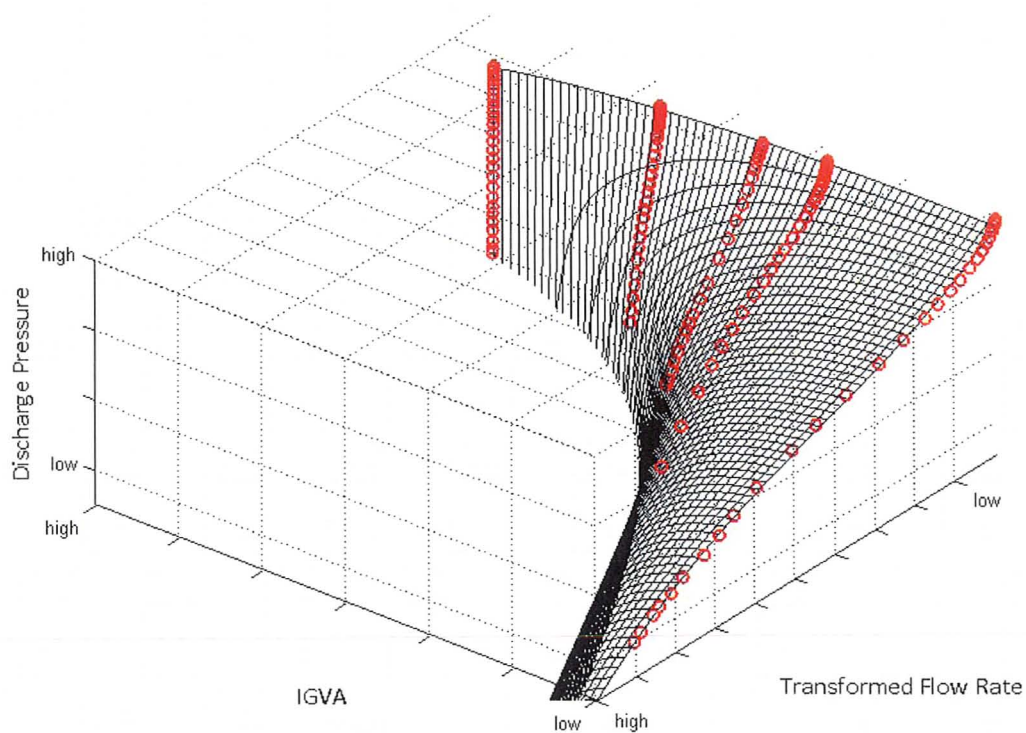


Figure 3.8: The surface fit for the discharge pressure map. Circles are data points collected from the compressor map.

the fan law gives :

$$\frac{\dot{V}_{original}}{\dot{V}_{scaled}} = \frac{\sqrt{H_{poly,original}}}{\sqrt{H_{poly,scaled}}} \quad (3.106)$$

where the subscripts *original* and *scaled* represent the original and scaled maps, respectively. For simplicity, the head is taken as the overall head of the compressor system, which was calculated using the overall compression ratio and the estimated polytropic exponent via Eqn. 3.97. However, neither linear scaling nor scaling according to the fan law would result in a compressor map that fits both the operating pressure range and the feed flow rate range of the pilot plant compressor system. As a result, scaling was performed to fit the operating pressure range. This means that the discharge pressure reading from the compressor map is scaled down by a factor of 1.25 and the corresponding polytropic head can then be estimated; after that, the scaled volumetric flow rate was estimated according to the fan law. This was performed to all the data collected for the original compressor map. It was noticed that when scaling down according to the Fan Law to fit the plant discharge pressure range, the resulting volumetric flow rate of the stream would be roughly 10 times greater than the plant operating flow rate. However, this scaled compressor map is still used with the volumetric flow rate accordingly divided by 10. Hence, the new scaled compressor map was generated as shown in Fig. 3.9 with a surface fit expressed similar to the original compressor map (i.e. Eqns. 3.103 to 3.105).

3.7 Turbine

A model is required to predict the discharge condition of the turbine (i.e. T and P) from the given inlet condition (i.e. T , P and composition). The initial attempt to model the turbine follows the approach in Smith *et al.* [2005] using thermal efficiency. However, due to limited information available for the turbine to adopt that approach, a model based on the assumption that the turbine in the pilot plant can be modelled in a similar way to a compressor is proposed. This implies the fan law is applicable to relate the discharge pressure, the volumetric flow rate and the speed of the turbine. This assumption was made as (1) measurements of the inlet and discharge conditions, as well as the rotating speed are

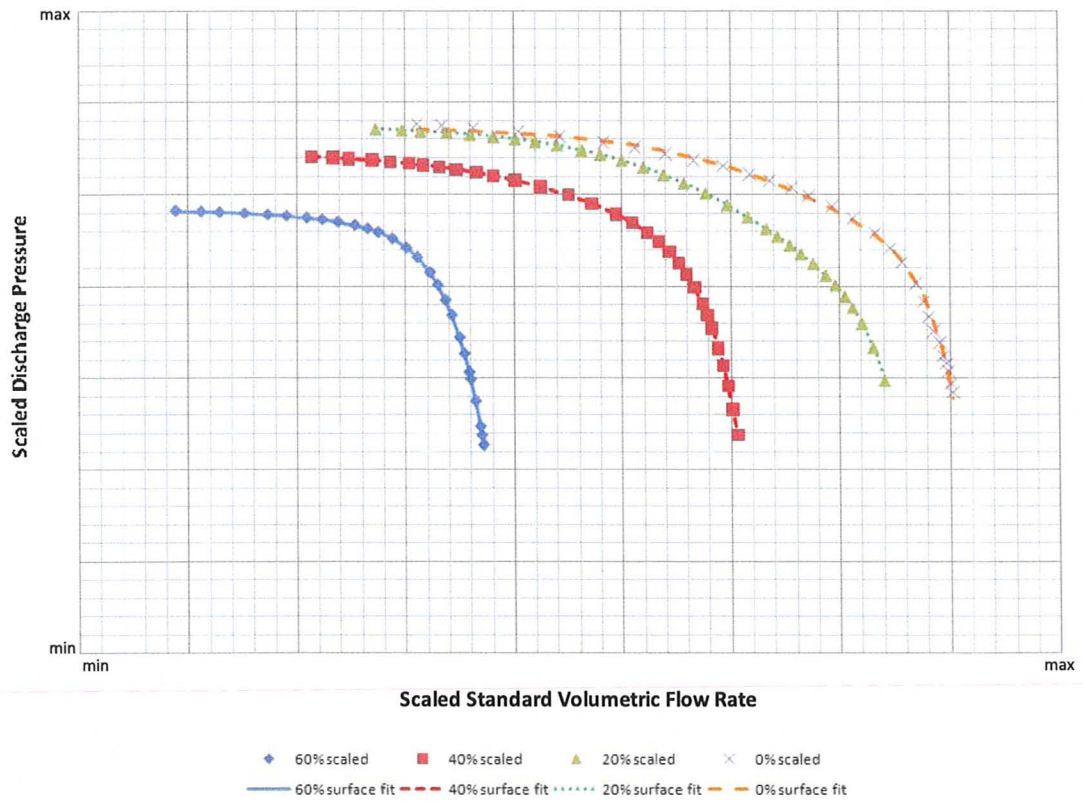


Figure 3.9: Scaled compressor map for the pilot plant. Scaled values were obtained according to the fan law and the predicted curves were generated using the surface fit expressions. Percentages correspond to the percentage closure of the IGVA.

available and (2) the fan law is applicable to pumps, fans and hydraulic turbines according to Lobanoff and Ross [1992].

The modeling equations used in this case are similar to those in the compressor model. According to Brown [2005], the fan law gives:

$$H_{poly}^{turb} \propto S^2 \quad \Rightarrow \quad H_{poly}^{turb} = f(S^2) \quad (3.107)$$

$$\dot{V} \propto S \quad \Rightarrow \quad S = f(\dot{V}) \quad (3.108)$$

where S is the speed of the turbine and \dot{V} is the stream volumetric flow rate. The polytropic head of the turbine can be estimated using Eqn. 3.97 with $N_{stage} = 1$. The vapor phase compressibility factor is calculated using the Peng-Robinson equation of state. In this case, the value of the polytropic exponent of the turbine was first regressed from plant measurements (i.e. suction and discharge pressures and temperatures) using Eqn. 3.95, and refined later in the parameter estimation stage. Correlations for (1) the calculated head and turbine speed and (2) the turbine speed and stream flow rate were deduced from available plant measurements.

In the turbine model, once the volumetric flow rate is available, the polytropic head is approximated from the correlations deduced. For a given set of suction temperature and pressure, the discharge pressure is estimated using Eqns. 3.93 and 3.97. Finally, the discharge temperature can be obtained via Eqn. 3.95.

3.8 Integrated Plant Model

In the integrated plant model, all the individual units are assembled in accordance with the plant configuration, Fig. 2.2. The inlet stream conditions of a unit are set to be equivalent to the outlet conditions of the preceding unit in the direction of the flow.

A set of suitable variable specifications for the integrated plant model are summarized in Table 3.1. Also, in the actual plant, there are other units between the compressor and the PHX, hence, besides the tabulated variables, the desired temperature at the air inlet to the PHX as well as the corresponding pressure drop have to be specified. Model parameters that need to be assigned are tabulated in Table 3.2. Some parameters are calculated from available information, while others are estimated in order for the model predictions to match the plant measurements. The parameter estimation is carried out using gPROMS.

3.9 Data Reconciliation and Parameter Estimation

To reconcile the model with given plant data, parameter estimation was applied with gPROMS. In this procedure, the integrated plant model supplied was the one with the index-reduced column model. This version included 329 differential modeling equations. The integrated plant model can be put into the form of DAE systems defined in Process System Enterprise Ltd [2009],

$$f(\mathbf{x}(t), \dot{\mathbf{x}}(t), \mathbf{y}(t), \mathbf{u}(t), \mathbf{p}, \boldsymbol{\theta}) = \mathbf{0}$$

where

$\mathbf{x}(t)$ = differential variables

$\mathbf{y}(t)$ = algebraic variables

$\mathbf{u}(t)$ = time-varying control variables

\mathbf{p} = time-invariant control variables/setting

$\boldsymbol{\theta}$ = parameters to be estimated

The idea is to obtain a set of parameters, $\boldsymbol{\theta}$, that would result in predictions that best match the plant measurements with given sets of $\mathbf{u}(t)$ and \mathbf{p} . The objective function for the gPROMS parameter estimation in this case is (Process System Enterprise Ltd [2009]):

$$\Phi_{PE} = \frac{N_m}{2} \ln(2\pi) + \frac{1}{2} \min_{\boldsymbol{\theta}} \left\{ \sum_{i=1}^{NV} \sum_{j=1}^{NM_i} \left[\ln(\sigma_{ij}^2) + \frac{(\tilde{z}_{ij} - z_{ij})^2}{\sigma_{ij}^2} \right] \right\} \quad (3.109)$$

Table 3.1: Set of variable specifications in the integrated plant model.

Variable	Unit Model	Additional Information
\dot{V}_{std}^{sp}	Compressor	Set point of feed flow rate. Recall the discharge condition of the compressor is controlled using the IGVA. However, required by our industrial collaborator, the IGVA is not directly specified, but is determined from the set point of the feed volumetric flow rate.
x_i	Compressor	Mole fraction of the air feed to the plant; air compositions (i.e. $x_{N_2} = 0.7811$, $x_{O_2} = 0.2096$ and $x_{Ar} = 0.0093$) assumed.
$T_{suction}, P_{suction}$	Compressor	Inlet temperature and pressure of air feed; ambient conditions assumed.
$F_{2,3}$ or $F_{air\ withdrawal}$	PHX	Flow rate of the liquid air to the column or the flow rate of the air withdrawal; $F_{2,3}$ was selected in the study.
$T_{ambient}$	Column	Ambient temperature used to calculate heat leakages.
$r_{gas\ draw}$ or F_{reflux}	Condenser	Gas draw fraction to the PHX or the flow rate of the reflux; $r_{gas\ draw}$ was selected in the study.
F_{LN_2}	Condenser	LN₂ production rate
P_{cond}	Condenser	Condenser pressure
P_{reb}	Reboiler	Reboiler pressure

Table 3.2: Parameters in the integrated plant model.

Parameter	Eqn Number	Estimated	Additional Information
$UA_{leakage}$	Eqn. 3.21	N	Calculated from the design memo.
A_s, H_{weir}, L_{weir}	Eqn. 3.33	N	Given tray design.
η_{spec}	Eqn. 3.34	Y	Estimated to match the model impurity prediction with measurement.
A_a	Eqn. 3.38	N	Given tray design.
ϕ, T_s	Eqns. 3.40, 3.41	N	Given tray design
V_{reb}, V_{sump}	Eqns. 3.63, 3.69	N	Calculated from reboiler and tray design.
$F_{drain}^{ss}, F_{sump}^{ss}$	Eqns. 3.64, 3.70	Y	Estimated to match plant data.
$l_{reb}^{ss}, l_{sump}^{ss}$	Eqns. 3.64, 3.70	N	
K_c^-, τ_I^-	Eqns. 3.64, 3.70	N	
b_j, t_j, N_j, t_{edge}	Eqn. 3.72	N	Given PHX design.
W, L, H, r_k	Eqn. 3.75, 3.78	N	Given PHX design.
ρ_{metal}, Cp_m	Eqn. 3.75, 3.82	N	Metal properties.
$UA_{k,j}^{base}$	Eqn. 3.76	Y	Estimated to match plant data; there are 6 UA values in total.
$F_{k,j}^{base}$	Eqn. 3.76	N	From design memo.
n_{poly}^{comp}	Eqn. 3.95	N	Calculated from compressor maps.
n_{poly}^{turb}	–	Y	Estimated to match plant data.
N_{tray}	–	N	–
$N_{k,segment}$	–	N	–

where

N_m = total number of measurements used

NV = number of variables measured

NM_i = number of measurements of variable i

σ_{ij}^2 = variance of the j^{th} measurement of variable i

\tilde{z}_{ij}, z_{ij} = j^{th} measured value and predicted value of variable j

For the parameter estimation, a steady state form of the integrated plant model was used by setting the time derivatives of the differential variables (i.e. $\frac{dm_{n,i}}{dt}$, $\frac{dm_{reb,i}}{dt}$, $\frac{dm_{sump,i}}{dt}$, $\frac{dE_{k,j,n}}{dt}$ and $\frac{dT_{k,n}^m}{dt}$) to zero at $t = 0$ with constant variable specifications and parameter assignments. In addition, the value of IGVA was set to its set point (i.e. $\alpha = \alpha^{sp}$), and the sump and reboiler liquid level were at the corresponding steady state conditions (i.e. $l_{sump} = l_{sump}^{ss}$, $l_{reb} = l_{reb}^{ss}$) at $t = 0$. The simulation was required to continue for a certain period of time (i.e. t_{PE}). The problem was formulated in such way in order to ensure that with the set of variable specifications and parameter assignments, the system is stable and at steady-state. The variable specifications given included: $T_{suction}$, $P_{suction}$ and x_i in the compressor model, P_{cond} in the condenser model, P_{reb} in the reboiler model, as well as $T_{ambient}$ in the column model (refer Table 3.1 for details). The non-estimated model parameters were assigned as well. Variables and parameters to be estimated included: \dot{V}_{std}^{sp} , $F_{2,3}$, $r_{gas\ draw}$, F_{LN2} , η_{spec} , F_{drain}^{ss} , F_{sump}^{ss} , $UA_{k,j}^{base}$ and η_{poly}^{turb} . The reader can refer to Tables 3.1 and 3.2 for details. For each variable having plant measurements, the average value of its first 4000 data points was used. The bounds were assigned either according to the physical meaning of the variable or as an order of magnitude down or up of the corresponding value of the initial guess obtained from pre-calculations. The variance model supplied to the parameter estimation was constant variance for the temperature and pressure sensors with standard deviations of 1.35 R and 0.4 psia, and constant relative variance for the flow sensor and the analyzer with relative standard deviations of 2 %. Values of standard deviations used were selected based on Swartz [1989].

Table 3.3: Table of the measured variables.

Measured Variable	ε %
Product impurity	3.33e-3 %
GN ₂ production rate	4.64e-2 %
Standard volumetric flow rate of the feed to the compressor	4.07e-1 %
Reboiler temperature	9.63e-2 %
Outlet temperature of GN ₂ from the PHX	4.00e-3 %
Vapor feed temperature to the column	1.04e-2 %
Liquid feed temperature to the column	5.68e-3 %
Discharge pressure of turbine	1.27 %
Discharge temperature of turbine	2.28e-2 %

Model variables having plant measurements are shown in Table 3.3. The absolute relative error of the model prediction for each measured variable after parameter estimation is calculated as:

$$\varepsilon \% = \frac{|\tilde{z}_{ij} - z_{ij}|}{\tilde{z}_{ij}} \cdot 100 \% \quad (3.110)$$

Note that we also have measurements for P_{reb} and P_{cond} . However, if P_{reb} and P_{cond} were also allowed to change, it was very challenging to obtain a solution. As a result, P_{reb} and P_{cond} were specified instead of estimated. As shown in Table 3.3, the reconciliation result is satisfactory; the maximum relative percent error after parameter estimation is less than 2 %.

3.10 Simulation Results

With the estimated model parameters, several simulation cases were conducted. Variables specified and parameters assigned are summarized in Tables 3.1 and 3.2. Initially, the system is at a steady state. Time derivatives of the differential variables (i.e. $\frac{dm_{n,i}}{dt}$, $\frac{dm_{reb,i}}{dt}$, $\frac{dm_{sump,i}}{dt}$, $\frac{dE_{k,j,n}}{dt}$ and $\frac{dT_{k,n}^m}{dt}$) were assigned to zero at $t = 0$. In addition, the value of IGVA was set to its set point (i.e. $\alpha = \alpha^{sp}$), and the sump and reboiler liquid level were at

the corresponding steady state conditions (i.e. $l_{sump} = l_{sump}^{ss}$, $l_{reb} = l_{reb}^{ss}$) at $t = 0$. It is worth mentioning that with the identical setup, the plant model with the column model following the general approach and allowing gPROMS performing auto index reduction took about 132 seconds (i.e. total CPU time) to complete initialization, while the one with the index-reduced column model requires only 3 seconds. Results (simulation and optimization) presented in the rest of this thesis correspond to a plant model implementation with the index-reduced column model.

Step tests were introduced in different inputs to the system. Fig. 3.10 shows the dynamic response of selected scaled plant variables to a negative 5 % step change in the inlet air volumetric flow rate while holding other inputs constant. The product impurity level in this project is defined by the oxygen level in the gas nitrogen product/top tray vapor stream. When there is a decrease in the air feed flow rate, the vapor feed to the column decreases. With a fixed gas draw fraction of the top tray to the primary heat exchanger, this leads to a decrease in GN_2 production. Meanwhile, the reflux flow rate also decreases, but the response is slower than the vapor feed to the column. Hence, a decrease in product impurity is observed initially. The system gradually equilibrates and reaches a new steady-state. At this steady-state, the product impurity level is slightly higher than before as the reflux rate is relatively lower than before due to a constant LN_2 production:

$$F_{reflux} = V_{top} (1 - r_{gas\ draw}) - F_{LN_2}.$$

Fig. 3.11 shows the dynamic response of selected scaled variables to a positive step change in the gas draw fraction to the PHX. Without changes in other inputs to the system, when the gas draw fraction increases, GN_2 production increases and the reflux rate decreases. Again the system gradually equilibrates and reaches a new steady-state. As the reflux rate relative to the air feed at the new steady state is much lower than before, a significant increase in the product impurity level is observed.

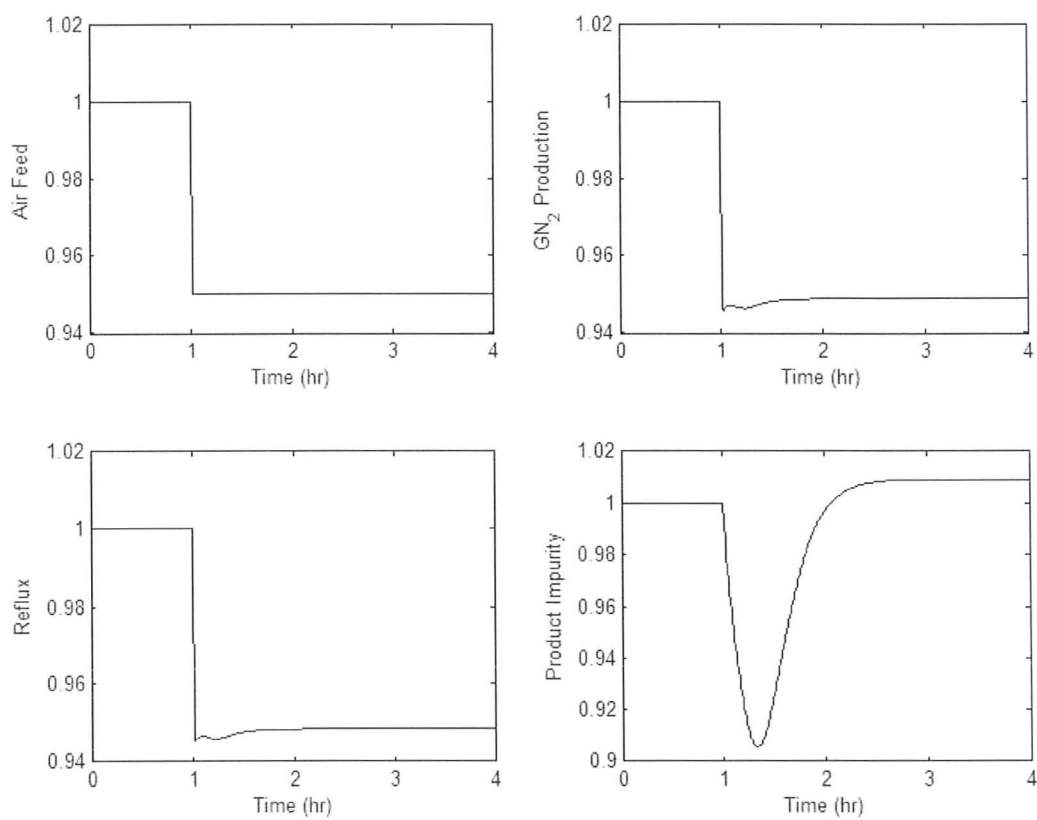


Figure 3.10: Dynamic response of selected scaled variables to a negative step change in the air feed.

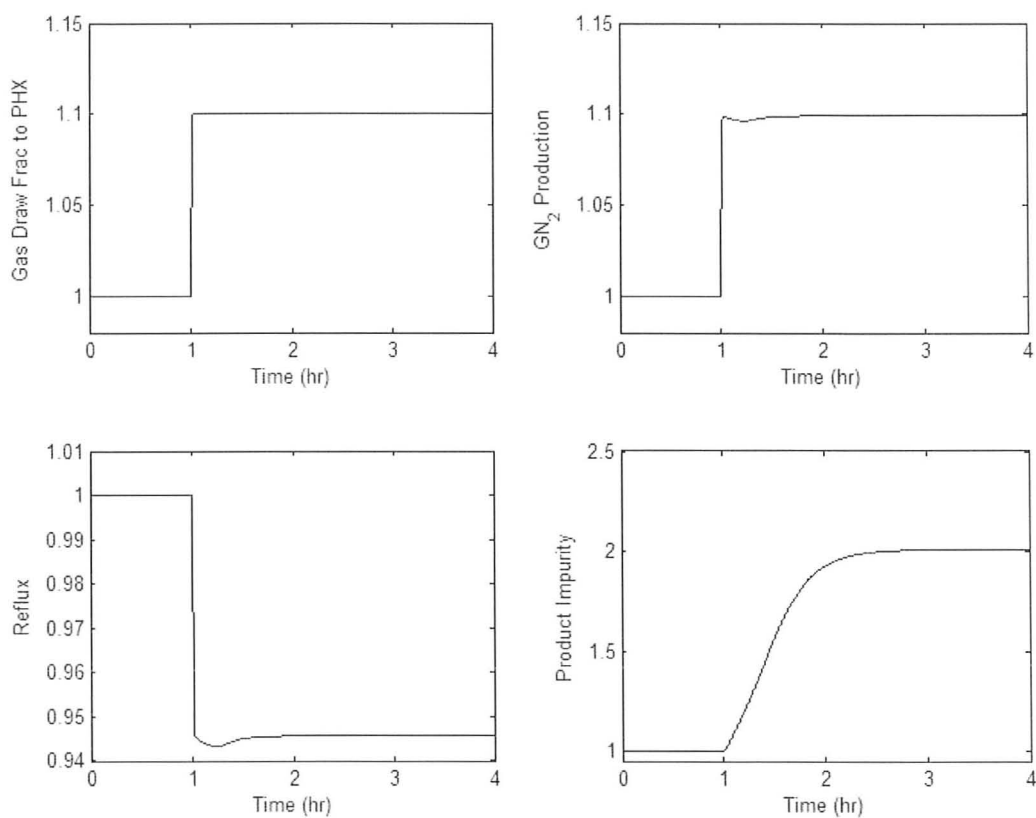


Figure 3.11: Dynamic response of selected scaled variables to a positive step change in the gas draw fraction to the primary heat exchanger.

Chapter 4

Optimization Formulation

This chapter will outline the optimization problem formulation, including the general methodology, the basic form of the objective function, constraint sets and decision variable handling.

4.1 Optimization Approach - Decomposition Strategy

The purpose of this study is to identify limiting factors that constrain the dynamic performance of the plant, and to obtain the best possible performance for the plant to transition between operating points in response to the dynamic market conditions via dynamic optimization. The underlying assumption is that except during transitions, the plant operates at steady state operating points. Thus, we ensure that under normal conditions, the steady state operating point is economically optimal. Note that this project is not intended for direct online application, but rather to serve as a guideline for design and control. The best possible plant performance obtained is independent of the plant control system, and would thus serve as a control performance benchmark.

The optimization methodology used in this project is a decomposition strategy. A base case design is specified and no uncertainties are considered. The first tier of the optimiza-

tion solves a constrained set-point optimization problem using the steady-state model to determine the economically optimal operating point corresponding to new market conditions (i.e. customer demand requirements or electricity price in this study). The second tier is to obtain a set of trajectories of the manipulated variables to achieve fast transitions to the pre-determined operating point subject to an extended set of constraints. Although step changes may be attractive, they could result in undesirable results like severe constraint violation during the transition, which necessitates the use of dynamic optimization.

Our optimization approach is similar in character to the two-level dynamic optimization and control strategy adopted in Kadam and Marquardt [2007]:

“The overall problem of economical optimization and control of dynamic processes should be decomposed into consistent and simple subproblems, and subsequently re-integrated using efficient techniques to handle uncertainty.”

4.2 Tier 1: Economic Steady-state Optimization

We remark first that the product demand must be satisfied, and can be done by evaporation of pre-stored liquid N₂ if the amount gas nitrogen (GN₂) produced by the plant is insufficient. By solving the first tier optimization problem, an economically optimal steady-state operation point is obtained (i.e. the desired GN₂ production rate, as well as the optimal control input values), which is then provided to the dynamic optimization formulation. Fig. 4.1 shows a plant configuration with indicated decision variables.

4.2.1 General Form

The steady-state optimization framework takes the following form:

$$\max_{\mathbf{u}, F_{evap}} \Phi_{ss} = C_{GN_2} (F_{GN_2, prod} + F_{evap}) - C_{elec} W_{poly} - C_{evap} F_{evap} \quad (4.1)$$

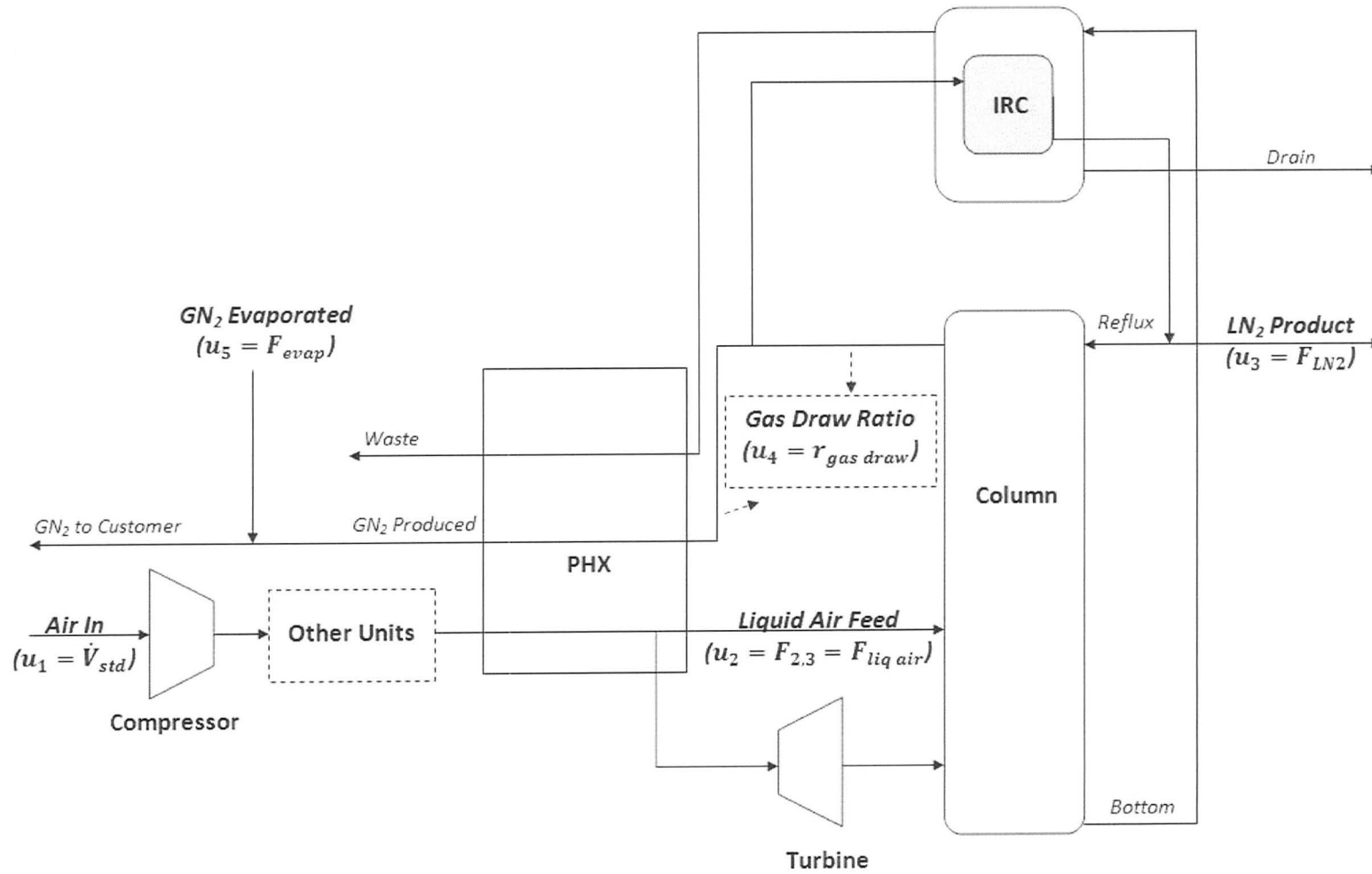


Figure 4.1: A nitrogen plant configuration with indicated decision variables for the optimization problems.

Subject to:

$$\mathbf{f}(\dot{\mathbf{x}} = \mathbf{0}, \mathbf{x}, \mathbf{z}, \mathbf{u}, \mathbf{p}) = \mathbf{0} \quad (4.2)$$

$$\mathbf{g}(\mathbf{x}, \mathbf{z}, \mathbf{u}, \mathbf{p}) = \mathbf{0} \quad (4.3)$$

$$\mathbf{h}(\mathbf{x}, \mathbf{z}, \mathbf{u}, \mathbf{p}) \leq \mathbf{0} \quad (4.4)$$

where:

\mathbf{x} = differential state vector

\mathbf{z} = algebraic state vector

\mathbf{u} = control input vector

\mathbf{p} = parameter vector

C_{GN_2} = sales price of gas nitrogen (GN_2)

$C_{\text{elec}}, C_{\text{evap}}$ = costs associated with compression and evaporation

$F_{\text{GN}_2, \text{prod}}$ = flow rate of GN_2 produced

F_{evap} = rate of evaporation of pre-stored liquid N_2

W_{poly} = power consumption of the compressor

\mathbf{f} and \mathbf{g} comprise the DAE plant model equations and \mathbf{h} includes variable bounds (i.e. for \mathbf{x} , \mathbf{z} , \mathbf{u}), operational constraints, product specification constraints and constraints required in the model.

4.2.2 Constraints

Operational constraints

Operational constraints in this phase include surge constraints at the compressor and the flooding constraints at all column trays.

- Compressor Surge Constraint

To prevent surging, the compressor should operate away from the surge line (i.e. described in Section 3.6). This means:

$$\dot{V}_{std} - \dot{V}_{critical} \geq \varepsilon_{surge} \quad (4.5)$$

where ε_{surge} is a specified non-negative surge margin.

- Flooding Constraint

At any column tray n , the fractional flooding should not be greater than 1:

$$1 - \alpha_n^{flooding} \geq \varepsilon_{flooding} \quad (4.6)$$

where $\alpha_n^{flooding}$ is the ratio of the gas velocity at tray n to the corresponding flooding velocity, and $\varepsilon_{flooding}$ is a non-negative pre-determined safety margin.

Production Specification Constraints

Regardless the market conditions, the plant product provided to the customer must meet certain product requirements.

- Demand Satisfaction

The customer demand has to be met either by production or LN₂ evaporation:

$$(F_{GN_2,prod} + F_{evap}) - D \geq 0 \quad (4.7)$$

where D is the customer demand. No offsets are allowed in this case as demand satisfaction is strictly required.

- No Overproduction

As the overproduced product will be vented, which represents a potential lose in revenue, overproduction has to be limited to be no more than a certain non-negative value, ε_{op} :

$$(F_{GN_2,prod} + F_{evap}) - D \leq \varepsilon_{op} \quad (4.8)$$

- Product Purity

Unsatisfactory product cannot be supplied to the customer. This imposes a strict constraint on the product purity:

$$Impurity - Impurity_{ss} \leq 0 \quad (4.9)$$

Modeling Constraints

Those constraints discussed previously are required by the actual process. However, there are other constraints which are not required by the actual plant but are enforced to ensure the model predictions are physically consistent.

- Pressure Constraints in the PHX

As the primary heat exchanger model developed assumes that a phase change occurs in the air stream after the turbine air withdrawal, the outlet pressure of the air feed from zone 2 has to be greater than the corresponding bubble point pressure. According to Smith *et al.* [2005], this yields:

$$P_{out,air} > \sum_{i=1}^{NC} y_{air,i} P_{out,i}^{sat} \quad (4.10)$$

with $P_{out,i}^{sat}$ evaluated using Antoine equation at the outlet temperature of air feed from zone 2 of the PHX. Similarly, the air stream at the air withdrawal point has to be in the vapor phase; hence, the stream pressure should not be greater than the corresponding dew point pressure:

$$P_{withdrawal,air} < \frac{1}{\sum_{i=1}^{NC} y_{air,i} / P_{withdraw,i}^{sat}} \quad (4.11)$$

with $P_{withdraw,i}^{sat}$ evaluated at the air withdrawal point.

- Temperature Difference in the IRC

As mentioned earlier, a temperature difference between the reboiler and the condenser (i.e. with the condenser temperature at a higher value) has to remain for the occurrence

and the correct direction of heat transfer. This gives a constraint that

$$\Delta T_{IRC} = T_{cond} - T_{reb} > 0. \quad (4.12)$$

4.3 Tier 2: Dynamic Optimization

The second tier of the optimization is to transition the plant optimally from the initial operating point to the determined new operating point. It would be desirable for the plant to move to a new production load immediately at the point of time that the changes occur without violating any constraints. Hence, the integral squared deviation from the desired production trajectory with a free end time roughly indicates the transition speed, as proposed in White *et al.* [1996].

4.3.1 General Form

The objective function at this stage is trajectory-tracking based, similar to White *et al.* [1996] with some modifications. The optimization problem is posed in the following manner:

$$\min_{\mathbf{u}(t), t_f} \Phi = t_f \left\{ \int_{t_0}^{t_f} \left[1 - \frac{F_{GN_2, prod}(t)}{F_{GN_2, prod}^*} \right]^2 dt + \sum_{i=1}^{N_u} w_i \left[1 - \frac{u_i(t_f)}{u_i^*} \right]^2 \right\} \quad (4.13)$$

Subject to:

$$\mathbf{f}(\dot{\mathbf{x}}(t), \mathbf{x}(t), \mathbf{z}(t), \mathbf{u}(t), \mathbf{p}, t) = \mathbf{0} \quad (4.14)$$

$$\mathbf{g}(\mathbf{x}(t), \mathbf{z}(t), \mathbf{u}(t), \mathbf{p}, t) = \mathbf{0} \quad (4.15)$$

$$\mathbf{h}(\mathbf{x}(t), \mathbf{z}(t), \mathbf{u}(t), \mathbf{p}, t) \leq \mathbf{0} \quad (4.16)$$

and

$$\dot{\mathbf{x}}(0) = \mathbf{0} \quad (4.17)$$

$$t_0 \leq t \leq t_f \quad (4.18)$$

where w_i is the penalty assigned for deviations in input variable i at t_f .

4.3.2 Constraints

In this stage, the optimal solution not only has to satisfy those constraints from the steady state optimization stage, but also some other constraints that regulate the system behavior during the transition.

Constraints from Steady State Optimization

Except the demand satisfaction constraint, all the constraints considered in Tier 1 are translated into path constraints. In this thesis, path constraints are transformed into combinations of interior-point constraints and end-point inequality constraints. Dummy variables are used to track the accumulated squared constraint violations over the time horizon. Similar approach have be adopted in studies of in White *et al.* [1996] and Feehery and Barton [1999]. In Bansal *et al.* [2002], an alternative approach is suggested. To illustrate, the product impurity constraint is formulated as the end-point inequality constraint:

$$\epsilon_{impurity}(t_f) \leq \epsilon_{impurity} \quad (4.19)$$

with $\epsilon_{impurity}$ defined as:

$$\frac{d\epsilon_{impurity}(t)}{dt} = [\max(0, Impurity(t) - Impurity_{path})]^2 \quad (4.20)$$

and the interior-point constraint

$$Impurity(\bar{t}_j) \leq Impurity_{path}, \quad j = 1, \dots, N_J \quad (4.21)$$

where $\epsilon_{impurity}$ is a pre-determined threshold and \bar{t}_j means at the time of the j th interior point. Also, as the value of maximum allowable impurity level during transition is different from that for the steady state case, it also requires the impurity level at the new operating point to be below the steady state operation requirements:

$$Impurity(t_f) \leq Impurity_{ss} \quad (4.22)$$

Reaching the New Steady-state

Similar to White *et al.* [1996], we also require that when the plant completes the transition, it has be at steady-state. This imposes two additional constraints: one on the manipulated variables

$$\mathbf{u}(\bar{t}_{N_{J-1}}) = \mathbf{u}(\bar{t}_{N_J}) \quad (4.23)$$

and the other on the differential state variables

$$\sum_{i=1}^{N_x} \left[\frac{dx_i(t_f)}{dt} \right]^2 \leq \varepsilon_{ss} \quad (4.24)$$

where ε_{ss} is a “sufficiently small” tolerance and N_x is the number of differential variables. Theoretically, when reaching the new steady state, Eqn. 4.24 should have a value of zero, but due to computation errors, enforcing Eqn. 4.24 may result in optimization difficulties. One only needs to enforce this constraint on the slowest variable. The selection of the slowest variable can be made based on dynamic simulation results.

Pinning Down Final States

To force the system to reach the pre-determined economically optimal operating point, we require the system inputs to reach a neighborhood of the desired values at the end of the time horizon,

$$-\varepsilon_i \leq 1 - \frac{u_i(t_f)}{u_i^*} \leq \varepsilon_i \quad (4.25)$$

and the desired production rate may also be required to reach the desired production rate at t_f :

$$-\varepsilon_{prod} \leq 1 - \frac{F_{GN_2,prod}(t_f)}{F_{GN_2,prod}^*} \leq \varepsilon_{prod} \quad (4.26)$$

ε_i and ε_{prod} are specified tolerances.

Liquid Level

During transition, no overflow or drying tank should be allowed in either the reboiler or the sump. This requires limiting the liquid level to be within certain lower and upper bounds:

$$l_{LB}^- \leq l_-(t) \leq l_{UB}^- \quad (4.27)$$

This path constraint is treated using the same method described earlier.

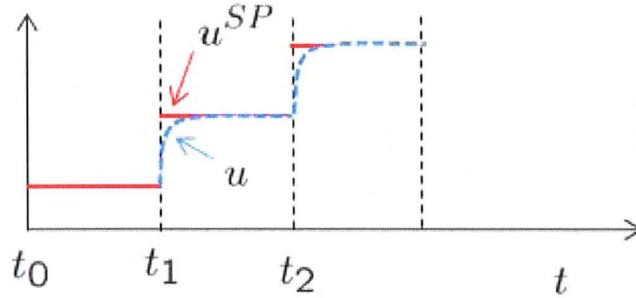


Figure 4.2: Filter on the inputs.

4.4 Handling Optimization Decision Variables

This section explains how the decision variables are handled in the optimization problem in the second tier.

4.4.1 Filter on the Inputs

In reality, when controllers receive control signals and adjust valves to change the manipulated inputs, delays always occur. The actual value of the manipulated variable requires some time to reach its set point. To roughly capture this phenomenon, we introduce a set of dynamic equations

$$\tau_i \frac{du_i}{dt} = u_i^{sp} - u_i, \quad i = 1, \dots, N_u \quad (4.28)$$

where τ_i is the response time constant and the superscript *sp* indicate set point. A graphic representation is shown in Fig. 4.2. In addition, this also helps to smooth the input trajectory, hence, reduces computation difficulties (Process System Enterprise Ltd [2010]). In this project, values of τ_i are set to be very small (i.e. a few seconds).

4.4.2 Control Vector Parametrization

To approximate the control actions, we implement the idea of control vector parameterizations. If we divide the time horizon of interest into N_J control intervals, the continuous

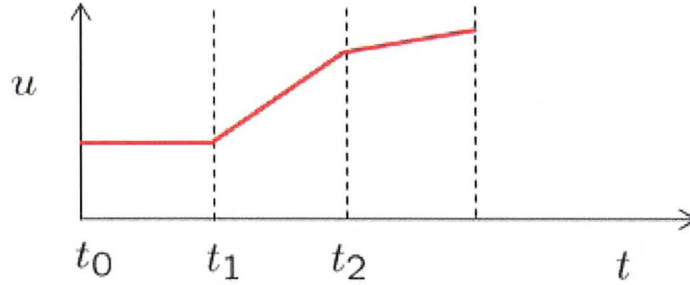


Figure 4.3: Piecewise linear control profile.

control action can be approximated using a piecewise linear profile with continuity at interval boundaries as shown in Fig. 4.3. Derived based on Process System Enterprise Ltd [2009], this adds some additional differential equations to the system. Using set points of the inputs, we have:

$$\frac{du_i^{sp}}{dt} = a_{i,j}, \quad t \in [\bar{t}_j, \bar{t}_j + \delta_j], \quad i = 1, \dots, N_u \quad (4.29)$$

where $a_{i,j}$ is the slope of the control trajectory of input i in control interval j ; \bar{t}_j and δ_j are starting time and duration time of control interval j . This also requires additional initial conditions. At initial steady state, system inputs should be at their set points

$$u_i^{sp}(0) = u_{i,0}, \quad i = 1, \dots, N_u \quad (4.30)$$

The initial steady state also implies that there is no change in the control trajectory (i.e. slopes in this case)

$$a_{i,0} = 0, \quad i = 1, \dots, N_u \quad (4.31)$$

The optimization variables are the set of parameters that define the control trajectory. In this case, it would be the slope set, namely

$$a_{i,j}, \quad i = 1, \dots, N_u; j = 1, \dots, N_J$$

The duration time of each control interval can be specified or optimized. In a study on switchability of distillation column (i.e. White *et al.* [1996]), control actions were also approximated using piecewise linear profiles. After applying these techniques, the true from

of the objective function for the second tier becomes:

$$\min_{\mathbf{a}, \delta} \Phi = t_f \left\{ \int_{t_0}^{t_f} \left[1 - \frac{F_{\text{GN}_2, \text{prod}}(t)}{F_{\text{GN}_2, \text{prod}}^*} \right]^2 dt + \sum_{i=1}^{N_u} w_i \left[1 - \frac{u_i(t_f)}{u_i^*} \right]^2 \right\} \quad (4.32)$$

Chapter 5

Case Studies

Optimization results following the proposed approach are presented in this chapter. Scenarios evaluated include both demand changes and electricity price fluctuations. The dynamic optimizations conducted are reactive, in the sense that no control actions take place prior to the change, either demand or electricity price, being introduced.

5.1 Optimization Platform

The commercial software package gPROMS 3.3.1 is used for simulation and optimization. The solver for DAEs in gPROMS is DASOLV, which solves the DAE set using backward differentiation formulae and following the predictor-corrector approach (Process System Enterprise Ltd [2004]). The solver selected for optimization is CVP_SS, which implements a single-shooting dynamic optimization algorithm. SRQPD, employing a sequential quadratic programming method, is used as the NLP (nonlinear programming) solver.

5.2 Steady-state Optimization

As explained in the formulation section, the steady state optimization is intended to obtain the desired operation points under the new scenarios. The decision variables selected in this study are:

- LN₂ production rate,
- gas draw fraction,
- volumetric flow rate of air feed under standard conditions,
- molar flow rate of liquid air feed to the column, and
- the rate of evaporation of LN₂ for unmet demand

as indicated in Table 3.1.

Scenarios considered in this study include: (1) demand fluctuations (i.e. positive and negative changes in demand requirements covering the range from +30 % to -30 %), and (2) electricity price increases (i.e. 2 and 4 times of the base case value) with and without the demand satisfaction requirement. Details of each scenario and corresponding steady state optimization results are tabulated in Table 5.1. Absolute and relative tolerances of the optimizer are set to 1e-5. ε_{surge} in Eqn. 4.5 is assigned to be 0. ε_{op} in Eqn. 4.8 is assigned to be $5e-5F_{prod,base}$. Safe margins are used on the modeling constraints (Eqns. 4.10 and 4.11):

$$P_{out,air} \geq \sum_{i=1}^{NC} y_{air,i} P_{out,i}^{sat} + 0.01$$

$$P_{withdrawal,air} \leq \frac{1}{\sum_{i=1}^{NC} y_{air,i} / P_{withdraw,i}^{sat}} - 0.01$$

If the value of the constrained variable is within $\pm 1e-4$ from the corresponding bound value, it is marked as an active constraint in Table 5.1. Data in the table are reported as ratios to

reference values. The evaporation rate is reported as percentage of the base case optimal (i.e. 0 % demand change) GN_2 production rate; the rest of the variables in Table 5.1 are presented as ratios to their corresponding base case values. The results presented are not guaranteed to be globally optimal due to the nonconvexity of the problem. However, while solving the problem, a number of different initial guesses were provided in each case, and the best solution point reported. The results of the case studies are discussed in the following sections.

5.2.1 Demand Fluctuation

The cases corresponding to demand changes were solved with all the constraints described in Section 4.2. Unmet demand and overproduction are both eliminated. As shown in Table 5.1, in the optimized cases, the LN_2 production is at its lower bound as there is no revenue associated with it. Note that the value 1 of LN_2 production in Table 5.1 corresponds to its lower bound. Also, the optimization results indicate that it is optimal to utilize available plant capacity before evaporating pre-stored LN_2 to meet the demand (i.e. evaporation only occurs with 20 % and 30 % demand increases, where the plant production is limited by the column flooding constraint). This is due to the high evaporation cost relative to the price of the GN_2 product. In all optimized cases, except the -30 % and -20 % demand change scenarios, the plant operates at its maximum allowable impurity level (i.e. indicated by the value of 1 in Table 5.1). By doing so, more GN_2 product can be generated from the same amount of feed. This can be seen from nitrogen recovery values in Table 5.1. Recall that the recovery of 1 corresponds to the base case value. In cases of -30 % and -20 % demand changes, it would be optimal in the absence of constraints for the plant to operate at the maximum allowable impurity level. However, it is impossible to reduce the feed flow rate to the value corresponding to the maximum allowable impurity as it is below the surge flow rate of the compressor. This is indicated by the active surge constraint of the compressor in these cases. Without overproduction, the plant operates with a lower recovery ratio and purer GN_2 product as more top tray vapor returns to the column as reflux rather than GN_2 product. The optimization results agree with expectation. For cases having large demand

Table 5.1: Steady-state optimization results for changing demand and electricity price.^a

		Demand							Electricity Price		
		0%	-30%	-20%	-10%	10%	20%	30%	$2P_{elec}$	$4P_{elec}$	$4P_{elec} + D$ ^b
Decision Variables	LN ₂ Production	1.00	1.00	1.00	1.00	1.00	1.00	1.00	1.00	1.00	1.00
	Gas Draw Fraction to PHX	1.00	0.79	0.90	1.00	1.00	1.01	1.01	1.01	1.00	1.00
	Air Feed	1.00	0.89	0.89	0.90	1.10	1.13	1.13	1.13	0.89	1.00
	Liquid Air	1.00	1.28	1.22	1.16	0.86	0.47	0.47	0.47	1.17	1.06
	Evaporation Rate	0	0	0	0	0	6.28	16.28	0	0	0
Objective Function		1.00	0.56	0.73	0.88	1.12	0.95	0.61	0.41	-0.97	-1.01
Tracking Variables	Nitrogen Recovery ^c	1.00	0.79	0.90	0.99	1.00	1.01	1.01	1.01	1.00	1.00
	GN ₂ Production	1.00	0.70	0.80	0.90	1.10	1.13	1.13	1.13	0.89	1.00
	Demand	1.00	0.70	0.80	0.90	1.10	1.20	1.30	N/A	N/A	1.00
	Impurity	1.00	0.25	0.50	1.00	1.00	1.00	1.00	1.00	1.00	1.00
Active Constraints	Maximum Allowable Impurity	X			X	X	X	X	X	X	X
	Surge Constraint		X	X						X	
	Bubble Point Constraint at PHX ^d	X	X	X	X					X	X
	Dew Point Constraint at PHX ^d						X	X	X		
	No Overproduction	X	X	X	X	X			N/A	N/A	
	Demand Satisfaction						X	X	N/A	N/A	X
	Flooding						X	X	X		

^a Data in the table are scaled values. Except for evaporation rate, which is reported as % of the base case air feed flow rate, the others are represented as ratios to their corresponding values at the base case (i.e. optimized 0 % demand change).

^b Solved with demand satisfaction requirement. The required demand is the base case production rate.

^c N₂ recovery rate in GN₂ and LN₂ products. Ratio of N₂ in product streams to N₂ in the air feed to the system.

^d Safe margins of 0.01 are used.

increases (i.e. +20 % and +30 %), the flooding constraint limits the plant performance. These active constraints imply that the operating window of the plant is defined by the flooding constraint (i.e. upper bound) and the surge constraint (i.e. lower bound) with respect to feed flow rate.

5.2.2 Electricity Price Change

For the electricity price change cases, without the demand satisfaction requirement, the total GN_2 supply (i.e. production plus evaporation) is not required to meet a particular demand, but it is not allowed to decrease below 70 % of a specified base case production rate (i.e. cases “ $2P_{elec}$ ” and “ $4P_{elec}$ ” in Table 5.1). The end-point inequality constraints on GN_2 production (Eqns. 4.7, 4.8) now become

$$(F_{\text{GN}_2,prod} + F_{evap}) - 0.7F_{prod,base} \geq 0.$$

When demand satisfaction is required (i.e. case “ $4P_{elec} + D$ ” in Table 5.1), Eqns. 4.7 is imposed. Other setups are the same as described in the demand change cases.

General trends observed in the electricity price scenarios are consistent with those in the demand fluctuation cases. Results of the “ $4P_{elec}$ ” case further support our argument that it is optimal to operate at the maximum allowable impurity level. As there is no constraint that eliminates overproduction in electricity price change scenarios, the plant is able to maximize the amount of top tray vapor drawn as GN_2 product, regardless of the actual demand requirement. In the “ $4P_{elec}$ ” case, with the similar amount of air feed (as in the 20 and 30 % demand decrease cases), the optimal policy is to maximize GN_2 production (or N_2 recovery) by operating at the maximum allowable impurity level. Again, when the feed flow rate reduces in the “ $4P_{elec}$ ” case, the surge constraint of the compressor becomes active and limits plant performance. Optimization results of the 2 times electricity price case agree with those of the +20 % and +30 % demand cases (i.e. operating at maximum allowable impurity and active flooding constraint). As GN_2 supply is not forced to meet a particular demand, LN_2 evaporation rates are kept at zero in the “ $2P_{elec}$ ” and “ $4P_{elec}$ ”

cases. When demand satisfaction is required (i.e. case “ $4P_{elec} + D$ ” in Table 5.1), it is still optimal to utilize the plant capacity to meet the demand instead of evaporating pre-stored LN_2 . This is expected due to the high evaporation cost used in the case study.

Remarks

Optimization results of the electricity price cases show an interesting point on the break-point between revenue from production and cost due to electricity consumption. When the electricity price increases, before it reaches a critical value, it is optimal to operate at the maximum plant capacity (defined by the flooding constraint). Within this range, the compression cost is still lower than the sale price of the GN_2 product. However, once the electricity price exceeds a break-point, it is beneficial to reduce production. Table 5.1 indicates that for the price information used in this study, the break point is between the 2 times and 4 times electricity price.

We can revisit the plant model presented in Chapter 3. The pressure drops within the column and the PHX are functions of the feed flow rate. However, such changes in the pressure profile of the plant would not be very large as indicated by the plant data which shows limited changes in pressure drops in response to changes in the flow rate. In addition, the condenser pressure is specified and constant in this study. Consequently, the discharge pressure of the compressor, hence the polytropic head of the compressor (defined by Eqn. 3.97), do not vary significantly. Recall that the power consumption of the compressor is a function of the flow and the polytropic head. This implies that the compressor power consumption is almost proportional to the feed flow rate in this case:

$$W_p \approx \alpha F_{feed} \implies 1 \text{ mol air feed} \approx \$ \alpha C_{elec} \text{ compression cost.}$$

On the other hand, as it is economically optimal to operate at the maximum allowable impurity level, the recovery rate of N_2 (i.e. $R_{recovery}$) is roughly constant. Recall that N_2 recovery rate is defined as ratio of N_2 in GN_2 and LN_2 product streams to the amount of N_2 in the air feed. The amount of GN_2 and LN_2 that can be generated from the feed is also

proportional to the feed flow rate. This gives

$$\begin{aligned} 1 \text{ mol air feed} &\implies 0.78 \text{ mol N}_2 \\ &\implies (0.78R_{recovery} - F_{LN2}) \text{ mol GN}_2 \implies \$ (0.78R_{recovery} - F_{LN2}) C_{GN_2} \text{ revenue.} \end{aligned}$$

Hence, the break-point can be roughly estimated as

$$C_{elec}^{bp} = \frac{0.78R_{recovery} - F_{LN2}}{\alpha} C_{GN_2} \quad (5.1)$$

Below this point, it would be beneficial to operate at maximum plant capacity, while above it, it is beneficial to cut back production. Applying Eqn. 5.1 to our case, the estimated break-point is consistent with the optimization result.

5.3 Dynamic Optimization for Existing Design

Case studies in this section consider transition to the optimized steady-state operating point without design modifications by using the first four inputs defined in Section 5.2. Note that the 2 times electricity price and the +30 % demand change cases have similar optimal steady state operating points as the +20 % demand case. Also, the steady-state optimization results for the 4 times electricity price, -30 % demand and -20 % demand scenarios are similar, except for the gas draw fraction and the liquid air flow rate. Hence, dynamic optimizations were only conducted for moving from the base case optimal point to the operating points of ± 20 % and ± 10 % demand change cases.

The objective function used is Eqn. 4.32, repeated here for convenience,

$$\min_{\mathbf{a}, \delta} \Phi = t_f \left\{ \int_{t_0}^{t_f} \left[1 - \frac{F_{GN_2,prod}(t)}{F_{GN_2,prod}^*} \right]^2 dt + \sum_{i=1}^{N_u} w_i \left[1 - \frac{u_i(t_f)}{u_i^*} \right]^2 \right\}$$

with the following weights assigned to the manipulated variables:

$$w_{air \text{ feed}} = w_{liq \text{ air}} = w_{gas \text{ draw}} = 1; \quad w_{LN_2} = 0.1.$$

The positive demand change cases were solved with 5 control intervals (i.e. $N_J = 5$) and absolute and relative tolerances of $1e-5$. In cases of negative demand changes, 6 control

Table 5.2: Dynamic Optimization Setup

	Number of Intervals	Duration Time	Input Slopes ^a
Initial Period ^b	1	Assigned (1 hr)	Assigned to 0
Control Period	N_J	Optimized $\left(\sum_{j=1}^{N_J} \delta_j\right)$	Optimized
Settling Period ^c	1	Assigned (3 hr)	Assigned to 0

^a $a_{i,j}$ in Eqn. 4.29.

^b This period is to ensure that the transition starts at the initial steady-state.

^c This period is to ensure that the system settles at a new steady-state.

intervals (i.e. $N_J = 6$) were used, and the absolute and relative tolerances were set to 1e-3. The number of control intervals is selected to be large enough to capture the control behavior, but not too large for undesired oscillations in the control trajectories to result. The tolerance setup is mainly due to the numerical challenges experienced.

The total time horizon was divided into 3 periods as shown in Table 5.2. The initial period is to ensure that transitions start at the initial steady-state operating point. At the end of the initial period, demand changes occur. In the control period, the plant takes action to respond to the market changes. Both the control trajectory slopes and control interval duration time are optimized. The final settling period is to ensure that the the system settles at a new steady-state and is stable after a period of time. Also, by introducing a settling period, the dynamic optimization solves more efficiently.

5.3.1 Positive 20 % Demand Change

Before applying dynamic optimization, a step test was performed to change the plant operation from the optimal base case to the optimized steady-state corresponding to a 20% demand increase. Fig. 5.1 plots the largest vapor velocity to flooding velocity ratio within the column. As shown, a direct step change is not desirable/applicable as it violates the

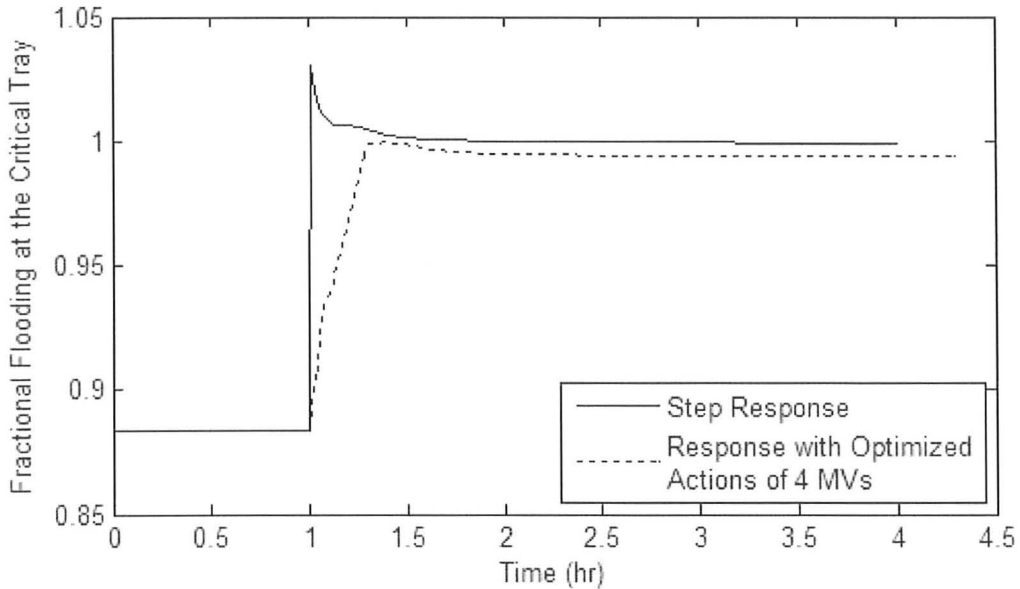


Figure 5.1: Fraction of vapor velocity to flooding velocity at critical tray for 20 % demand increase case

flooding constraint during the transition. This provides an incentive for performing dynamic optimization.

Fig. 5.2 presents dynamic responses of the GN_2 production and product impurity as well as the optimized control actions of the four manipulated variables. The variables are scaled in the same manner as in Table 5.1. The large magnitude of the scaled LN_2 production rate is because of its reference has a very small magnitude that is close to zero. Recall that the base case LN_2 production rate is at its lower bound. The trajectory of resulting GN_2 production is close to a step with small offsets at the beginning. The response of the product impurity is consistent with observations from the dynamic simulations in Section 3.10. There is an initial peak in product impurity with a decreasing internal L/V ratio due to:

- an increasing vapor air feed to the column due to an increase in air feed and a decrease in liquid air to column,
- a transient increasing LN_2 production, and

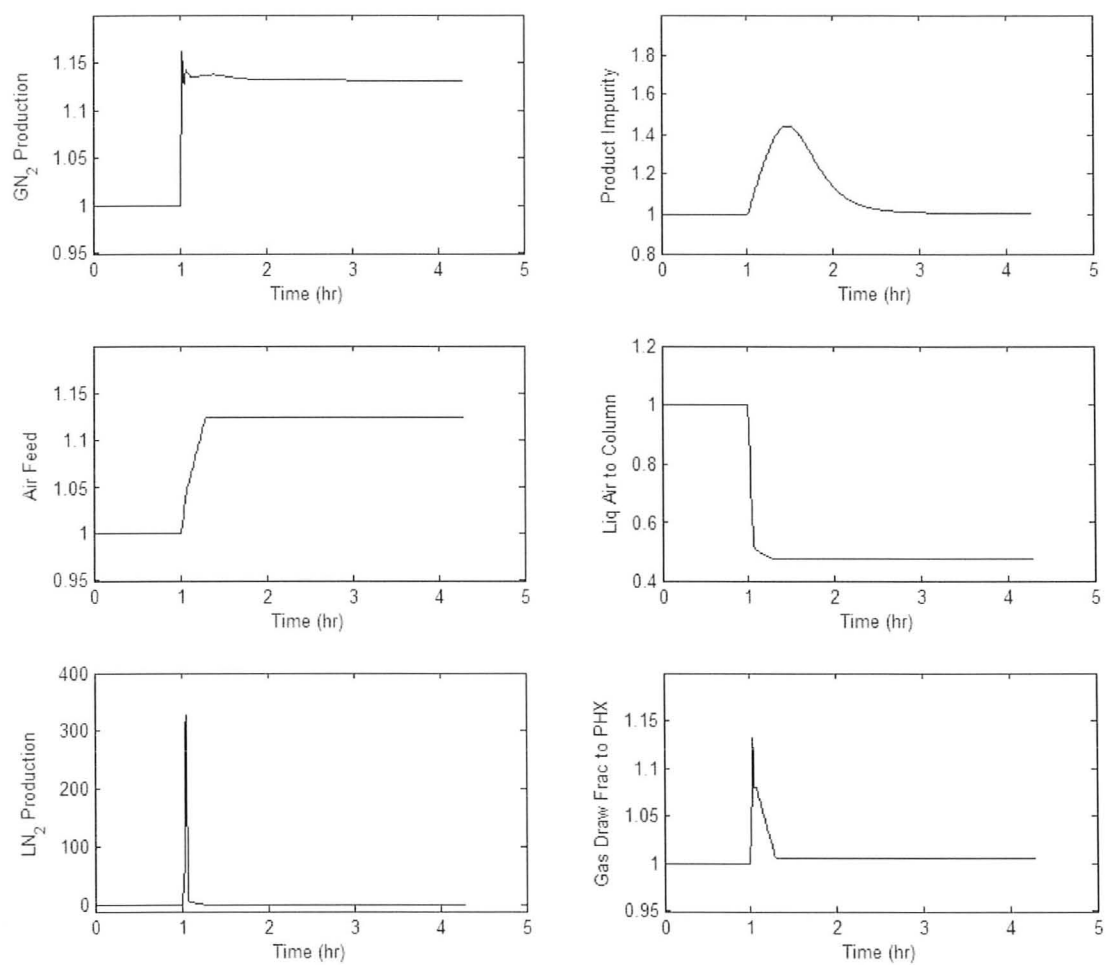


Figure 5.2: Responses of the scaled variables for the 20 % demand increase case with optimized control actions.

- an initial peak in gas draw fraction to the PHX.

The first factor leads to an increase in internal vapor flow while the other two lead to a relative decrease in internal liquid flow initially. Moreover, all variables reach steady-states at the end, with manipulated variables settling at their desired values within allowable tolerances. In contrast to the result for the direct step change, with the optimized control actions, the flooding constraint is active but not violated anymore (i.e. in Fig. 5.1). The dew point constraint at the PHX is another active constraint declared by the gPROMS solver.

5.3.2 Positive 10 % Demand Change

In Fig. 5.3, optimal dynamic responses to a 10 % demand increase in GN_2 production, product impurity, and the control actions of the four manipulated variables are plotted. Similar to the +20 % demand change case, the system reaches a steady-state at the end of the time horizon. The product impurity level peaks initially but the magnitude is smaller than that in the 20 % demand increase case. The four manipulated variables settle at their desired values within allowable tolerances. The speed of response is very similar in these two demand increase cases (i.e. in the GN_2 production). In both cases, the resulting GN_2 production experiences step like behavior. However, a relatively smaller initial overshoot, as well as smaller offsets during the transition, were observed in the GN_2 production trajectory in the 10 % demand increase case. The only active constraint declared by the gPROMS solver during the transition is the bubble point constraint at the PHX.

5.3.3 Negative 20 % Demand Change

Fig. 5.4 shows the optimal dynamic responses of the GN_2 production, product impurity, and control actions of the four manipulated variables for a 20 % decrease in GN_2 product demand. Consistent with observations from dynamic simulations in Section 3.10 and results of previous studies on increasing demands, the product impurity in this case decreases first then increases to the new steady-state value. However, as the impurity level at the new

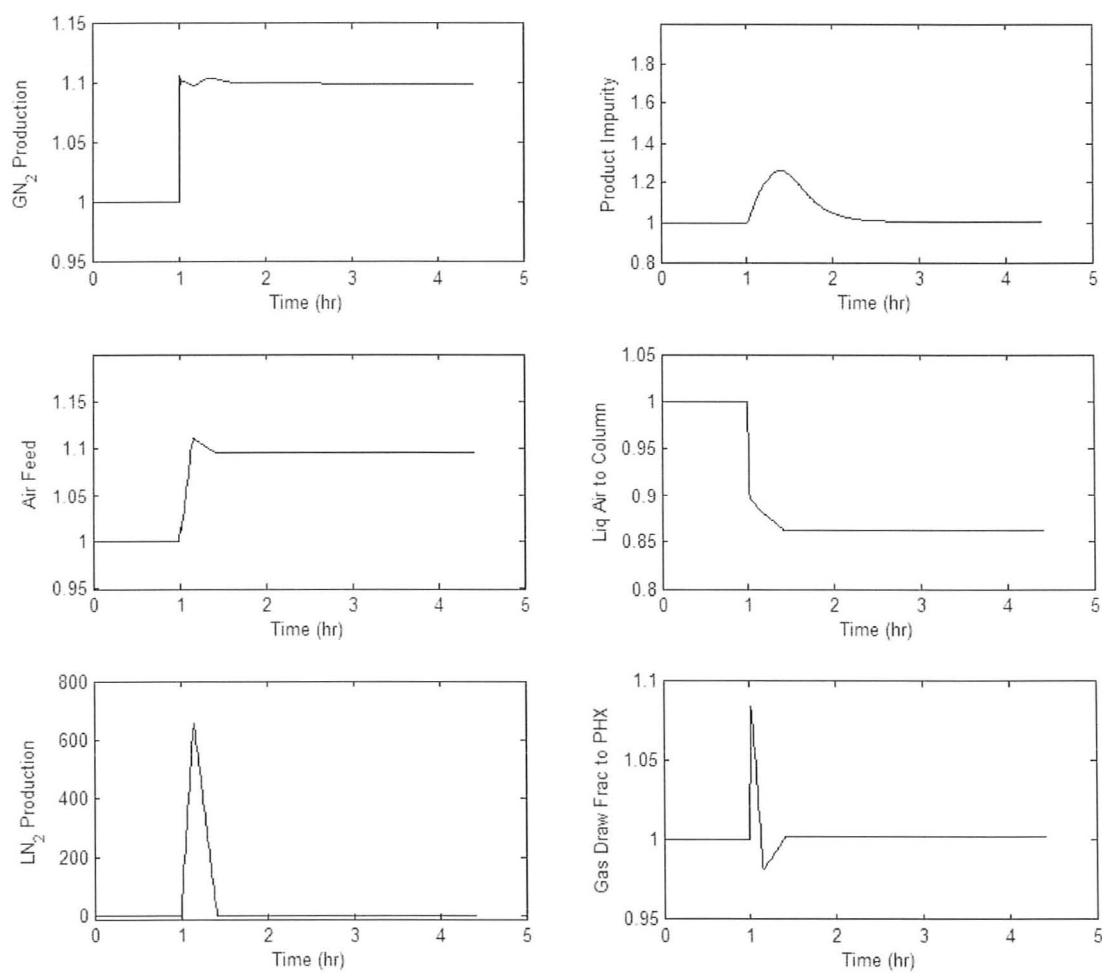


Figure 5.3: Responses of the scaled variables for the 10 % demand increase case with optimized control actions.

operating point is low, the trough is not that noticeable. Again, the system reaches a stable operating point with all control inputs at their optimal values and negligible offsets in GN_2 production. The response of the GN_2 production is step like. The surge constraint of the compressor and the bubble point constraint at the PHX are active during the transition.

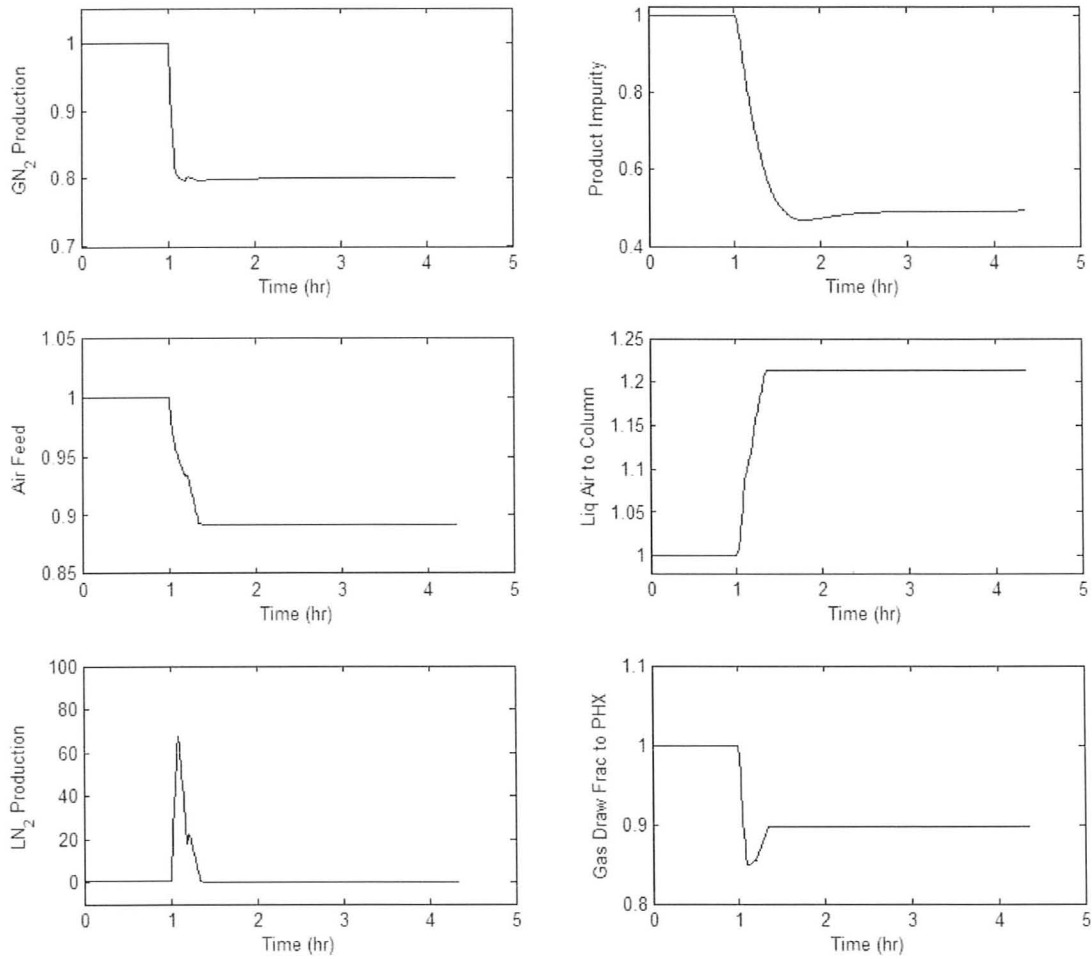


Figure 5.4: Responses of the scaled variables for the 20 % demand decrease case with optimized control actions.

5.3.4 Negative 10 % Demand Change

Dynamic responses of the GN_2 production and product impurity to the optimized control actions of the four manipulated variables for the -10 % demand change are plotted in Fig. 5.5. This time, the minimum in the product impurity is more clear. At the end of the time horizon, the system stabilizes at the pre-determined optimal operating point. The only active constraint declared by the optimizer is the bubble point constraint at the PHX. Compared to the GN_2 production trajectories in the demand increase cases, it was observed

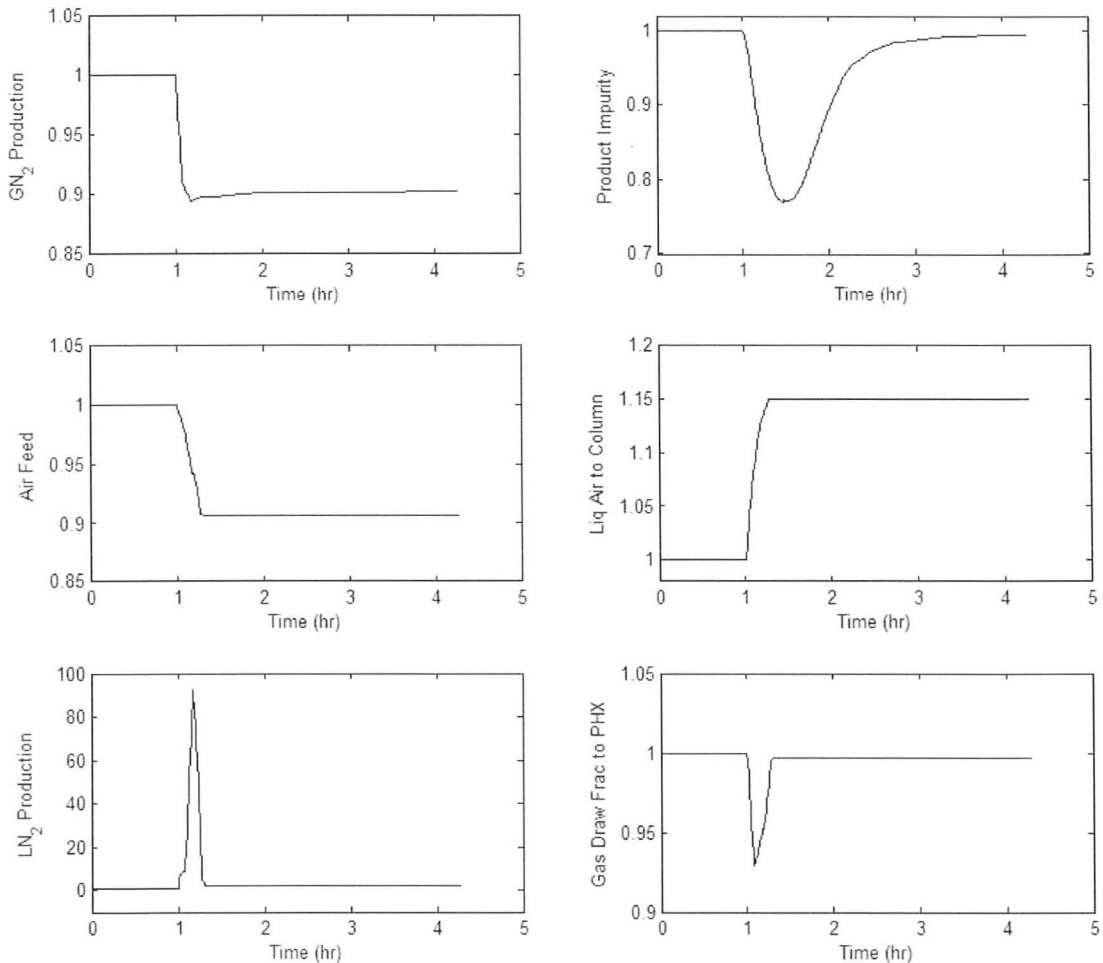


Figure 5.5: Responses of the scaled variables for the 10 % demand decrease case with optimized control actions.

that the system performs slightly worse in response to negative demand changes in a sense that the GN_2 production trajectories are not as steep as in the demand increase cases. In particular, the duration for the GN_2 production to first time reach the new steady state value in the demand decrease case is roughly five times of that in the demand increase case. Note that this is not the time required for the GN_2 production to stabilize at the new steady state value, but indicates the steepness of the initial decrease/increase in the GN_2 trajectory. However, we should not conclude that the dynamic performance for the demand decrease cases cannot be improved. There are many factors may influence the final results, such as: (1) profiles used to parameterize the control trajectories, e.g. piecewise constant versus piecewise linear, (2) the number of control intervals selected, and (3) the initial guess supplied for the optimization.

5.4 Effect of Introducing External Liquid Nitrogen during Transitions

In this section, the effect of introducing pre-stored external liquid nitrogen back to the column is studied. Miller *et al.* [2008a] demonstrated that re-introducing external liquid to the column can reduce start-up times. As the flooding constraint limits the plant performance during transitions for demand increase cases, it might be beneficial to introduce pre-stored LN_2 back to the column during transitions without altering the tray design. Fig. 5.6 illustrate the design modification for introducing pre-stored LN_2 . For simplicity, we assumed that the pre-stored LN_2 is at the same conditions and hence has the same properties as the reflux to the column. Control profiles of the external liquid nitrogen flows are treated in the same way as other system inputs as described in Chapter 4. The general form of the

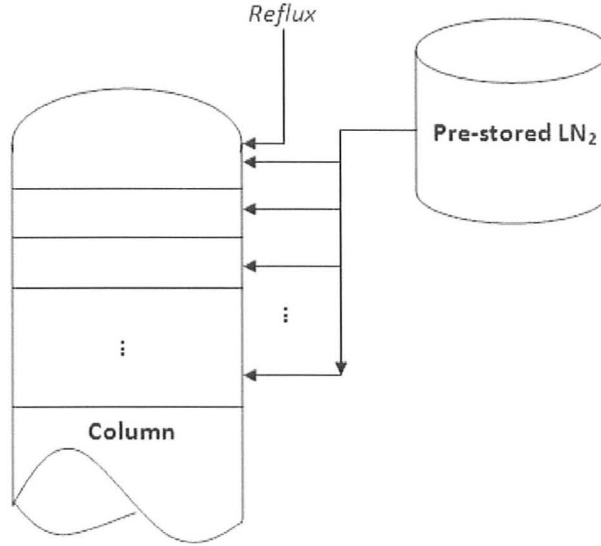


Figure 5.6: A schematic representation of the design modification for introducing pre-stored liquid nitrogen.

objective function used for evaluating this design modification is:

$$\min_{\mathbf{a}, \mathbf{b}, \delta} \Phi = t_f \left\{ \int_{t_0}^{t_f} \left[1 - \frac{F_{\text{GN}_2, \text{prod}}(t)}{F_{\text{GN}_2, \text{prod}}^*} \right]^2 dt + \sum_{i=1}^{N_u} w_i \left[1 - \frac{u_i(t_f)}{u_i^*} \right]^2 + w_{\text{acc}} \int_{t_0}^{t_f} \left[\sum_{k=1}^{N_{\text{ext}}} F_{\text{ext}, k}(t) \right]^2 dt + w_{\text{ext liq}} \sum_{k=1}^{N_{\text{ext}}} [F_{\text{ext}, k}(t_f)]^2 \right\} \quad (5.2)$$

\mathbf{b} is a matrix containing slopes of trajectories of the external LN_2 streams; w_{acc} and $w_{\text{ext liq}}$ are weights assigned to penalize the overall external LN_2 usage and the sum of squared deviations of LN_2 streams from zeros at t_f . $F_{\text{ext}, k}$ is the flow rate of the external LN_2 stream k . The integral term $\int_{t_0}^{t_f} \left[\sum_{k=1}^{N_{\text{ext}}} F_{\text{ext}, k}(t) \right]^2 dt$ is the squared overall usage, and together with the associated weighting parameter, is used to represent the cost associated with introducing external LN_2 to the column. The external liquid can only be used to help transitions, and is required to be zero at the final steady state. This gives an additional set of constraints in the dynamic optimization

$$F_{\text{ext}, k}(t_f) \leq \varepsilon_{\text{ext}}, \quad k = 1, \dots, N_{\text{ext}}. \quad (5.3)$$

Note this design alteration requires modifications of tray material and energy balances with or without manual index reductions. For trays having external LN₂ entering, there would be an additional term in the balances. To illustrate, for a regular column tray having an external liquid nitrogen feed, $F_{ext,k}$, the material balance on component i at tray n becomes,

$$\frac{dm_{n,i}}{dt} = l_{n+1,i} + v_{n-1,i} - l_{n,i} - v_{n,i} + x_{LN_2,i} F_{ext,k}.$$

The scenario selected is the 20 % demand increase case as the flooding constraint is active.

5.4.1 Multiple Trays

Base Case Impurity Specification

Case studies conducted under this category enforced a base case impurity constraint during transitions. It was assumed that the maximum allowable impurity level during transitions is two times of that at steady state. In other words, the plant keeps a safety margin of 100 % (i.e. according to steady state impurity upper bound) to allow the system to complete dynamic transitions without violating customer specifications at both steady state conditions and during transitions. This set of studies conducted allowed the introduction of pre-stored LN₂ to the top three column trays. Dynamic optimizations were performed and the result compared against the scenario without external liquid nitrogen (i.e. Section 5.3.2). Different combinations of control actions and control interval durations could result in similar dynamic performance. In other words, when both duration times and slopes are allowed to change, there are too many degrees of freedom (DOF). As a result, the duration times of the control intervals were fixed at the optimal values obtained in the previous study to reduce the DOF in the problem and provide a clearer comparison between cases with and without external LN₂. Weights assigned for the external LN₂ are:

$$w_{ext\ liq} = 100, w_{acc} = 0$$

without cost consideration, and

$$w_{ext\ liq} = 100, w_{acc} = 0.01$$

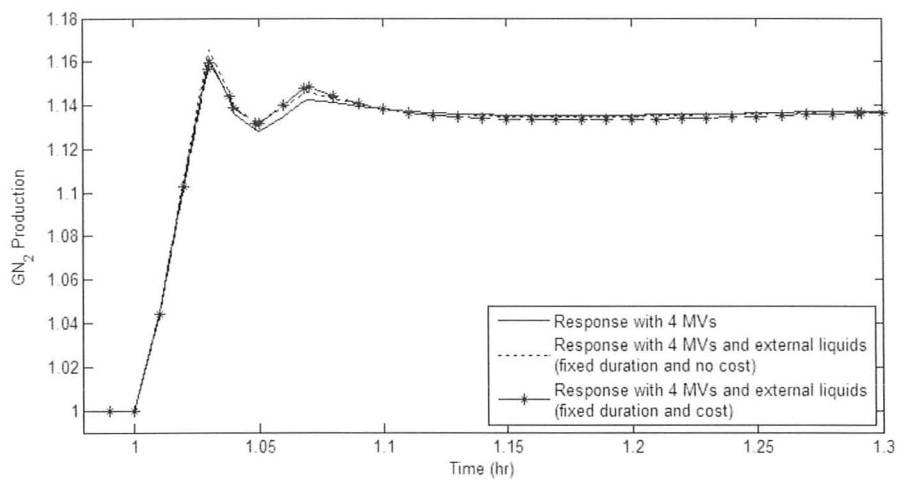
with cost consideration.

- Without Cost Consideration

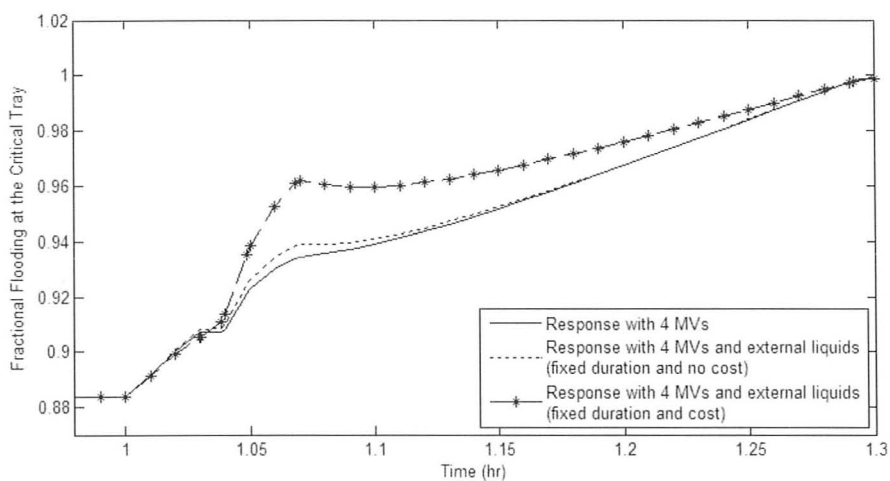
Here, we will outline the optimization results of introducing external LN_2 without considering the associated cost. Fig. 5.7 plots a magnified view of gas nitrogen production and fractional flooding at the critical tray in responses to the optimized control actions. With external LN_2 introduced, the system performs slightly better than the case without external liquid (i.e. a marginally more rapid change in the GN_2 production level with a slightly bigger overshoot), as illustrated in Fig. 5.7a. The fractional flooding is away from the constraint and is similar to that in the no external LN_2 case as shown in Fig. 5.7b. The optimal control trajectories are shown in Fig. 5.8. Gas nitrogen, product impurity, air feed, liquid air to the column, liquid nitrogen production, gas draw fraction and reflux flow are scaled according to their corresponding optimal base case values. External liquid flow rates of the top three trays are scaled as percentage of base case gas nitrogen production rate. The trajectories of the manipulated variables are very close to the case with no external liquid, except those of the liquid air feed to the column. Also, the reflux flow rate is slightly lower and the gas draw fraction to the PHX is slightly higher during the transition in the external LN_2 case. This was expected as the external liquid acts as additional reflux; hence, more top tray vapor can be drawn to the PHX instead of being sent back to the column. A more significant point is that with external LN_2 , the product impurity peak is lower during the transition. Active constraints in this scenario are: (1) dew point and bubble point constraints at the PHX, and (2) the flooding constraint in the column.

- With Cost Consideration

When the cost of introducing external LN_2 is considered, the overall amount of external liquid used during the transition is reduced to a level close to zero (Fig. 5.9). However, as shown in Fig. 5.7, the GN_2 production has a similar response as the other two cases (i.e. overshoots initially and reaches a new steady state at the end). The response of GN_2 production is slightly better than that in the no external liquid case, but worse than that in the no cost penalty case. Except the liquid air to the column, other manipulated variables have similar profiles to the no external liquid case. The fractional flooding is still away from



(a) Magnified view of gas nitrogen production.



(b) Fractional flooding at the critical tray.

Figure 5.7: Magnified views of gas nitrogen production and fractional flooding at the critical tray in responses to: optimized control actions of only the four manipulated variables (MVs); four MVs together with external LN₂ with and without cost considerations.

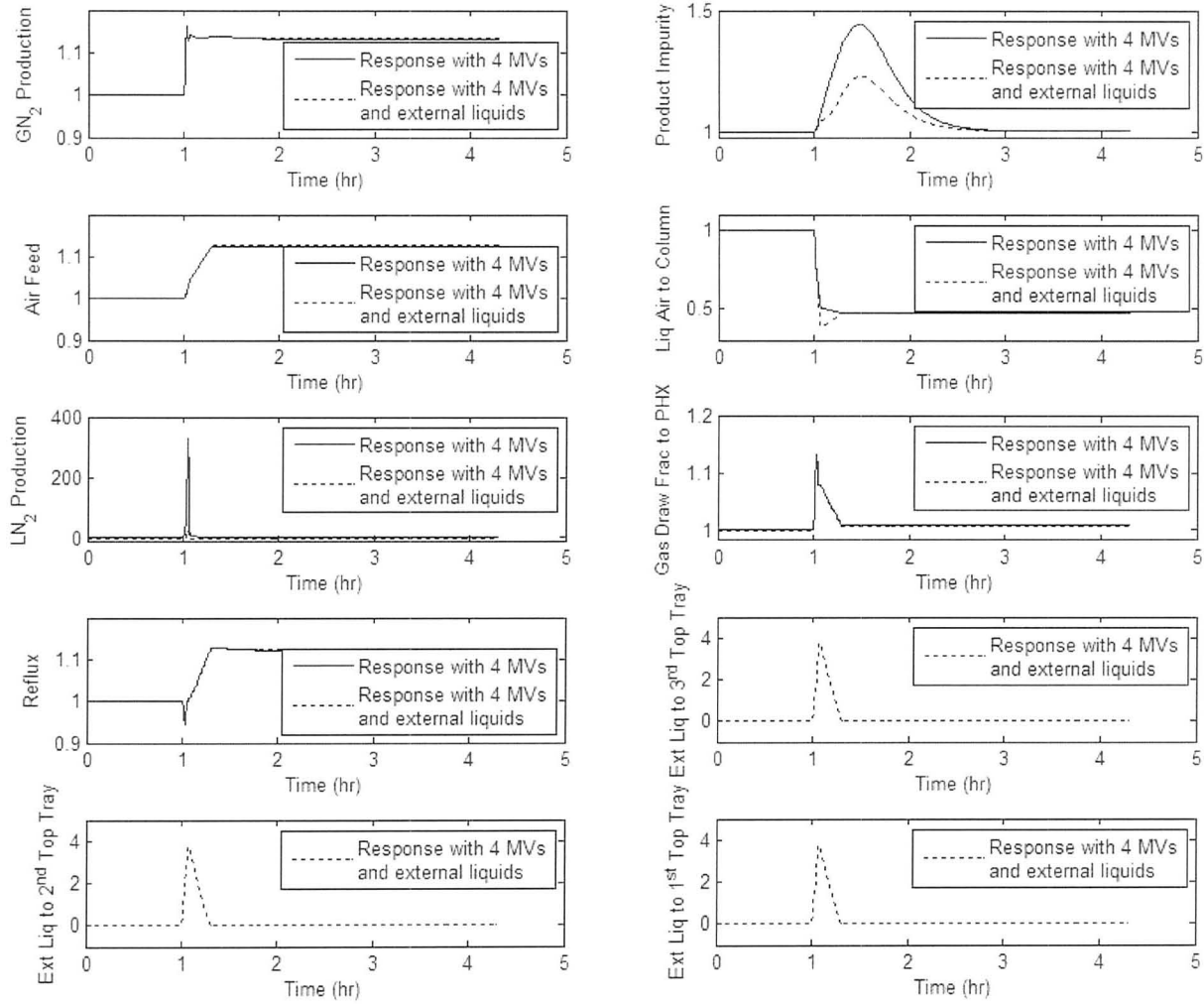


Figure 5.8: Optimized trajectories of scaled variables for 20 % demand increase cases with and without external liquid nitrogen. No cost penalty applied to external liquid.

its upper bound during the transition, but the response is worse than the case without the cost penalty. Note that the response of product impurity in this case is very close to that in the no external LN_2 case. However, the product impurity constraint is not a limiting factor for the plant performance. This indicates that there may be little incentive for introducing external LN_2 during transitions for this plant if associated costs are considered under the base case impurity requirement. Active constraints are: (1) dew point and bubble point constraints at the PHX, and (2) the flooding constraint in the column.

Tightened Impurity Constraint During Transitions

Case studies under this category were motivated by the observation that introducing external LN_2 can improve the plant dynamic performance during transitions in terms of product impurity level. This leads to the question, “What will happen when the product impurity constraint during transitions is tightened?” Case studies were subsequently conducted with the maximum impurity constraint level during transitions reduced to 120 % of the steady state impurity upper bound. This set of studies conducted allowed the introduction of pre-stored LN_2 to the top three column trays, and solved in a similar approach as the base case impurity level scenarios. The problem was solved first with four inputs only (optimizing both trajectory slopes and control interval durations). When external LN_2 was introduced, control durations times were fixed at the corresponding optimized durations, and trajectory slopes were optimized. No cost penalty was considered in this set of case studies.

Optimized trajectories are presented in Fig. 5.10. As shown, when the impurity constraint during transitions is tightened, with only the four inputs, the speed of transition deteriorates, with the GN_2 production rate well below the desired value for a period of approximately 20 minutes. As indicated in Table 5.3, the impurity constraint is active during the transition. When external LN_2 is allowed, a significant decrease in the transition speed can be achieved. The GN_2 production has a step-wise response as in the base case impurity cases (i.e. the GN_2 production almost immediately reaches and remains no lower than the desired value during the transition). Active constraints for the tightened impurity constraint cases are summarized in Table 5.3.

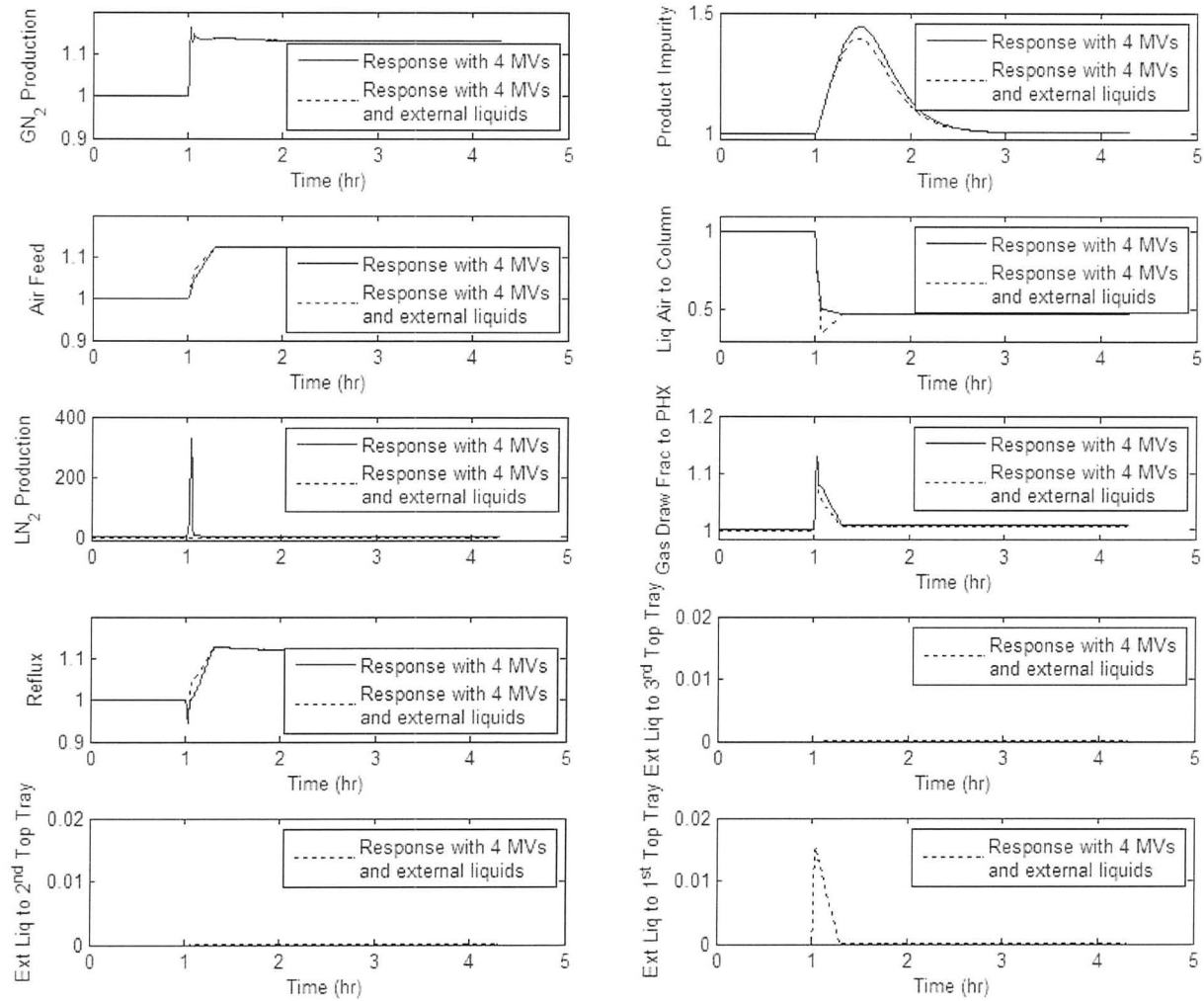


Figure 5.9: Optimized trajectories of scaled variables for 20 % demand increase case with cost penalty for external LN₂ usage.

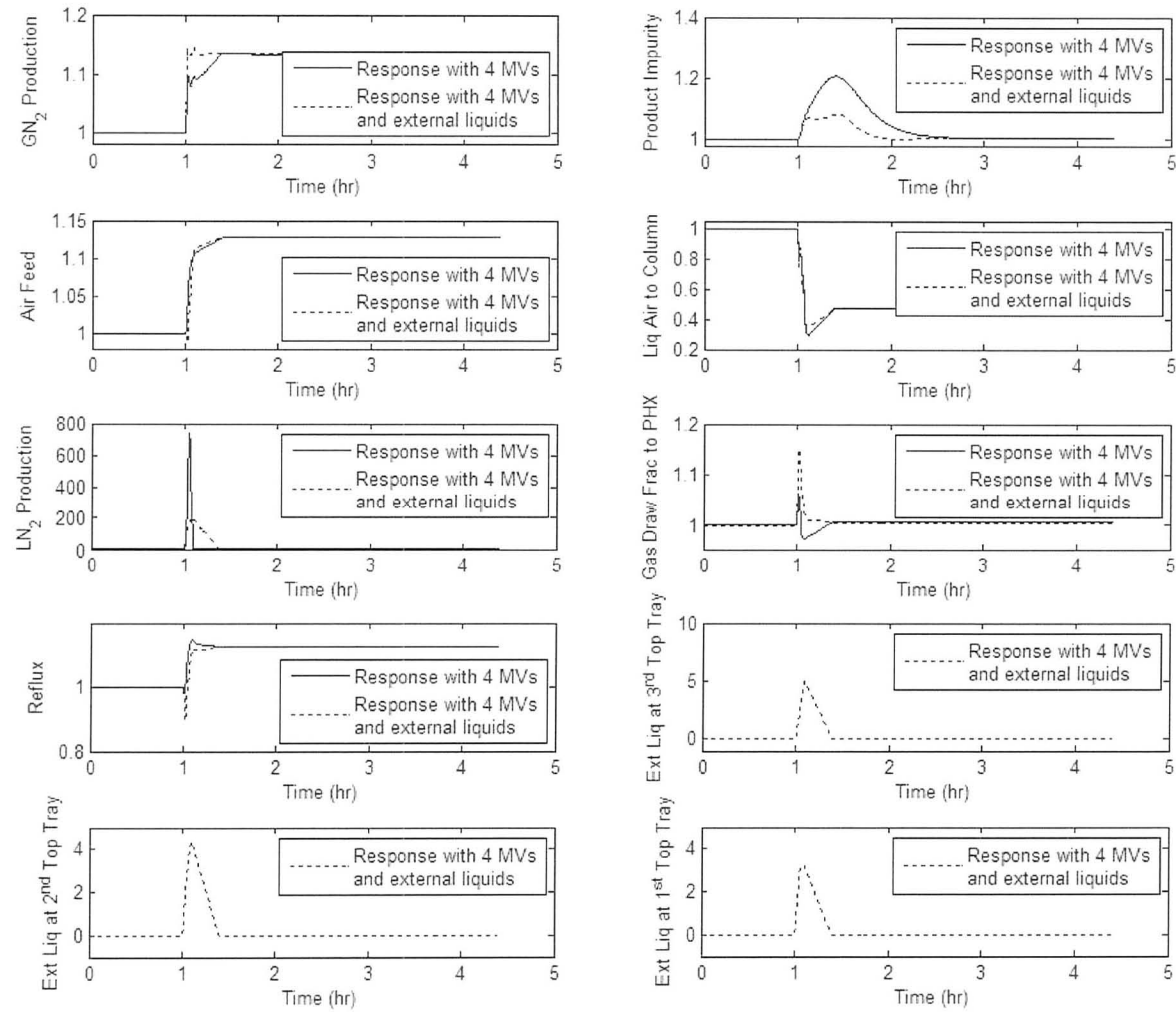


Figure 5.10: Optimized trajectories of scaled variables for 20 % demand increase case without cost penalty for external LN₂ usage and with tightened impurity constraint.

Table 5.3: Active constraints for case studies with tightened impurity constraints during transitions with and without external LN₂ to multiple trays.

Four Inputs Only	With External LN ₂ to Multiple Trays
<ul style="list-style-type: none"> • Maximum allowable impurity level, • flooding constraint in the column, and • dew point and bubble point constraints at the PHX. 	<ul style="list-style-type: none"> • Flooding constraint in the column, and • dew point and bubble point constraints at the PHX.

5.4.2 Single Tray

One may argue that even if introducing external liquid to multiple trays could be beneficial, it may not be practical to employ multiple external LN₂ streams due to the capital cost and operation considerations. Hence, a new set of case studies were compiled for introducing external LN₂ to only the top tray. The objective function and constraints are the same as the multiple tray case. This plant modification was evaluated under both the base case impurity requirement and the tightened impurity requirement. Responses are presented in Appendix C. General trends in this new set of studies are consistent with those in the multiple tray case. Under the base case impurity requirement, we have: faster transition in GN₂ production with initial overshoot; improvement in product purity during transitions in the case without cost consideration; and fractional flooding away from the bound. However, in the single tray case, the improvement in the product impurity level during transition becomes smaller compared to the corresponding multiple tray case. When the impurity constraint was tightened, a noticeable improvement in the transition speed was observed in the GN₂ production trajectories, but this improvement is not as significant as that in the multiple tray case (i.e. for a period of time initially, the GN₂ production cannot meet the desired value).

5.4.3 Remarks

These studies demonstrate that introducing external LN_2 to the column during transition can improve the dynamic performance of the system. For this particular plant setup, i.e. impurity requirements and tray design, etc., introducing external LN_2 may not be very cost-effective as the improvement is not that significant. This may be due to the fact that external LN_2 is only allowed during the transition and with only the four manipulated variables, the system is capable of achieving an acceptable dynamic performance without violating the flooding constraint during transition. However, when the impurity constraint during transitions is tightened, there is a great incentive to allow the introduction of external LN_2 during transitions as significant reductions in transition speed (i.e. in terms of GN_2 production rate) can be achieved when external LN_2 is introduced. This suggests that when introducing external LN_2 is allowed, the plant does not require as large a safety margin to avoid violations of the customer purity specification during transitions. This also implies that the plant can operate with a higher maximum impurity level at steady state. Incorporate the results from steady state case studies, this further leads to a higher profit.

5.5 Effect of Vent after the Compressor

Recall that the surge line of the compressor defines the limiting operation range of the compressor. Under normal conditions, the compressor operates on the right hand side of the surge line. Once the feed flow rate to the compressor reduces quickly below the restricted value, defined by the surge line (with fixed IGVA in our case), a reversal of flow occurs as the compressor is incapable of working against the already-compressed gaseous stream downstream (Neerken [1984], Brown [2005]). Allowing a vent stream at the outlet of the compressor is the simplest form anti-surge control (Neerken [1984]). As the surge constraint can be an active constraint during transition in the decreasing demand case, the option of allowing a vent stream at the outlet of the compressor is studied. The objective

function used in this case is derived similarly as in the external LN₂ studies,

$$\min_{\mathbf{a}, \mathbf{b}, \delta} \Phi = t_f \left\{ \int_{t_0}^{t_f} \left[1 - \frac{F_{\text{GN}_2, \text{prod}}(t)}{F_{\text{GN}_2, \text{prod}}^*} \right]^2 dt + \sum_{i=1}^{N_u} w_i \left[1 - \frac{u_i(t_f)}{u_i^*} \right]^2 + w_{\text{acc}} \int_{t_0}^{t_f} [F_{\text{vent}}(t)]^2 dt + w_{\text{vent}} [F_{\text{vent}}(t_f)]^2 \right\} \quad (5.4)$$

F_{vent} is the flow rate of the vent stream,

$$F_{\text{air to compressor}} = F_{\text{vent}} + F_{\text{compressor discharge}}.$$

The accumulated vent flow rate is minimized as the vent stream has a compression cost but no revenue associated with it. An additional endpoint inequality constraint is also introduced:

$$F_{\text{vent}}(t_f) \leq \varepsilon_{\text{vent}} \quad (5.5)$$

The weights are assigned as $w_{\text{acc}} = 0.001$ and $w_{\text{vent}} = 10$.

The problem was solved with fixing the control interval duration times at the optimal values determined in Section 5.3.3. Trajectories with the optimized control actions are presented in Fig. 5.11. Gas nitrogen, product impurity, air feed, liquid air to the column, liquid nitrogen production, gas draw fraction and reflux flow are scaled according to their corresponding optimal base case values. The vent flow rate is scaled as percentage of base case gas nitrogen production rate. Note that the vent flow rate is low, about 0.15 % of the base case GN₂ production rate. With this set of control actions, the resulting trajectories are not much different from those in the case without the vent stream. The improvement in the transition speed is not significant. This may be due to the fact that the surge constraint is not the only active constraint during the transition. However, with the vent stream, the fraction to surge moves slightly away from the bound. The surge constraint at the compressor and the bubble point constraint at the PHX are active in this case.

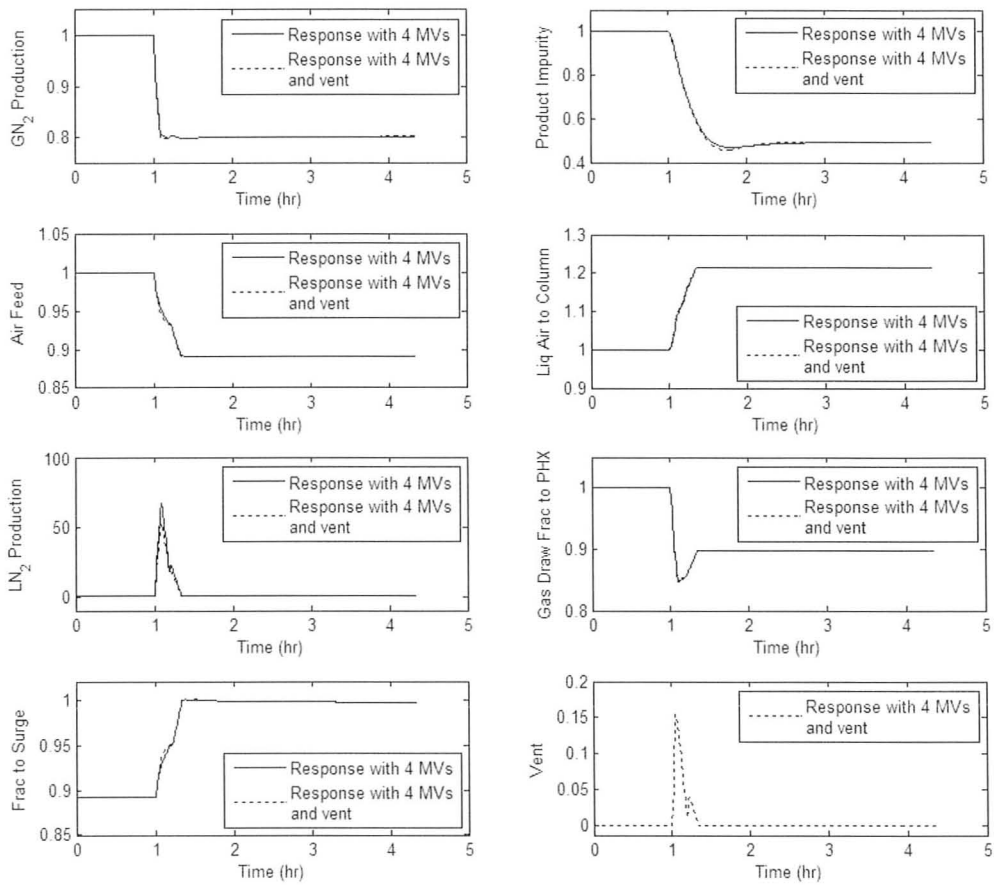


Figure 5.11: Optimized trajectories of scaled variables for 20 % demand decrease case, with and without a vent stream.

Chapter 6

Conclusions and Recommendations

6.1 Conclusions

This thesis considered an optimization-based framework for improving agility of a N_2 plant in response to a highly dynamic market, particularly demand and electricity price fluctuations. Rigorous dynamic models for the plant were developed and served as a foundation for the later optimization studies. The discussion below summarizes key findings and contributions of this thesis.

6.1.1 Process Modeling

Depending the assumptions made during model development, dynamic distillation models following the general approach as presented in Chapter 3 often result in systems of high-index DAEs. High-index DAE models impose numerical challenges in simulations and optimizations. An index reduction procedure utilizing the vapor-liquid phase equilibrium correlation and the dynamic energy balances has shown to be effective in improving model robustness and reducing simulation time. The time required in the initialization phase is shortened by a factor of more than 40 in the case presented. Discontinuities in the vapor phase enthalpy are handled using hyperbolic tangent function approximations, which have

been shown to be more efficient and less numerically challenging than IF-ELSE statements. Logarithmic transformations for the minor components can be used to improve variable scaling.

The dynamic model proposed for the primary heat exchanger considers phase change in the air feed stream after air withdraw occurs in the interior of the heat exchanger. This allows for separate liquid and vapor air feed to the column at different locations, which is consistent with the actual operating practice. Using three separate countercurrent processing streams, namely air feed, gaseous N_2 product and waste, in the model instead of combining GN_2 product and waste, as done in Miller *et al.* [2008a], also provides a closer representation of reality.

The surface fits obtained in the compressor model yield accurate predictions with the compressor maps available. By obtaining surface fits, the discharge pressure of the compressor is expressed as a continuous function of the inlet guide vane angle and the flow rate of the processing stream. Hence, model complexity is greatly reduced without significant losses in prediction accuracy. The turbine is modelled in a similar fashion as the compressor.

After parameter estimation, model predictions yield an adequate consistency with plant measurements, with a maximum relative error of 1.27 %. In addition, trajectories of dynamic simulations in response to step changes in different system inputs also have good agreement with expectation. When there is a decrease in the air feed flow rate, the vapor feed to the column decreases. As the gas draw fraction is fixed, this further leads to a reduction in GN_2 production rate. Due to differences in the dynamic time constant, a decrease in product impurity is observed initially. When there is an increase in the gas draw fraction, the reflux rate relative to the air feed at the new steady state is much lower than before and a significant increase in the product impurity level was observed.

6.1.2 Steady State Optimization

Steady state optimization is the first tier of the optimization problem. In this stage, different scenarios in terms of demand changes and electricity price fluctuations were explored. The decision variables selected are the system specifications (i.e. air feed volumetric flow rate, liquid air feed flow rate to the column, gas draw fractions to the PHX and LN₂ production rate), together with the option of evaporating liquid nitrogen for meeting unsatisfied demand. Even though results obtained in these studies are not guaranteed to be globally optimal due to the structure of the problem, the general trends are still important.

In all optimized cases, the LN₂ production rate and rate of evaporation remain at their lower bounds. These results agree with expectation considering the zero revenue for LN₂ product and the high cost of evaporation. Also, operating close to the maximum allowable impurity level is optimal as it gives a high recovery rate. There are two major findings in the steady state optimization studies:

Operating window of the plant

The operating window of the plant is defined by the flooding constraint of the distillation column and the surge constraint of the compressor when the feed flow rate is considered.

Break-even points of fluctuating electricity price

It is optimal under the base case electricity price to operate at the highest possible production rate. When electricity price increases, before reaching a critical value, it is still economically optimal to remain at high production levels; however, once the electricity price exceeds that value, it is beneficial to reduce production.

6.1.3 Dynamic Optimization

Dynamic optimizations were performed to switch the system from the base case operating point to the new operating point determined from the steady state optimization without vi-

olating plant constraints. A trajectory tracking objective function with endpoint inequality constraints to “pin-down” the final states to the pre-determined optimal values was solved in each case. As discussed earlier, such a formulation would enforce rapid transitions to the pre-determined economically optimal steady state operating points. Without the optimized control actions, severe constraint violation may occur during transitions as shown in the 20 % demand increase case. With optimized control action, a fast transition without constraint violations can be achieved. As demonstrated by the resulting trajectories, with the four control inputs selected, plants can complete the transition in less than 30 minutes. Moreover, responses of GN_2 production are step-like. The plant achieves the new production rate rapidly.

In addition, two design alternatives to improve the dynamic performance were investigated:

Introducing external LN_2 during transitions

Case studies demonstrate that introducing external liquid to the column during transition can improve the dynamic performance of the system. Positive impacts of this design alternative on avoiding column flooding and preventing impurity constraint violations were observed. Even though for this particular plant setup, i.e. impurity requirements and tray design, etc., introducing external LN_2 may not be cost-effective, this design modification is very attractive as it allows a smaller operating safety margin, which could result in more profitable steady-state operation.

Vent stream after the compressor

Allowing a vent stream after the compressor to prevent compressor surge does not result in a significant improvement in the dynamic performance. This could be due to the fact that there are other active constraints during transition. This design alternative is not that attractive especially considering the associated cost. However, when working with a different plant, it is worth re-evaluating.

6.2 Recommendations for Further Work

This project opens many opportunities for future work - the most interesting of which are summarized below.

6.2.1 Distillation Column Modeling

The first interesting avenue to explore lies in modeling of distillation columns. As explained in Section 3.2.2, several authors remarked that the high-index issue of dynamic distillation model following the general approach could be due to neglecting vapor holdups at each tray. Hence, it is worth developing a dynamic model considering the dynamics of vapor holdups together with the liquid holdups at each column tray. In this case, the energy balances are recommended to be derived using internal energy as done in Bansal *et al.* [2002].

Also, performing a systematic analysis on the index of the distillation model following approaches proposed in Gani and Cameron [1992] would be helpful. However, considering the size of the problem, it might be too expensive to accomplish this task. Another alternative is to employ available software packages. For example, DAETS is stated to be able to determine the underlying structure of DAE systems at its structural analysis stage (Nedialkov and Pryce [2009]). Moreover, the structural analysis also indicates variables to be specified for consistent initialization. These may serve as a starting point to more fully understand and resolve the high-index issue of dynamic distillation models. Issues to be investigated include variable selections (e.g. explicit vs. implicit variables), process specification, forcing function (e.g. pressure drop as driving force for vapor flow), etc.

6.2.2 Varying Efficiency

In this thesis, we assume a constant tray efficiency regardless of the load of the system. However, in reality, tray efficiency changes in accordance with column loads and tray conditions (Lockett [1986]). When the tray condition is closer to critical tray conditions, such

as weeping (i.e. due to insufficient vapor flow) and flooding (i.e. due to excessive vapor flow), dramatic changes in separation efficiency occur. Lockett [1986] provides an extensive summary of correlations for predicting tray efficiencies. An alternative approach would be to develop empirical correlations for the column load and separation efficiency.

6.2.3 Disturbance and Uncertainty

This project did not consider the presence of either disturbances or uncertainty. In the dynamic energy balance, we consider a “heat leakage term”, which is the heat transfer between the cold box and the ambient surrounding due to the temperature difference. Also, air separation processes use ambient air as the raw material. Hence, fluctuations in ambient conditions would be an important disturbance on the system performance. In all studies performed, the ambient temperature was assumed to be constant. However, in reality, there are temperature fluctuations within a day (e.g. day and night) and repeated seasonal cycles. Even though this project is not intended for disturbance rejection, the control profiles to achieve fast transitions may differ with disturbances introduced.

Zhu *et al.* [2010] summarized uncertainties that should be considered for process flexibility: process performance, product demand and pricing, as well as process input availability and pricing. In the area of our interest, uncertainty could be in customer demand and electricity price. It might be interesting to investigate process performance under these uncertainties. The problem could be formulated using the multi-scenario approach as in the study of Zhu *et al.* [2010].

6.2.4 Multiple Column Air Separation Plants

N₂ plants are the simplest representation of an air separation plant, but it still capture the essential structures of more complex plant configurations. Studies in this project have shown promising results in improving plant agility utilizing an optimization-based approach. It would be interesting to apply this approach to a multiple column air separation plant as

described in Chapter 2. This topic will require developing dynamic models for the upper column and the super-stage argon column prior to optimization following either a manual index reduction approach or refined approach through detailed index analysis. When the model index is 1, dynamic optimization can be performed with other available commercial packages that implement different solution algorithms that may be more suitable and robust for large scale nonlinear dynamic optimization.

List of References

- ALPEMA (2000). *The standards of the Brazed Aluminium Plate-Fin Heat Exchanger Manufacturers' Association*. Brazed Aluminium Plate-Fin Heat Exchanger Manufacturers' Association, 2 edition.
- ASCHER, U. M. AND PETZOLD, L. R. (1998). *Computer Methods for Ordinary Differential Equations and Differential-Algebraic Equations*. Society for Industrial and Applied Mathematics.
- AVEROUS, D., HAMMADI, K., PINGAUD, H., JOULIA, X., AND GUITTARD, P. (1999). Dynamic simulation of brazed plate-fin heat exchangers. *Computers & Chemical Engineering*, **23**(Supplement 1), S447 – S450.
- BAKER, R. AND SWARTZ, C. L. E. (2004). Simultaneous solution strategies for inclusion of input saturation in the optimal design of dynamically operable plants. *Optimization and Engineering*, **5**(1), 5 – 24.
- BALLARD, D., BROSILOW, C., AND KAHN, C. (1978). Dynamic simulation of multicomponent distillation columns. In *AIChE Meeting, Paper No. 42a, Miami, Miami, USA, October*.
- BANSAL, V., PERKINS, J. D., AND PISTIKOPOULOS, E. N. (2002). A case study in simultaneous design and control using rigorous, mixed-integer dynamic optimization models. *Industrial & Engineering Chemistry Research*, **41**(4), 760 – 778.

- BANSAL, V., ROSS, R., PERKINS, J. D., AND PISTIKOPOULOS, E. N. (2000). The interactions of design and control: Double-effect distillation. *Journal of Process Control*, **10**, 219 – 227.
- BIAN, S., HENSON, M. A., BELANGER, P., AND MEGAN, L. (2005a). Nonlinear state estimation and model predictive control of nitrogen purification columns. *Industrial & Engineering Chemistry Research*, **44**(1), 153 – 167.
- BIAN, S., KHOWINIJ, S., HENSON, M. A., BELANGER, P., AND MEGAN, L. (2005b). Compartmental modeling of high purity air separation columns. *Computers & Chemical Engineering*, **29**(10), 2096 – 2109.
- BIEGLER, L. T. (2000). *Differential-Algebraic Equations (DAEs)*. Chemical Engineering Department, Carnegie Mellon University, Pittsburgh, PA.
- BIEGLER, L. T. (2007). An overview of simultaneous strategies for dynamic optimization. *Chemical Engineering and Processing: Process Intensification*, **46**(11), 1043 – 1053.
- BIEGLER, L. T., CERVANTES, A. M., AND WÄCHTER, A. (2002). Advances in simultaneous strategies for dynamic process optimization. *Chemical Engineering Science*, **57**(4), 575 – 593.
- BIEGLER, L. T. AND GROSSMANN, I. E. (2004). Retrospective on optimization. *Computers & Chemical Engineering*, **28**(8), 1169 – 1192.
- BROWN, R. N. (2005). *Compressors: Selection and Sizing*. ELSEVIER.
- CANNEY, W. M. (1996). Model predictive control method for an air-separation system (United States patent 5522224). United States Patent.
- CAO, Y., BISS, D., AND PERKINS, J. D. (1996). Assessment of input-output controllability in the presence of control constraints. *Computers & Chemical Engineering*, **20**(4), 337 – 346.
- CERVANTES, A. AND BIEGLER, L. T. (2009). Optimization strategies for dynamic systems. In Floudas, C. A. and Pardalos, P. M. (Eds.), *Encyclopedia of Optimization*, pp. 2847 – 2857. Springer Science+Business Media, 2 edition.

- CHACHUAT, B. (2009). *Optimal Control (Lecture 19 - 20): Direct Solution Method*. Department of Chemical Engineering. McMaster University, 1280 Main Street West, Hamilton, ON, Canada.
- CHO, Y. S. AND JOSEPH, B. (1983). Reduced-order steady-state and dynamic models for separation processes. Part II. Application to nonlinear multi-component systems. *AIChE Journal*, **29**, 270 – 276.
- COSTA Jr., E. F., VIEIRA, R. C., SECCHI, A. R., AND BISCAIA Jr., E. C. (2003). Dynamic simulation of high-index models of batch distillation processes. *Latin American Applied Research*, **33**, 155 – 160.
- ESPIE, D. M. AND PAPAGEORGAKI, S. C. (1998). Validation of dynamic simulation models of cryogenic air separation processes. In *11th Intersociety Symposium, Houston, Texas, USA*, pp. 91 – 98, Houston, Texas, USA, January.
- FEEHERY, W. F. AND BARTON, P. I. (1999). Dynamic optimization with equality path constraints. *Industrial & Engineering Chemistry Research*, **38**(6), 2350 – 2363.
- FIKAR, M., LATIFI, M. A., AND CREFF, Y. (1999). Optimal changeover profiles for a industrial depropanizer. *Chemical Engineering Science*, **54**, 2715 – 2720.
- GANI, R. AND CAMERON, I. T. (1992). Modelling for dynamic simulation of chemical processes : the index problem. *Chemical Engineering Science*, **47**(5), 1311 – 1315.
- GEORGIADIS, M. C., SCHENK, M., PISTIKOPOULOS, E. N., AND GANI, R. (2002). The interaction of design, control and operability in reactive distillation systems. *Computers & Chemical Engineering*, **26**, 735 – 746.
- GREEN, D. W., MALONEY, J. O., AND PERRY, R. H. (1997). *Perry's Chemical Engineers' Handbook*. McGRAW-HILL.
- HANGOS, K. AND CAMERON, I. (2001). Dynamic models — lumped parameter systems. In Stephanopoulos, G. and Perkins, J. (Eds.), *Process Modeling and Model Analysis*, Vol. 4 of *Process System Engineering*. Academic Press.

- HANSON, T. C. (1993). Statistical process control for air separation process (United States patent 5257206). United States Patent.
- HEATH, M. T. (2002). *Scientific Computing: An Introductory Survey*. McGraw-Hill, Boston, 2 edition.
- HUANG, R., ZAVALA, V. M., AND BIEGLER, L. T. (2009). Advanced step nonlinear model predictive control for air separation units. *Journal of Process Control*, **19**(4), 678 – 685.
- HUSS, R. S. AND WESTERBERG, A. W. (1996). Collocation methods for distillation design. 1. model description and testing. *Industrial & Engineering Chemistry Research*, **35**(5), 1603 – 1610.
- INFOCHEM COMPUTER SERVICES LTD (2008). *User Guide for Models and Physical Properties*. Infochem Computer Services Ltd.
- KADAM, J. AND MARQUARDT, W. (2007). Integration of economical optimization and control for intentionally transient process operation. In Findeisen, R., Allgöwer, F., and Biegler, L. (Eds.), *Assessment and Future Directions of Nonlinear Model Predictive Control*, Vol. 358 of *Lecture Notes in Control and Information Sciences*, pp. 419 – 434. Springer Berlin / Heidelberg.
- KIENLE, A. (2000). Low-order dynamic models for ideal multicomponent distillation processes using nonlinear wave propagation theory. *Chemical Engineering Science*, **55**(10), 1817 – 1828.
- LOBANOFF, V. S. AND ROSS, R. R. (1992). *Centrifugal Pumps: Design & Application*. Gulf Professional Publishing, 2 edition.
- LOCKETT, M. J. (1986). *Distillation Tray Fundamentals*. Cambridge University Press.
- MILLER, J., LUYBEN, W. L., BELANGER, P., BLOUIN, S., AND MEGAN, L. (2008a). Improving agility of cryogenic air separation plants. *Industrial & Engineering Chemistry Research*, **47**, 394 – 404.

- MILLER, J., LUYBEN, W. L., AND BLOUIN, S. (2008b). Economic incentive for intermittent operation of air separation plant with variable power costs. *Industrial & Engineering Chemistry Research*, **47**, 1132 – 1139.
- MOHIDEEN, M. J., PERKINS, J. D., AND PISTIKOPOULOS, E. N. (1996). Optimal design of dynamic systems under uncertainty. *AIChE Journal*, **42**, 2251 – 2272.
- MORARI, M. (1983). Design of resilient processing plants–III : A general framework for the assessment of dynamic resilience. *Chemical Engineering Science*, **38**(11), 1881 – 1891.
- NARRAWAY, L. T. AND PERKINS, J. D. (1993). Selection of process control structure based on linear dynamic economics. *Industrial & Engineering Chemistry Research*, **32**(11), 2681 – 2692.
- NEDIALKOV, N. S. AND PRYCE, J. D. (2008-2009). *DAETS User Guide, Version 1.1*.
- NEERKEN, R. F. (1984). Keys to compressor selection. In Greene, R. (Ed.), *The Chemical Engineering Guide to Compressors*, pp. 14 – 30. MCGRAW-HILL.
- PENG, D.-Y. AND ROBINSON, D. B. (1976). A new two-constant equation of state. *Industrial & Engineering Chemistry Fundamentals*, **15**(1), 59 – 64.
- PROCESS SYSTEM ENTERPRISE LTD (2004). *gPROMS Introductory User Guide*. Process System Enterprise Ltd.
- PROCESS SYSTEM ENTERPRISE LTD (2009). *Optimisation and Model Validation with gPROMS*. Process System Enterprise Ltd.
- PROCESS SYSTEM ENTERPRISE LTD (2010). Personal Communication.
- PROKOPAKIS, G. J. AND SEIDER, W. D. (1983). Dynamic simulation of azeotropic distillation towers. *AIChE Journal*, **29**, 1017 – 1029.
- RAGHUNATHAN, A. U., SOLEDAD DIAZ, M., AND BIEGLER, L. T. (2004). An MPEC formulation for dynamic optimization of distillation operations. *Computers & Chemical Engineering*, **28**(10), 2037 – 2052.

- RAVINDRAN, A., RAGSDELL, K. M., AND REKLAITIS (2006). *Engineering Optimization: Methods and Applications*. John Wiley & Sons, Inc., New York, 2 edition.
- REID, R. C., PRAUSNITZ, J. M., AND SHERWOOD, T. K. (1977). *The Properties of Gases and Liquids*. McGRAW-HILL, 3 edition.
- ROFFEL, B., BETLEM, B. H. L., AND RUIJTER, J. A. F. (2000). First principles dynamic modeling and multivariable control of a cryogenic distillation process. *Computers & Chemical Engineering*, **24**, 111 – 123.
- SAKIZLIS, V., PERKINS, J. D., AND PISTIKOPOULOS, E. N. (2004). Recent advances in optimization-based simultaneous process and control design. *Computers & Chemical Engineering*, **28**(10), 2069 – 2086.
- SIRDESHPANDE, A. R., IERAPETRITOU, M. G., ANDRECOVICH, M. J., AND NAUMOVITZ, J. P. (2005). Process synthesis optimization and flexibility evaluation of air separation cycles. *AIChE Journal*, **51**(4), 1190 – 1200.
- SMITH, J. M., VAN NESS, H. C., AND ABBOTT, M. M. (2005). *Introduction to Chemical Engineering Thermodynamics*. McGRAW-HILL, 7 edition.
- SWARTZ, C. L. E. (1989). Data reconciliation for generalized flowsheet applications. In *American Chemical Society National Meeting*, Dallas, TX.
- SWARTZ, C. L. E. (1996). A computational framework for dynamic operability assessment. *Computers & Chemical Engineering*, **20**(4), 365 – 371.
- TRIERWEILER, J. AND ENGELL, S. (2000). A case study for control structure selection: air separation plant. *Journal of Process Control*, **10**(2 - 3), 237 – 243.
- UNGER, J., KRÖNER, A., AND MARQUARDT, W. (1995). Structural analysis of differential-algebraic equation systems — theory and applications. *Computers & Chemical Engineering*, **19**(8), 867 – 882.
- VAN SCHIJNDEL, J. M. G. AND PISTIKOPOULOS, E. N. (2000). Towards the integration of process design, process control & process operability – current status & future trends.

- In Malone, M., Trainham, J., and Carnahan, B. (Eds.), *Foundations of computer aided process design 99*, number 323 in AIChE symposium series, pp. 99 – 112. American Institute of Chemical Engineers.
- WHITE, V., PERKINS, J. D., AND ESPIE, D. M. (1996). Switchability analysis. *Computers & Chemical Engineering*, **20**(4), 469 – 474.
- ZHU, G., HENSON, M. A., AND MEGAN, L. (2001). Low-order dynamic modeling of cryogenic distillation columns based on nonlinear wave phenomenon. *Separation and Purification Technology*, **24**, 467 – 487.
- ZHU, Y., LEGG, S., AND LAIRD, C. D. (2010). Optimal design of cryogenic air separation columns under uncertainty. *Computers & Chemical Engineering*, **34**(9), 1377 – 1384.
- ZHU, Y., LIU, X., AND ZHOU, Z. (2006). Optimization of cryogenic air separation distillation columns. In *6th World Congress on Intelligent Control and Automation, Dalian, China*, pp. 7702 – 7705.

Appendix A

Numerical Issues

A.1 Step-wise Discontinuity

In this project, step-wise discontinuity occurred in vapor phase molar enthalpy estimation under cryogenic conditions. Recall from Section 3.2.1 the expression for the vapor phase molar enthalpy

$$h^{vap} = \sum_{i=1}^{NC} \left[y_i \left(a_j^{vap} + b_j^{vap} T \right) \right]$$

where a_j and b_j are piecewise constant with respect to pressure. The discontinuity in these coefficients is shown in Fig. A.1.

Discontinuity of this type could be handled using IF-ELSE statements in gPROMS as

IF $P_{j-1} < P \leq P_j$

$$h^{vap} = \sum_{i=1}^{NC} \left[y_i \left(a_j^{vap} + b_j^{vap} T \right) \right]$$

ELSEIF $P_j < P \leq P_{j+1}$

$$h^{vap} = \sum_{i=1}^{NC} \left[y_i \left(a_{j+1}^{vap} + b_{j+1}^{vap} T \right) \right]$$

...

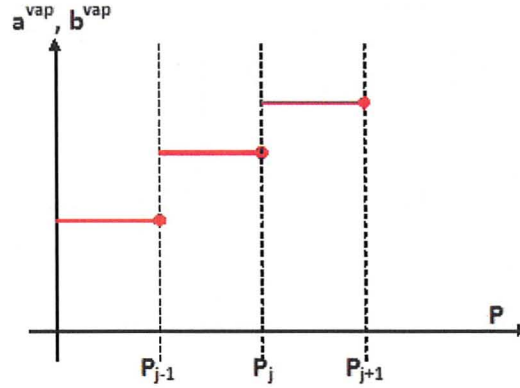


Figure A.1: Step-wise discontinuity in vapor phase molar enthalpy coefficients.

However, with this formulation, the problem is much more difficult to solve, especially dynamic optimization. This discontinuity can be translated into

$$h^{vap} = \sum_{j=1}^{N_P} \left\{ 0.25 [1 + \text{TANH}(\beta(P_j - P))] [1 - \text{TANH}(\beta(P_{j-1} - P))] \sum_{i=1}^{N_C} \left[y_i \left(a_j^{vap} + b_j^{vap} T \right) \right] \right\} \quad (\text{A.1})$$

using hyperbolic tangent function. The use of hyperbolic tangent function to capture step-wise discontinuity has been well practiced in many research studies such as Bansal *et al.* [2002]. In the equation, N_P denotes the number of pressure ranges considered and β is the steepness factor. The greater the β is the closer the resulting profile is to a step-wise change. The value assigned to β should be big enough to capture the step-wise transition, but not too big that would result in numerical problems while deriving the first order derivative with respect to the variable, P . The value of β used in our study is 50.

To illustrate how this expression works, let us take $P \in (P_1, P_2)$ and $N_P = 3$. Then,

$$(P_0 - P) < 0 \Rightarrow \text{TANH}(\beta(P_0 - P)) = -1$$

$$(P_1 - P) < 0 \Rightarrow \text{TANH}(\beta(P_1 - P)) = -1$$

$$(P_2 - P) > 0 \Rightarrow \text{TANH}(\beta(P_2 - P)) = +1$$

$$(P_3 - P) > 0 \Rightarrow \text{TANH}(\beta(P_3 - P)) = +1$$

gives

$$\begin{aligned}
 h^{vap} &= 0.25[1 + (-1)][1 - (-1)] \sum_{i=1}^{NC} [y_i (a_1^{vap} + b_1^{vap}T)] \\
 &\quad + 0.25[1 + (+1)][1 - (-1)] \sum_{i=1}^{NC} [y_i (a_2^{vap} + b_2^{vap}T)] \\
 &\quad + 0.25[1 + (+1)][1 - (+1)] \sum_{i=1}^{NC} [y_i (a_3^{vap} + b_3^{vap}T)] \\
 &= \sum_{i=1}^{NC} [y_i (a_2^{vap} + b_2^{vap}T)]
 \end{aligned}$$

which is consistent with the result using the IF-ELSE statement. When the pressure is right at the boundary value, e.g. $P = P_2$, it can be easily shown that the estimated vapor phase enthalpy has the following expression

$$h^{vap} = 0.5 \left\{ \sum_{i=1}^{NC} [y_i (a_2^{vap} + b_2^{vap}T)] + \sum_{i=1}^{NC} [y_i (a_3^{vap} + b_3^{vap}T)] \right\}$$

The predicted value is shown to be reasonably accurate based on available information. With the hyperbolic tangent function formulation, Eqn. A.1, the optimization problem can be solved more efficiently. Significant reductions in execution time and the number of optimization failures are observed when Eqn. A.1 is implemented instead of the IF-ELSE statement.

A.2 Variable Scaling

Poor variable scaling could result in numerical difficulties in the problem solution. Many authors have stressed the importance of variable scaling in eliminating numerical difficulties and obtaining solutions for optimization problems, such as Ravindran *et al.* [2006]. Throughout the course of this research project, issues of variable scaling are also encountered. As in this project, variables are usually in the form of an array (i.e. column temperature profile); in later discussions, we will use a variable array to denote variables that belong to the same family.

If elements in the same variable array have roughly the same magnitude, and the change in values with respect to time are not that significant, variable scaling can be easily performed by using methods like linear transformations:

$$\mathbf{y} = a\mathbf{x} \tag{A.2}$$

where a is a constant, \mathbf{y} is an array of transformed variables, and \mathbf{x} is an array of actual variables. However, not all the variables in the model would belong to this category, and impose numerical challenges for dynamic simulation and/or dynamic optimization. There are techniques that can be applied to transform such variables. However, depending on the robustness of the solver and the solution approach, such reformulations may not be required.

Logarithmic transformation is one solution implemented in our study for the bad scaling of the variables. For example, the composition of the minor components in the column is badly scaled and changes from 1e-1 to 1e-6 or 1e-7 in a high purity distillation column. But its natural log is much better scaled:

$$\ln(1e-1) = -2.3$$

$$\ln(1e-6) = -13.8$$

However, logarithmic transformation is not suggested for variables that could have values close to 1. In the case of high purity columns, logarithmic transformation is not recommended for scaling the composition of the major component, as

$$\ln(0.999999) = -1e-6$$

Bad scaling still remains. The closer the variable is to 1, the closer the value of the log transformation is to 0.

Introducing a constant to transform the variable linearly is another approach adopted in our study. For example, we have

$$y = \sum_{i=1}^{NC} \frac{dx_i}{dt}$$

which should have a value of zero at steady state and nonzero during transition, e.g. 1. Due to computation errors, instead of zero, the variable y may take a value of $1e-24$ at steady state. This again is a scaling problem. Introducing a constant,

$$z = y + 1,$$

helps to overcome the problem as the range of z is $[1, 2]$.

A.3 Constraint Formulation

With different constraint formulations, it was observed that control trajectories during iterations and/or the convergence point could differ. For example, if a constraint requires

$$|x - x^*| \leq 0.01,$$

there are several mathematically equivalent expressions:

$$f_1(x) = \sqrt{(x - x^*)^2}, \quad f_1(x) \leq 0.01$$

$$f_2(x) = (x - x^*)^2, \quad f_2(x) \leq 0.0001$$

$$f_3(x) = x - x^*, \quad -0.01 \leq f_3(x) \leq 0.01$$

$$f_4(x) = |x - x^*|, \quad f_4(x) \leq 0.01.$$

Depending on which expression is included in the optimization formulation, with the same setup, with gPROMS, it could result in “optimization failure” or “solution found”. This may be due to the way gPROMS evaluates the Jacobian. The Jacobian elements corresponding to the constraint formulations are:

$$J_1(x) = \frac{df_1}{dx} = \frac{1}{2} \frac{1}{\sqrt{(x - x^*)^2}} 2(x - x^*)$$

$$J_2(x) = \frac{df_2}{dx} = 2(x - x^*)$$

$$J_3(x) = \frac{df_3}{dx} = 1$$

$$J_4(x) = \frac{df_4}{dx} = \begin{cases} 1, & x > x^*; \\ 0, & x = x^*; \\ -1, & x < x^*; \end{cases}$$

As a result, the Jacobian of the constrained problem is different even if that of the unconstrained system (i.e. system having no constraints imposed)

$$\begin{aligned} \mathbf{f}(\dot{\mathbf{x}}(t), \mathbf{x}(t), \mathbf{z}(t), \mathbf{u}(t), \mathbf{p}, t) &= \mathbf{0} \\ \mathbf{g}(\mathbf{x}(t), \mathbf{z}(t), \mathbf{u}(t), \mathbf{p}, t) &= \mathbf{0} \end{aligned}$$

is the same. By looking at the Jacobian, it seems using f_3 to formulate the problem might be the best approach as it does not introduce nonlinearity and discontinuity to the constrained system. However, experience in this study, while working with different constraint formulations, indicated that when solving the dynamic optimization, there is no guarantee which formulation is the most efficient/effective. It is recommended that when the optimization problem cannot be solved efficiently, various constraint reformulations could be attempted.

Appendix B

Manual Index Reduction

Differentiating and applying chain rule to the total energy holdup expression, Eqn. 3.18

$$E_n = M_n h_n^{liq\ mix}$$

gives:

$$\frac{dE_n}{dt} = M_n \left[\frac{\partial h_n^{liq\ mix}}{\partial T_n} \cdot \frac{dT_n}{dt} + \sum_{i=1}^{NC} \left(\frac{\partial h_n^{liq\ mix}}{\partial x_{n,i}} \cdot \frac{dx_{n,i}}{dt} \right) \right] + h_n^{liq\ mix} \cdot \frac{dM_n}{dt} \quad (B.1)$$

Equivalent algebraic expressions for $\frac{dT_n}{dt}$, $\frac{dx_{n,i}}{dt}$ and $\frac{dM_n}{dt}$ need to be derived.

Derivations of Composition and Holdup Time Derivative Expressions

As at each tray

$$\frac{m_{n,i}}{M_n} = \frac{l_{n,i}}{L_n} = x_{n,i} \Rightarrow m_{n,i} = M_n x_{n,i} \quad \text{and} \quad \sum_{i=1}^{NC} m_{n,i} = M_n$$

it can be shown that, for a common column tray n ($1 \leq n \leq N_{tray}$, $n \neq N_{feed}, N_{tray}$), following expressions hold

$$\frac{dx_{n,i}}{dt} = \frac{1}{M_n} \left[\frac{dm_{n,i}}{dt} - x_{n,i} \frac{dM_n}{dt} \right] \quad (B.2)$$

$$\frac{dM_n}{dt} = L_{n+1} + V_{n-1} - L_n - V_n \quad (B.3)$$

For the feed tray and reflux, there are additional terms in Eqn. B.3.

Derivations of the Temperature Time Derivative Expression

To determine the expression for $\frac{dT_n}{dt}$, we need to revisit the VLE model (Section 3.1.1). At each tray, differentiating and applying the chain rule to

$$\sum_{i=1}^{NC} K_{n,i} x_{n,i} = 1$$

results in

$$\sum_{i=1}^{NC} \left(\frac{dK_{n,i}}{dt} x_{n,i} + \frac{dx_{n,i}}{dt} K_{n,i} \right) = 0 \quad (\text{B.4})$$

From the Modified Raoult's Law and Antoine equation, we have that:

$$\frac{dK_{n,i}}{dt} = \frac{\gamma_{n,i}}{P_n} \frac{\partial P_{n,i}^{sat}}{\partial T_n} \frac{dT_n}{dt} + \frac{P_{n,i}^{sat}}{P_n} \left(\frac{\partial \gamma_{n,i}}{\partial T_n} \frac{dT_n}{dt} + \sum_{j=1}^{NC} \frac{\partial \gamma_{n,i}}{\partial x_{n,j}} \frac{dx_{n,j}}{dt} \right) + \left(-\frac{\gamma_{n,i} P_{n,i}^{sat}}{P_n^2} \right) \frac{dP_n}{dt} \quad (\text{B.5})$$

Expressions of $\frac{\partial P_{n,i}^{sat}}{\partial T_n}$, $\frac{\partial \gamma_{n,i}}{\partial T_n}$ and $\frac{\partial \gamma_{n,i}}{\partial x_{n,j}}$ can be derived from the Antoine and Margules equations.

From the Antoine equation:

$$P_{n,i}^{sat} = \exp \left(A_i + \frac{B_i}{T_n + C_i} \right) \quad (\text{B.6})$$

we have:

$$\frac{\partial P_{n,i}^{sat}}{\partial T_n} = -\frac{P_{n,i}^{sat} B_i}{(T_n + C_i)^2} \quad (\text{B.7})$$

The Margules equation gives

$$\gamma_{n,i} = \exp \left[\frac{1}{R_{gas} T_n} \sum_{j=1}^{NC} \sum_{k=1}^{NC} \left(A_{ji}^{Margules} - \frac{1}{2} A_{jk}^{Margules} \right) x_{n,j} x_{n,k} \right] \quad (\text{B.8})$$

Let

$$g_{n,i} = \sum_{j=1}^{NC} \sum_{k=1}^{NC} \left(A_{ji}^{Margules} - \frac{1}{2} A_{jk}^{Margules} \right) x_{n,j} x_{n,k} \quad (\text{B.9})$$

we get

$$\frac{\partial \gamma_{n,i}}{\partial T_n} = -\gamma_{n,i} \frac{g_{n,i}}{R_{gas} T_n^2} \quad (\text{B.10})$$

and

$$\frac{\partial \gamma_{n,i}}{\partial x_{n,j}} = \gamma_{n,i} \frac{1}{R_{gas} T_n} \frac{\partial g_{n,i}}{\partial x_{n,j}} \quad (\text{B.11})$$

For our system having 3 components, we have

$$\frac{\partial g_{n,1}}{\partial x_{n,1}} = A_{11}^{Margules} = 0 \quad (\text{B.12})$$

$$\frac{\partial g_{n,1}}{\partial x_{n,2}} = 2A_{21}^{Margules} x_{n,2} + (A_{21}^{Margules} - A_{23}^{Margules} + A_{31}^{Margules}) x_{n,3} \quad (\text{B.13})$$

$$\frac{\partial g_{n,1}}{\partial x_{n,3}} = 2A_{31}^{Margules} x_{n,3} + (A_{31}^{Margules} - A_{32}^{Margules} + A_{21}^{Margules}) x_{n,2} \quad (\text{B.14})$$

$$\frac{\partial g_{n,2}}{\partial x_{n,1}} = 2A_{12}^{Margules} x_{n,1} + (A_{12}^{Margules} - A_{13}^{Margules} + A_{32}^{Margules}) x_{n,3} \quad (\text{B.15})$$

$$\frac{\partial g_{n,2}}{\partial x_{n,2}} = A_{22}^{Margules} = 0 \quad (\text{B.16})$$

$$\frac{\partial g_{n,2}}{\partial x_{n,3}} = 2A_{32}^{Margules} x_{n,3} + (A_{32}^{Margules} - A_{31}^{Margules} + A_{12}^{Margules}) x_{n,1} \quad (\text{B.17})$$

$$\frac{\partial g_{n,3}}{\partial x_{n,1}} = 2A_{13}^{Margules} x_{n,1} + (A_{13}^{Margules} - A_{12}^{Margules} + A_{23}^{Margules}) x_{n,2} \quad (\text{B.18})$$

$$\frac{\partial g_{n,3}}{\partial x_{n,2}} = 2A_{23}^{Margules} x_{n,2} + (A_{23}^{Margules} - A_{21}^{Margules} + A_{13}^{Margules}) x_{n,1} \quad (\text{B.19})$$

$$\frac{\partial g_{n,3}}{\partial x_{n,3}} = A_{33}^{Margules} = 0 \quad (\text{B.20})$$

These expressions are consistent with results from MAPLE. Hence, in Eqn. B.5,

$$\sum_{j=1}^{NC} \left(\frac{\partial \gamma_{n,i}}{\partial x_{n,j}} \frac{dx_{n,j}}{dt} \right) = \gamma_{n,i} \frac{1}{R_{gas} T_n} \sum_{j=1}^{NC} \frac{\partial g_{n,i}}{\partial x_{n,j}} \frac{dx_{n,j}}{dt} \quad (\text{B.21})$$

with $\frac{\partial g_{n,i}}{\partial x_{n,j}}$ given by Eqn. B.12 to Eqn. B.20.

After rearranging terms in Eqn. B.5, an expression of $\frac{dT_n}{dt}$ can be obtained:

$$\begin{aligned}
 f_T = \frac{dT_n}{dt} &= \frac{\sum_{i=1}^{NC} \left[K_{n,i} \frac{dx_{n,i}}{dt} + x_{n,i} \frac{P_{n,i}^{sat}}{P_n} \left(\sum_{j=1}^{NC} \frac{\partial \gamma_{n,i}}{\partial x_{n,j}} \frac{dx_{n,j}}{dt} \right) - x_{n,i} \frac{\gamma_{n,i} P_{n,i}^{sat}}{P_n^2} \frac{dP_n}{dt} \right]}{\sum_{i=1}^{NC} \left[- \left(\frac{\gamma_{n,i}}{P_n} \frac{\partial P_{n,i}^{sat}}{\partial T_n} + \frac{P_{n,i}^{sat}}{P_n} \frac{\partial \gamma_{n,i}}{\partial T_n} \right) x_{n,i} \right]} \\
 &= \frac{\sum_{i=1}^{NC} \left\{ K_{n,i} \frac{dx_{n,i}}{dt} + x_{n,i} P_{n,i}^{sat} \gamma_{n,i} \left[\left(\frac{1}{P_n R_{gas} T_n} \sum_{j=1}^{NC} \frac{\partial g_{n,i}}{\partial x_{n,j}} \frac{dx_{n,j}}{dt} \right) - \frac{1}{P_n^2} \frac{dP_n}{dt} \right] \right\}}{\sum_{i=1}^{NC} \left\{ \frac{P_{n,i}^{sat}}{P_n} \gamma_{n,i} \left[\frac{B_i}{(T_n + C_i)^2} + \frac{g_{n,i}}{R_{gas} T_n^2} \right] x_{n,i} \right\}} \quad (B.22)
 \end{aligned}$$

The $\frac{dP_n}{dt}$ term in Eqn. B.22 can be dropped if the top tray pressure is specified and a linear pressure profile is assumed. However, in our model, the pressure profile is a changing with the plant conditions.

$$P_{Ntray} = P_{cond} \quad (B.23)$$

$$P_n = P_{n-1} + \Delta P, \quad n = 1, \dots, N_{tray} - 1 \quad (B.24)$$

gives

$$P_n = P_{cond} - (N_{tray} - n)\Delta P, \quad n = 1, \dots, N_{tray} \quad (B.25)$$

Hence, we have

$$\frac{dP_n}{dt} = \frac{dP_{cond}}{dt} - (N_{tray} - n) \frac{d\Delta P}{dt} \quad (B.26)$$

As P_{cond} is specified and constant,

$$\frac{dP_n}{dt} = -(N_{tray} - n) \frac{d\Delta P}{dt}. \quad (B.27)$$

The pressure drop in Eqn. B.26 is a function of vapor flow rate

$$\frac{d\Delta P}{dt} = \frac{df(F_{vap})}{dt} = \frac{\partial f}{\partial F_{vap}} \frac{dF_{vap}}{dt} = \frac{\partial f}{\partial F_{vap}} \left(\beta \frac{d\dot{V}_{std}}{dt} - \frac{dF_{2,3}}{dt} \right) \quad (B.28)$$

where β is a constant unit conversion factor. Recall that \dot{V}_{std} is the volumetric flow rate of the air feed and $F_{2,3}$ is the liquid air feed from the PHX to the column, which are two system inputs. Exact forms of $\frac{d\dot{V}_{std}}{dt}$ and $\frac{dF_{2,3}}{dt}$ used in the study are:

$$\frac{d\dot{V}_{std}}{dt} = \frac{1}{\tau \dot{V}_{std}} \left(\dot{V}_{std}^{sp} - \dot{V}_{std} \right) \quad (B.29)$$

$$\frac{dF_{2,3}}{dt} = \frac{1}{\tau_{F_{2,3}}} (F_{2,3}^{sp} - F_{2,3}) \quad (\text{B.30})$$

considering the dynamics of the filter.

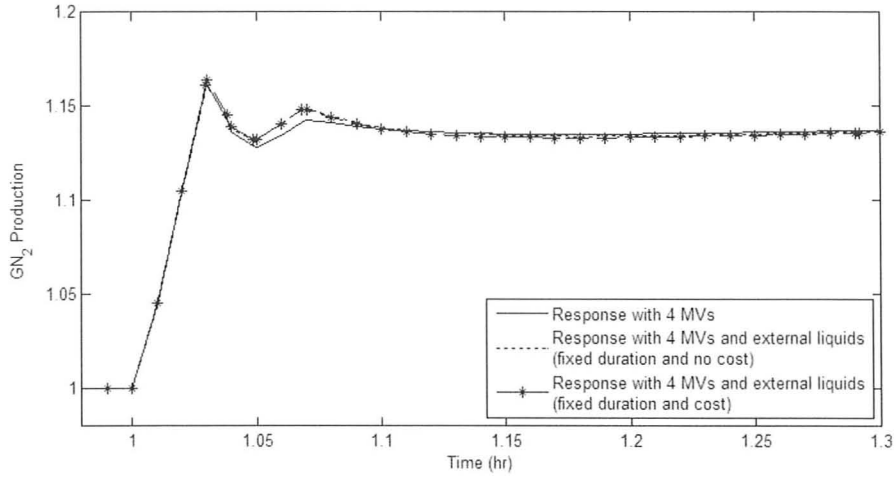
Appendix C

Results of Introducing External Liquid Nitrogen to Top Tray

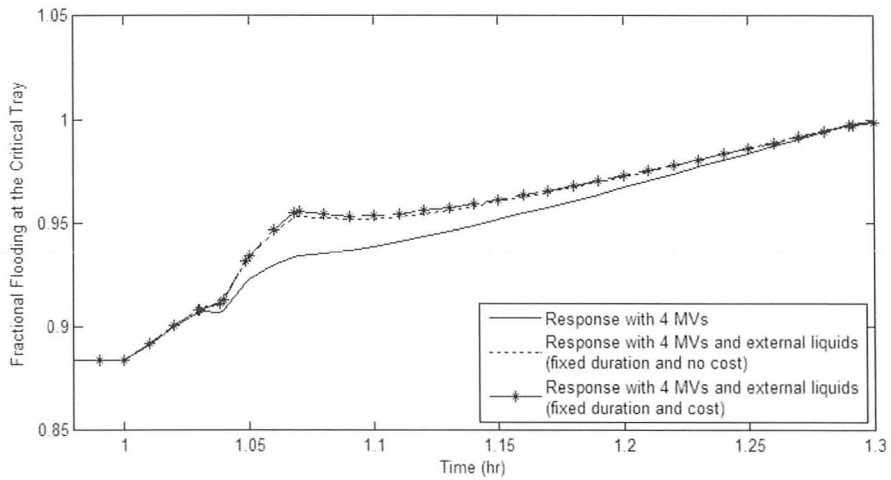
This section presents the dynamic optimization results of introducing external liquid nitrogen to only the top column tray due to capital cost and operation considerations. The same optimization problem formulation and procedures were applied as described in Section 5.4.

Base Case Impurity Specification

Fig. C.1 to Fig. C.3 present the dynamic optimization results with the base case impurity requirement during transitions and the single tray setup.



(a) Magnified view of gas nitrogen production.



(b) Fractional flooding at the critical tray.

Figure C.1: Magnified views of gas nitrogen production and fractional flooding at the critical tray in responses to: optimized control actions of only the four manipulated variables (MVs); four MVs together with external LN₂ with and without cost considerations.

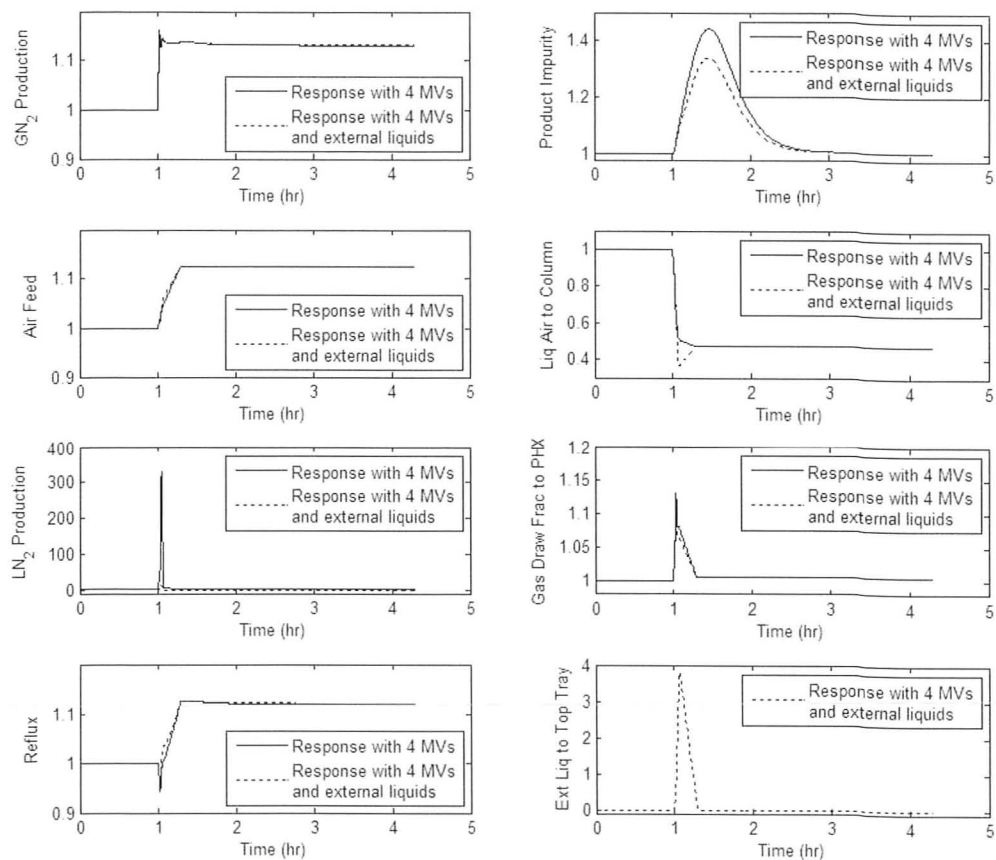


Figure C.2: Optimized trajectories of scaled variables for 20 % demand increasing case with fixed duration time and no cost penalty applied to using external LN₂.

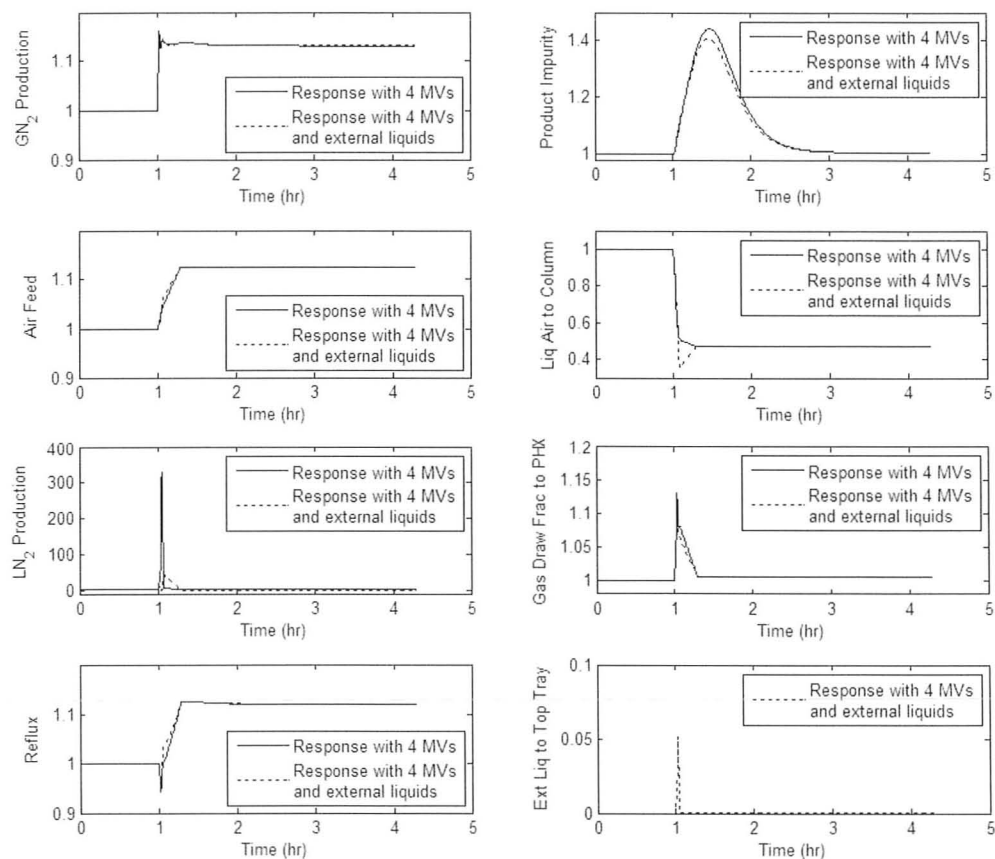


Figure C.3: Optimized trajectories of scaled variables for 20 % demand increasing case with fixed duration time and cost penalty applied to using external LN₂.

Tightened Impurity Requirement

Fig. C.4 and Table C.1 present the dynamic optimization results with tightened impurity requirement during transitions and the single tray setup.

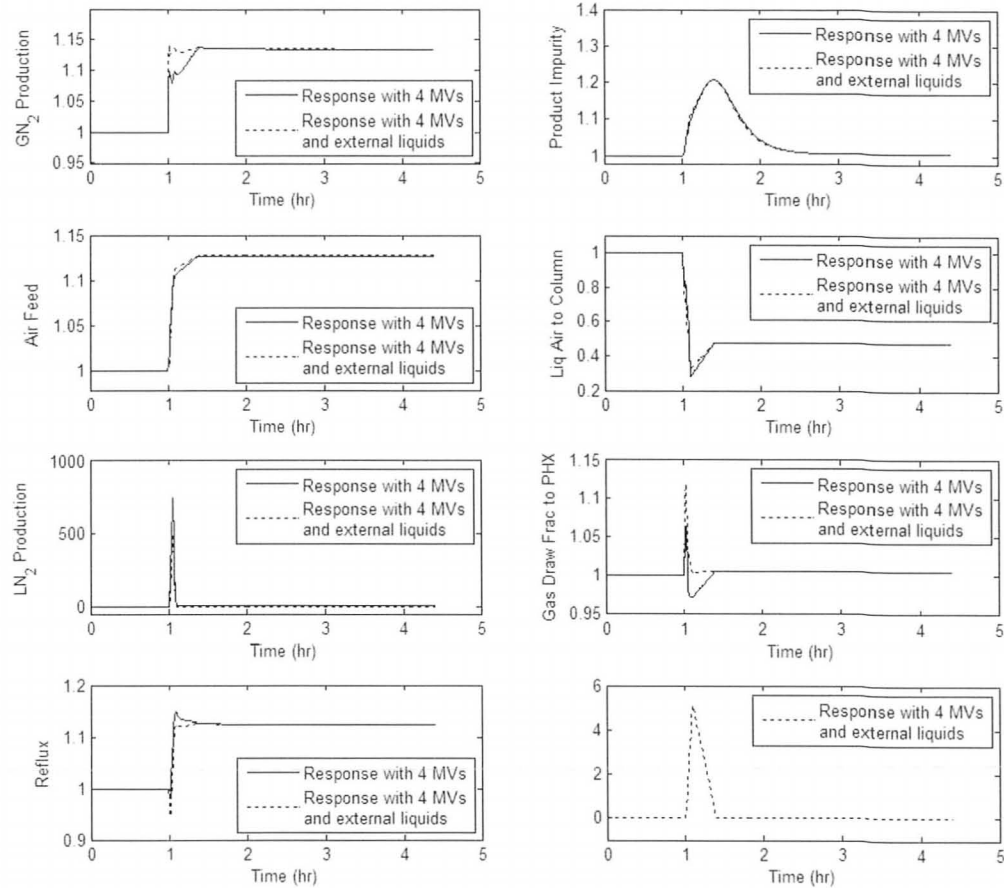


Figure C.4: Optimized trajectories of scaled variables for 20 % demand increase case without cost penalty for external LN₂ usage and with tightened impurity constraint.

Table C.1: Active constraints for case studies with tightened impurity constraints during transitions with and without external LN₂ to single tray.

Four Inputs Only	With External LN ₂ to Single Tray
<ul style="list-style-type: none">• Maximum allowable impurity level,• flooding constraint in the column, and• dew point and bubble point constraints at the PHX.	<ul style="list-style-type: none">• Maximum allowable impurity level,• flooding constraint in the column, and• dew point and bubble point constraints at the PHX.